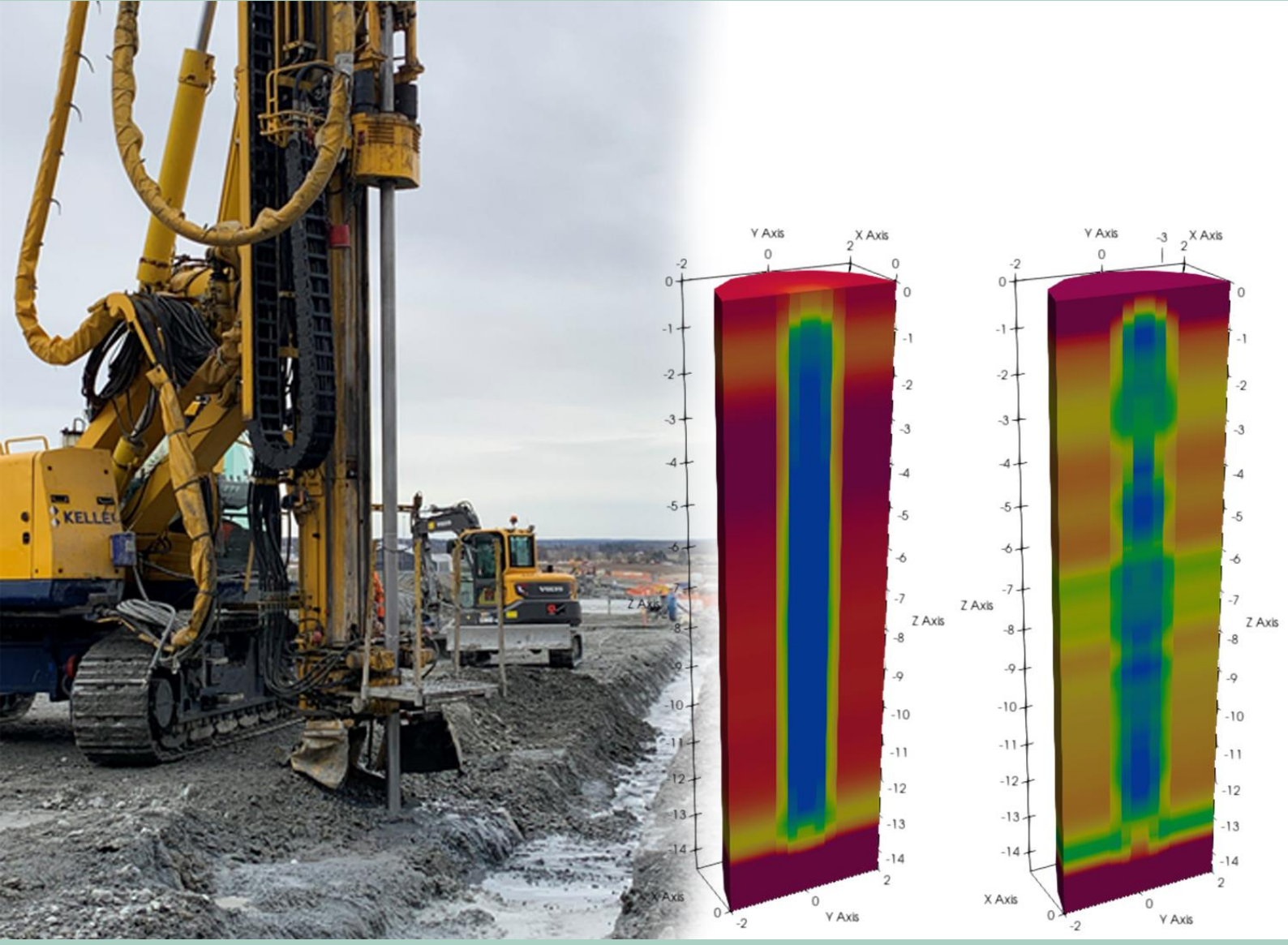

APPLICATION OF ERT FOR QUALITY ASSURANCE IN JET GROUTING COLUMNS

A development of an alternative quality control

Edvin Nilsagård

Rebecka Knutsson

Master of Science Thesis 30HP
ISRN LUTVDG(TVTG-5175)/1-84/(2022)

Engineering geology
Faculty of Engineering
Lund university

Application of ERT for Quality Assurance in Jet Grouting Columns

A development of an alternative quality control

Edvin Nilsagård & Rebecka Knutsson

LUND UNIVERSITY

THESIS

Submitted to the Division of Engineering Geology, Faculty of Engineering, Lund University in Partial Fulfilment of the Requirements for the Degree of Master of Science in Civil Engineering.

Lund 2022

Cover picture: Edvin Nilsagård

Lund University, Faculty of Engineering
Division of Engineering Geology

Application of ERT for Quality Assurance of Jet Grouting Columns

- A development of an alternative quality control

Tillämpning av ERT för kvalitetssäkring av jet-pelare

Author(s): Nilsagård, Edvin; Knutsson, Rebecka

Supervisor(s): Martin, Tina (LTH); Jonsson, Peter (LTH)

Examiner: Rossi, Matteo

ISRN LUTVDG/(TVTG—5175)/1-84/(2022)

Keywords: jet grouting, ERT, quality control, resistivity, pygimli, resdinv
Language: English

The work is performed in collaboration with Lunds Tekniska Högskola, Keller

Digital edition Lund 2022

Abstract

With the increased urbanization major cities are facing, expansion of larger facilities and households are inevitable. Expansion means larger areas of the surface needs to be used where the risk of varying subsurface soil properties increases with larger surface areas. This can result in soil properties that might not be stable enough to support these constructions. A potential solution to solve this problem is the soil improvement method of jet grouting. Jet grouting is a versatile soil improvement method used for various geotechnical aspects in construction projects worldwide. By eroding and mix in-situ soil with fluid binders from a high-pressure jet, improved geotechnical properties of the soil body could be achieved. When achieving the desired stability of the column it is crucial that the geometry and homogeneity correlates with the preliminary design standards. Thereby, quality controls are routinely performed on the column however, existing quality controls vary in methodology efficiency as well as the level of accuracy obtained from the controls. The thesis therefore aspired to find and compare an alternative quality control to the existing quality controls based on Electrical Resistivity Tomography (ERT) practice. ERT is a geophysical measuring technique for determining the electric properties of the subsurface. This technique consists of placing electrodes in contact with a specific medium and inject current via the electrodes to create an electric potential field. The electrodes will then measure the potential differences of the potential field which are translated to resistivity properties of the medium.

In this thesis a composed cable consisted of electrode cables and temperature sensors were inserted into a freshly produced test column. By injecting current the potential differences in the column and the surrounding soil were measured and the apparent resistivity properties of the underground could be determined. The measurements were performed at different times to study the curing process. The apparent resistivity measurements were inverted for two software: Res2DInv and pyGIMLi. Due to the borehole design, the resistivity measuring was performed differently than the traditional surface ERT-measurement, a geometry adapted to the data had to be applied for obtaining suitable inversion models of the column.

The measured data contained several outliers and errors which increased during the curing process of the column. This was most likely due to a corrosive action taking place on the electrode surfaces. The inversion models resulted in relatively large uncertainties as well, however the pyGIMLi inversion models showed better correlation with the intended geometry of the column compared to Res2DInv. Even though uncertainties of the inversion models were found, a resistivity contrast between the treated and untreated soil was identified throughout the curing process which decreased with curing time.

The conclusion of this thesis is that the ERT-method has potential to be applicable to quality assuring jet grouting columns. The quality parameter for determining the geometry and homogeneity of the column would be defined by the boundary of which the resistivity contrast between the treated and untreated soil was located in the inversion models or how the relative resistivity changes during the curing process. However, this quality control was not ideally executed, neither with the set of inversion models developed in this thesis, nor the set of equipment used when measuring as it was less adaptive to the column conditions and the installation procedure. The developed quality control of this thesis was not validated and it could therefore not be compared with the accuracy existing quality controls have. But we believe that the ERT-method could

potentially be a more time-effective and accurate quality control compared to existing quality controls with refinement in routine application, measuring equipment and inversion models.

Sammanfattning

Med den ökade urbaniseringen som de flesta städer står inför, är utbyggnad av större anläggningar och hushåll oundviklig. Denna expansion medför ett behov av mer tillgänglig markyta att bygga på, vilket även innebär att platser med varierande markförhållandena behöver utnyttjas. Detta kan resultera i att markegenskaperna inte alltid är passande för stora anläggningar. En lösning till detta problem är att stabilisera marken med den så kallade jetinjekterings-metoden. Jetinjektering är en mångsidig markförbättringsmetod som används för olika geotekniska aspekter i byggprojekt världen över. Genom att erodera marken och blanda cementslurry tillsammans med den befintliga jorden på platsen med hjälp av en högtrycksstråle, bildas en pelare som förbättrar markförhållandet. Vid tillverkningen av en jet-pelare är det viktigt att geometrin och homogeniteten stämmer överens med den förbestämda standarden. Därför genomförs kvalitetskontroller på pelarna för att säkerhetsställa detta. De befintliga kvalitetskontrollerna varierar i metodisk effektivitet samt i nivå av noggrannhet. Syftet med denna rapport är därför att undersöka en alternativ kvalitetskontroll som utförs med hjälp av ERT-mätningar (Electric Resistivity Tomography), samt att jämföra denna metod med de befintliga kvalitetskontrollerna. ERT är en geofysisk undersökningsmetod som mäter de elektriska egenskaperna i marken. Metoden går ut på att placera ut elektroder i kontakt med ett specifikt medium och via dessa elektroder injicera ström som skapar ett elektriskt potentialfält. Elektroderna mäter sedan potentialskillnaden i potentialfältet som omvandlas till resistivitetsegenskaper hos mediet.

I detta projekt fördes en kabel med elektroder och temperatursensorer ner i en nyproducerad kolumn. Genom att injicera ström i kolumnen och den omkringliggande jorden, kunde potentialskillnaden i potentialfältet som skapades bestämmas. Denna process gjordes vid flera tillfällen för att kunna studera härdningsprocessen. Med denna information kunde den skenbara resistiviteten för marken att räknas ut. Den skenbara resistiviteten gjordes om till den verkliga resistiviteten genom inversioner i olika datorprogram. De datorprogram som användes i detta arbete var Res2DInv och pyGIMLi. Eftersom mätningarna i detta arbete inte utfördes på samma sätt som de traditionella ERT-mätningarna på jordytan, definierades en ny geometri som var bättre anpassad till kolumner och på så sätt blev inversionmodellerna mer trovärdiga.

Den uppmätta data som erhölls efter mätningarna innehöll ett antal extremvärden och fel som ökade under härdningsprocessen av kolumnen. Detta berodde antagligen främst på korrosion på elektrodernas yta. Inversionsmodellen resulterade i relativt stora osäkerheter, men pyGIMLi-inversionsmodellerna hade bättre korrelation med den avsedda geometrin för kolumnen jämfört med Res2DInv. Trots en del osäkerheter gick det att urskilja en resistivitetskontrast mellan den obehandlade jorden och den behandlade jorden under härdningsprocessen, vilket dock minskade över tid.

Slutsatsen i detta examensarbete är att ERT-mätning har potential att användas som kvalitetskontroll för jet-pelare. Kvaliteten gällande geometrin och homogeniteten i kolumnen definieras utifrån var resistivitetskontrasten i inversionsmodellen är lokaliserad eller hur den relativa resistivitetsökningen ser ut under härdningsprocessen. I detta arbete utfördes inte kvalitetskontrollen på ett optimalt sätt då inversionsmodellerna utvecklade i detta arbete inte var idealiska med den samlade mätningsdatan, samt att utrustningen som användes vid mätningarna inte var anpassade för förhållandena och

installationsprocessen. Kvalitetskontrollen i detta arbete har inte validerats och kunde därför inte jämföras med de befintliga kvalitetskontrollernas noggrannhet. Med förbättrade rutintillämpningar, utrustning och inversionsmodeller kan ERT-metoden potentiellt vara en mer tidseffektiv och noggrann kvalitetskontroll jämfört med befintliga kvalitetskontroller.

Preface

We would like to thank our consultants and supervisors for helping us to complete this thesis. Tina Martin, Torleif Dahlin and Peter Jonsson from LTH: this would not be possible without your consultation and guidance to help us achieve this.

We would also like to thank the company Keller for allowing us to visit your site in Moss and get the opportunity to measure a jet grouting column as well as sharing your great knowledge of jet grouting.

Thomas Guenther, thank you for showing and helping us with the pyGIMLi software. It was massively appreciated.

We hereby complete our 5-year journey at LTH to become Master of Science in Civil Engineering-graduates. We want to thank everyone that shared this journey with us, with all the great memories that will last for as long as we live. And also, a special thank you to our families for supporting us through thick and thin.

Lund, September 2022

Content

1 Introduction

The population of the world's cities is expanding in a rapid manner, with an estimated 55.3% of the world's population living in urban settlements according to the United Nations (2018), while a third of the world's population is projected to live in cities with at least half a million inhabitants by year 2030. The urbanization of larger cities will prove to be challenging for the infrastructure and the demand of the expansion of households. To avoid succumbing to the challenges major cities are facing, expansion of urban land and production of larger facilities are an inevitability when finding solutions to these problems (The World Bank, 2020). This creates a necessary goal of producing stabilized foundations provided to these solutions. A risk for the expansion of urban land is the variation of soil conditions resulting in unplanned expansions that may not inherit suitable soil conditions for building facilities on. One soil improvement technique which could be proved useful to this situation is jet grouting.

This soil improvement technique uses in-situ soil mixed with a binder, by injecting a grout mixture through a high-pressure monitor in a pre-drilled hole. The mixture will destabilize the in-situ soil and mix it with the binder to form a column which will achieve desirable soil properties after curing (Croce, et al., 2014). This finished mixture is known as soilcrete.

Introduced in Japan during the 1970s, the development of the jet grouting technology has since advanced by specialist contractors (Keller, 2022) and researchers (Croce, et al., 2014; Essler & Yoshida, 2004; Bruce, 1994). By applying different types of treatment systems and exploiting knowledge to streamline the jet grouting procedure, it has popularised the technique throughout the world.

Much of its early development was based on practical experience accumulated through each project. By applying this experience to the academic community, additional development was made towards establishing empirical and theoretical methods for predicting the column properties (Ribeiro & Cardoso, 2017). The most important properties of achieving a desirable quality for the jet grout column is the geometry and homogeneity of the treated soil (Essler & Yoshida, 2004). To verify the quality of the column as well as the predictive method's credibility, quality controls are routinely performed by measurements for finished columns. Several methods of performing these quality controls differ in theories and results (Croce, et al., 2014) with varying credibility and accuracy without intruding the surrounding soil in which the column is installed in. Electrical Resistivity Tomography (ERT) methods have proved to be useful in jet grouting research but are largely unexplored for site investigations (Bearce, et al., 2016).

For this reason, the thesis aspires to find and test another method based on ERT-measurements in site investigations. This is where a potential to identify a resistivity contrast between the treated and the untreated soil can resolve in quality assuring the geometry and homogeneity of the jet grout column.

1.1 Purpose and aim

The purpose of this thesis is to investigate how the ERT-method can be applied for the quality assurance of jet grouting columns. It will aim to combine the knowledge of jet grouting, ERT and existing quality controls to find a suitable methodology of the ERT-measurements and establish an alternative quality control method for geometry and homogeneity of jet grouted columns.

Thereby, this thesis aims to answer the following questions:

- Can the ERT-method be used to assess the quality of jet grouted columns?
- How can the ERT-measurements be performed?
- What quality parameter can be defined based on the ERT-method and are they comparable to the existing quality controls as well as the methodology?

1.2 Method

The thesis will be divided into three sections: a literature study about jet grouting, ERT and existing quality controls, the application of the ERT-method and results with developed model as well as an analysis.

The literature study will consist of chapters describing the jet grouting technology, electrical resistivity methods and existing quality controls.

The methodology of the ERT-method was based on the principle of ERT practice and existing quality controls combined with the knowledge of jet grouting referred in the literature study.

The results will present the inversion models as well as error estimations based on the ERT-measurements. The analysis is based on the interpretation of the inversion models as well as by discussing the interaction of the soil and the resistivity progression throughout the curing process. Potential sources of errors in the methodology are also analysed and discussed.

1.3 Focus

The focus of this thesis is to find a suitable ERT-method for estimating the geometry and homogeneity of the jet grouted column as well as develop a methodology to perform the ERT-measurements. The measurements were performed on a specific construction site in the urban area of Moss in Norway. These measurements were considered for test columns with no interaction of the structure during the field investigation. Furthermore, the measurements were assessed by a double fluid system in the production of the test columns with a specific grout mix.

2 Jet grouting

2.1 Background

Jet grouting is a versatile and popular soil improvement method used for various geotechnical aspects in construction projects worldwide (Croce, et al., 2014; Wang, et al., 2013). By eroding and mix in-situ soil with fluid binders from a high-pressure jet, improved geotechnical properties of the soil body can be achieved. This can in hand reduce the settlements of new or existing projects, as well as supporting open or underground excavations in ongoing projects.

Jet grouting was considered to be first developed in Japan in the 1970s by reusing high-speed jets in rock cutting to be applied for ground improvement purposes instead (Croce, et al., 2014). A patent approved in 1974 presented a method of forming an underground wall comprising of several columns in the subsurface soil (Nakanishi, 1974). By drilling vertically using a rotationally moveable hollow shaft mounted with drilling functions as well as a nozzle to a predetermined depth, a cavity could be formed in the subsurface soil. The hollow shaft could then retract from the cavity whilst simultaneously rotating and radially injecting a solidification and densification liquid agent through the nozzle into the in-situ soil to mix and form a continuous column along the cavity.

The principle of the jet grouting procedure is largely unchanged however, the jet grouting technology has since progressed in development for decades, improving the soilcrete properties and streamlining the operation.

2.1.1 Applications

There are many different applications that jet grouting can be used for and the method works in the whole spectrum of soils from the coarsest gravels to the finest clays. Applications can be in any direction but are often divided into vertical or horizontal jet grouting (Bruce, 1994). According to Essler and Yoshida (2004) jet grouting is often applied to improve the soil in four different categories: groundwater control, movement control, ground support and for environmental aspects.

When jet grouting is used for groundwater control it is usually to prevent flow from getting into an excavation, either through the sides or the base of the excavation. Jet grouting can control groundwater during tunnel construction, as it prevents the groundwater from entering the tunnel. The method can also be applied to prevent water seepage through a water retention, such as a dam or flood defence structure as well as preventing or reducing contamination flow through the ground. Jet grouting can reduce ground or structure movement during excavation or tunnelling. The purpose of jet grouting in tunnels is to support the face or sides during construction and maintenance (Essler & Yoshida, 2004).

Jet grouting can also increase the factor of safety of embankments or cuttings, or to provide support to piles or walls to prevent or reduce lateral movement. Another important function of jet grouting is to support buildings during excavation or tunnelling. The method can also be applied to improve the ground to prevent failure through inadequate bearing or to transfer foundation load through weak material to a competent layer. The environmental aspects of jet grouting include providing lateral or vertical barriers to contaminant flow. It also applies for encapsulating contaminants in the ground to reduce or prevent contamination off-site or into sensitive water systems (Essler & Yoshida, 2004).

2.2 The process of jet grouting installation and different systems

2.2.1 The process of modern jet grouting

The jet grouting procedure consists of three parts: drilling, lifting and rotation. According to Croce et al. (2014), jet grouting is accomplished by using a jet grouting string consisting of several combined rods. In the rods there are one, two or three conduits that convey the fluids to a steel cylinder placed at the end of the string called “monitor”. On the monitor there are one or several nozzles with a small diameter that convert the high-pressure fluids flow in the string to high-speed jets. At the bottom of the monitor a drilling bit is attached.

Jet grouting is usually performed by using the same rig for both drilling and grouting. The rig can regulate the rotations and translation of the string and the monitor. The initial stage is the drilling, where the drilling bit is active and creates a borehole with a predetermined depth (see figure 1a). The drilling bit is larger than the pipe string, which enables a space between the pipe and the borehole wall (Croce, et al., 2014). After the drilling reaches the predetermined depth (see figure 1b), the lifting sequence starts, and the fluids are injected into the soil at high speed through the nozzles. The grout pipe is rotated at a constant rate and slowly raised towards the ground surface with the jet injecting into the soil radially from the jet grouting string (see figure 1c). After some time, the grout solidifies in the ground, formatting a quasi-cylindrical cement soil body (Modoni, et al., 2006). Depending on project requirements and soil types, the curing time for soilcrete varies between three to fourteen days (Shorr, et al., 2007).

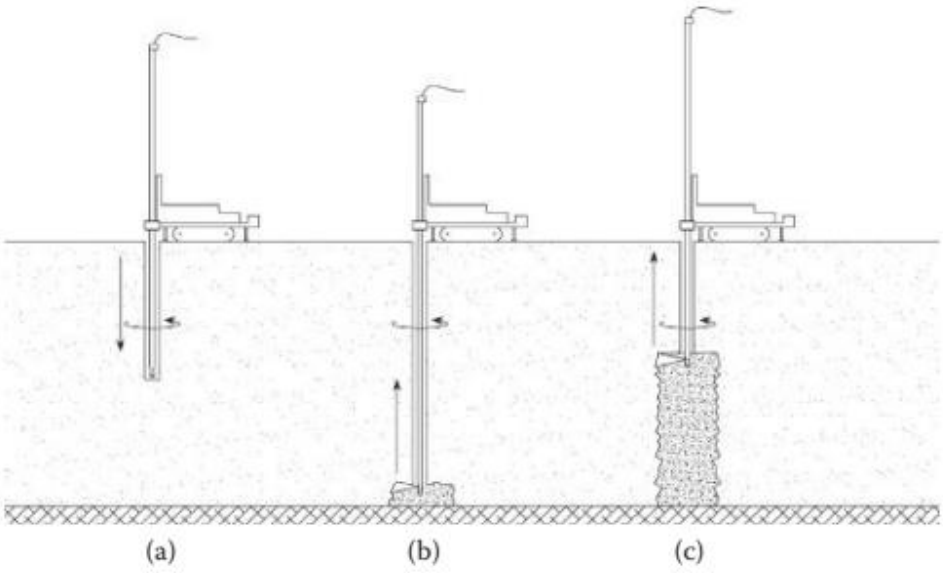

Figure 1 Process of jet grouting adapted from Croce, et al. (2014)

The lifting sequence can be done in two different ways. The most common method is intermittently lifting. This method is performed by lifting with subsequent steps of 40 to 100 mm with each step rotating several times. In the other method the pipe is lifted towards the ground at a constant rate and the jet grout creates a spiral shaped column (Croce, et al., 2014).

According to Croce & Flora (2000), the jet grouting procedure is performed in three stages which is presented in figure 2. In the first stage the grout is produced by mixing cement powder and water for prescription proportions. The grout is then subjected to high pressure and pumped into the monitor. From the monitor the grout is transported through tubes and then through the hollow metallic injection stem, eventually reaching the monitor nozzles where the grout is injected into the soil. After the injection, the second stage consists of the grout to be absorbed by the soil while the rest flows towards the ground surface. A part of the grout will not be absorbed by the soil and will therefore pass through the space between the perforation holes and the injection stem which becomes a waste product called spoil. The outflow of grout and eroded soil can vary between 0-80%. The third and last stage consists of the cementing process. The grout retained by the ground will solidify after some time due to the hydration of the cement particles by the water in the grout and in the natural soil (Croce & Flora, 2000).

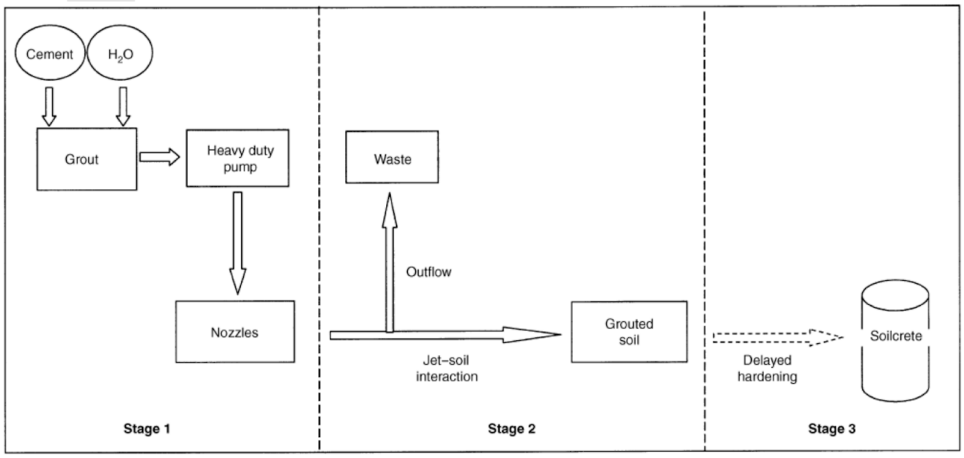

Figure 2 Schematic of the different stages of the jet grouting procedure (Croce & Flora, 2000)

2.2.2 Different jet grouting systems

There are three different types of jet grouting techniques that are commonly used. These methods are categorized according to the number of fluids injected into the subsurface soil: single-fluid system (grout), double-fluid system (air + grout) and triple-fluid system (water + air + grout).

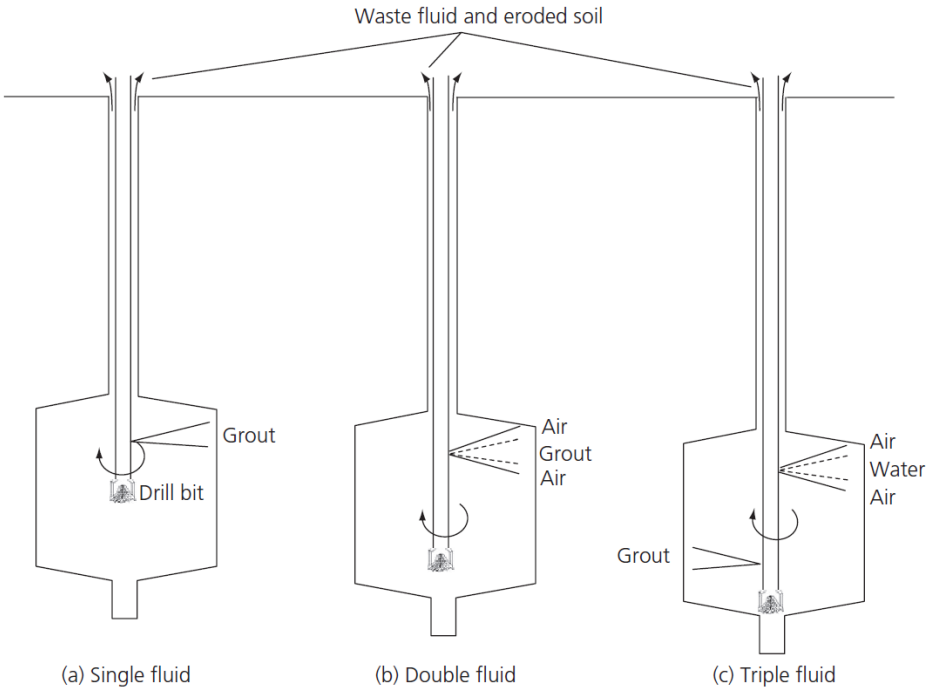

Figure 3 (a) Illustration of the process of single fluid system. (b) Illustration of the process of the double fluid system. (c) Illustration of the system of the triple fluid system. (Croce, et al., 2014)

In the **single fluid system** in figure 3 (a), only grout is injected into the ground. The single fluid system is the most economical and the most flexible system of them all. Therefore, it is often the most convenient solution (Croce & Flora, 2000). In the single fluid system, the soil remoulding and the subsequent cementation are both caused by the injected grout (Croce, et al., 2014)

The **double fluid system** in figure 3 (b), has two versions. In the conventional double fluid system, the soil remoulding and the cementation are still caused by the grout. The difference between the two systems is that in the classic double fluid system the jet of grout is shrouded by a jet of air. In the other version of the double fluid system both water and grout are injected into the soil. Water goes through a nozzle placed in the upper part of the monitor and the grout gets injected through a nozzle placed in the lower part of the monitor. In this system the eroding and remoulding is caused by water while the grout is cementing the soil (Croce, et al., 2014).

In the **triple fluid system** in figure 3 (c), grout, air and water is injected into the soil and the remoulding and the cementation is separated. The water jet is surrounded by an air jet which remoulds the soil. The grout is injected through another nozzle in the lower part of the monitor and is only used for cementation. In the standard triple fluid system, the velocity of the grout injection is lower than the air and water jet, since a high velocity is only necessary when it is used for erosion of the soil. In another type of triple fluid system, both the water jet and the grout are injected at a very high speed since both fluids are used for remoulding. By enabling two erosion stages, the penetration depth of the jet grout can enhance, which is called the eroding distance (Croce, et al., 2014).

2.3 Potential factors affecting jet grouting columns

This section will focus on the factors affecting the jet grouting process and the general theory of jet grouting interaction. The chapter will distinguish effects regarding the soil conditions and the equipment used for installation, describing potential risks and how to prevent them.

2.3.1 Soil conditions

Jet grouting can be performed in most soil conditions (Bruce, 1994). The efficiency of the injection can depend on the fluid system employed but the main consideration is the characteristics of the in-situ soil. The heterogeneity of the in-situ soil is caused by layers of variable physical properties with different depths and anisotropic characteristics. The layers inherit variable soil resistance, causing the erosive process from the jet to be uneven in the soil. Gravels and sands have a lower resistance towards erosion than clay for instance (Burke, 2004). For larger depths, increased confining stresses as well as consolidation will increase the soil resistance. This can result in inhomogeneous treatment and inconsistent geometries, exhibiting over- or undersized columns which potentially risk larger settlements than intended. Geotechnical and hydrological surveys performed before the jet grouting procedure can provide essential information for the contractors to adjust operation parameters to achieve desirable results.

Another important aspect is the impact of groundwater levels since they vary during the year (Fetter, Jr., 2014). Groundwater presence and groundwater chemistry can affect the seepage effect (later described in section 3.3) of the grout as well as decreasing the strength quality of the soilcrete. Therefore, it is important to ensure the right injection parameters are set before the jet grouting procedure (Bruce, 1994).

Croce et al. (2014) categorized 3 different mechanisms for the jet-soil interactions: seepage, erosion and cutting, illustrated in figure 4. The conclusion was based on various experiments presented from the literature. The seepage effect describes the penetration

in the voids between soil particles which are filled with the grouted material (see figure 4a). The erosion effect is when the fluids of the jet erode the soil material, flushing away particles which create space for filling of grouted material (see figure 4b). The final mechanism is the cutting effect which enables the jet to cut a bigger piece from loose soil creating space for grout to fill (see figure 4c).

For very coarse soils (gavels and sandy gravels), the main mechanism is erosion, whereas for clean gravel, grout seepage contributes to the expansion of a pillar. The erosion mechanism is also more relevant for coarse soils (gravelly sands, silty sands, and sand). This is due to the small particles being subsequently removed by the dragging action from the jet.

For clay or silty clay soil (cohesion soil), soil disaggregation and remoulding become more difficult. The adhesive forces between particles are much larger here resulting in a low efficiency of the erosive mechanism. If homogeneity of the pillar should be achieved, longer operational time of the jet to break through the voids between the particles is needed. Since clayey soils have a low permeability, the resistance to grout seepage is much higher. Therefore, the main mechanism for these soil types is jet cutting (Croce, et al., 2014).

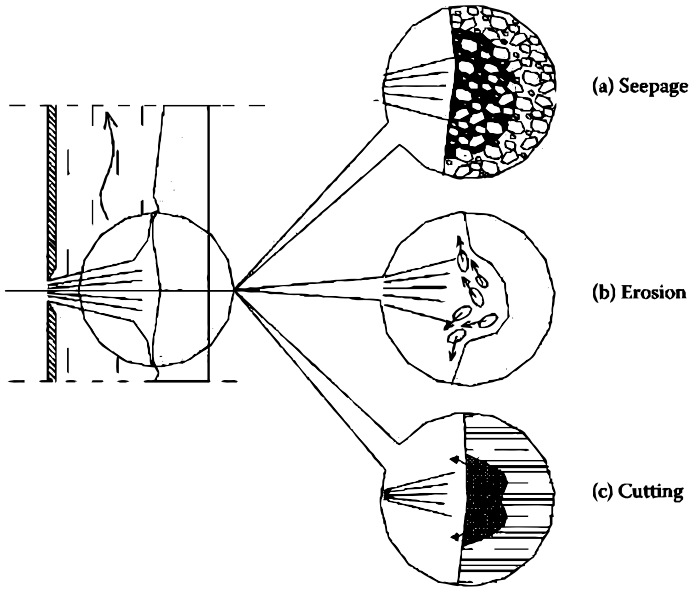

Figure 4 The three main mechanisms of jet-soil interaction regarding grout intrusion modified from Croce et al. (2014)

The concept of shadow effect is caused by a soil particle being too big for the jet to erode or too cohesive for the jet to cut, illustrated in figure 5. The particle can also disable the seepage mechanism if the cutting time is not long enough. This results in soilcrete columns to have a section with a smaller diameter compared to the rest of the cross-section since the jetting fluids could not penetrate the larger soil particle (Bellato, et al., 2018). With the columns interacting as a cohesive formation, spots of weaknesses for water ingress can be obtained making this a vital consequence when jet grouting is used for sealing water cut-offs.

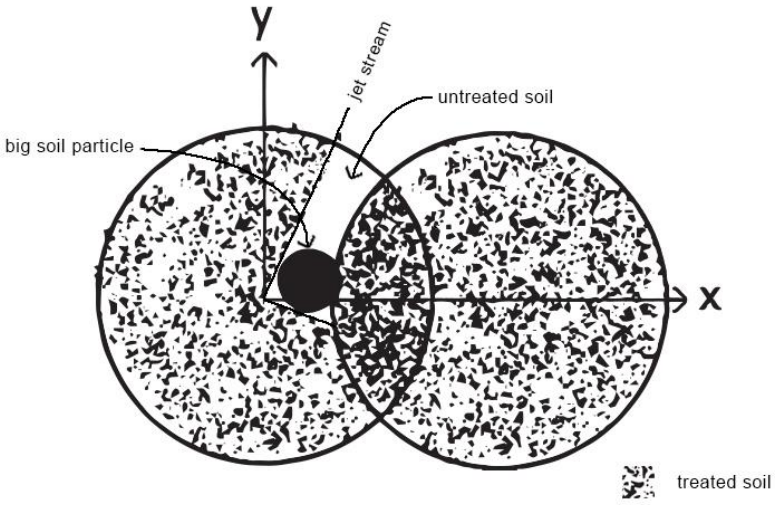

Figure 5 Illustration of the shadow effect in jet grout columns modified from Bellato, et al. (2018)

2.3.2 Equipment effects

There are further aspects that affect the efficiency of the jet grouting process, for example equipment effects (Essler & Yoshida, 2004; Croce, et al., 2014). The general effects are pressure from the jet, flow rate from the nozzle, grouting mix and spoil.

The effect of pressure from the water jet is important to the relation of the eroding distance. The typical jet pressures can range from 20 to 60 MPa depended on soil conditions (Bruce, 1994). Generally, increased jet pressure follows an increased eroding distance in the soil. The same eroding distance can also be obtained with a lower pressure, but the jet grouting process must be operational for a longer time period (slower rotating and lifting speed of the jet) (Essler & Yoshida, 2004; Croce, et al. 2014). Croce et al. (2014) summarized the erosive process from the water jet by two main factors. The action of the fluid threads, which cause the soil particles to drag away from their original position and, the increase of pore-pressure when the fluid seeps through cavities of the grains, reducing the contact force between the grains. Therefore, the soil's relative density can be related to the jet penetration rate. Looser soils enable the grout to expand faster due to larger cavities between grains, with higher relative density resulting in the opposite. For constant operational jetting times, the relative density can therefore influence the dimension of a column.

The grout mix is composed of water and cement according to weight ratio (W/C). The relation typically ranges from a value of 0.6 to 1.3 (Bruce, 1994). The decision of choosing the appropriate relation is largely depended on the column's purpose and the soil conditions. Generally, increased W/C results in more erosive efficiency from the grout material but obtaining lower strength when curing. This can be problematic if the jet grouting column is used for stabilization purposes, but almost irrelevant when used for water sealing. The type of cement used is not specified but needs to be taken into consideration depending on the site conditions. The rigidity, viscosity and rheology should be low to increase the column diameter. In soils of low permeability, the seepage effect is greatly reduced enabling a lower strength of the soilcrete than for granular soil.

As previously described the spoil is a waste product from the column installation. For decreasing production cost, the waste product should evidently be decreased as much as

possible. But for establishing an effective treatment of the pillar, a moderate amount of spoil is necessary (Croce, et al., 2014). The spoil ensures that no leakage occurs along the borehole during upward flow which otherwise can result in ground heave. If no connection between the annular space around the jet and the surface is found for the backflow, the consequence could lead to increased grout pressure, fracturing the soil when the grout pressure is larger than the soil resistance. This can result in thin grout layers. For preventing this scenario, the borehole walls should be sustained, by either installing casing or by circulation of bentonite or cement during drilling.

3 Existing Quality Controls

Several established quality controls regarding the homogeneity and geometry of jet grouting columns exists. Quality control is used to certify and quantify the comparison to the columns preliminary design standard. If a column inherits a lower quality than the design standard, a potential failure of the structure can occur. Considering jet grouting uses in-situ soils, which varies in its geotechnical properties, the level of uncertainty becomes more relevant, and the effect of soil improvement techniques and performance controls is therefore useful for supporting the decision-making process in ground improvement projects. Quality control is also considered a necessary tool for presenting a quality for a company, establishing its reputation and experience in its production and performance (Croce, et al., 2014).

The testing of the column's geometry can either be performed directly or indirectly (SS-EN 12716:2018). Direct method (measuring the diameter directly) obtains the most complete and accurate inspection but is not always possible and can be inefficient for certain situations. Indirect methods are an alternative way to effectively reduce the cost and time of performing the quality controls by using variables based on less intrusive measurements (Essler & Yoshida, 2004).

Jet grouting controls is categorized into three main aspects according to Croce et al. (2014). The first one is the treatment aspect, ensuring the dimensions and properties of the columns are desirable. The second one is the interaction between the column and the in-situ soil, checking the behaviour of the jet grouting components. The third aspect is the undesired effect on the surrounding environment, where neighbouring structures are of main concern. For this thesis, the treatment aspect and interaction will be of most relevance, why the following existing quality controls will mostly describe the methodology and what is obtained from these controls in relation to these aspects.

3.1 Direct quality control methods

3.1.1 Excavation

The most direct method of checking a column's dimensions and homogeneity is by physically looking and measuring it. This enables inspection for the smallest details, defects and highlights (Essler & Yoshida, 2004). Since the column installation is directly injected to the soil an excavation of the surrounding soil of the column must be performed for obtaining any intel of an ocular inspection. Data accumulated from this inspection can establish certain relationships between the average diameter of the column and the injection parameters of the jet grouting machine for the specific site (Croce, et al., 2014). As this control is intrusive it would not be possible to execute for a ground improvement structure thereby, trial columns with no relation to the structure are installed into nearby soil instead. The procedure is expensive and time consuming and assumes the same conditions as the columns for the actual structure as well. This potentially risks an

undesired treatment process. For columns designed for larger depths, an indirect method would be preferrable as excavation of long pillars is difficult to execute. A diameter quality control from excavation is shown in figure 6.

Figure 6 Diameter quality control of jet grout column by excavation (Croce, et al., 2014)

3.1.2 Calliper

Another direct method of verifying the diameter of the column is to use a calliper. This method is less invasive than excavating the column (Croce, et al., 2014). A calliper consists of two arms connected to a centre hydraulic jack (see figure 7a). The hydraulic jack can increase the pressure to open the two arms, enabling a jack chamber to penetrate the treated soil. The treated soil must be freshly made for fluid to be collected into the jack chamber. This tool is inserted in various depths of the column with different pressures to measure the volume variation of the fluid in the chamber. By expanding the two arms, a larger resistive force caused by the untreated soil compared to the treated soil will affect the pressure-volume relation, showcasing deviations (see figure 7b). This will mark the boundary between the treated and untreated soil, establishing the diameter of the column. A risk of performing this method is if the calliper is misaligned with the column axis when inserted into the column, giving uncertain measurements.

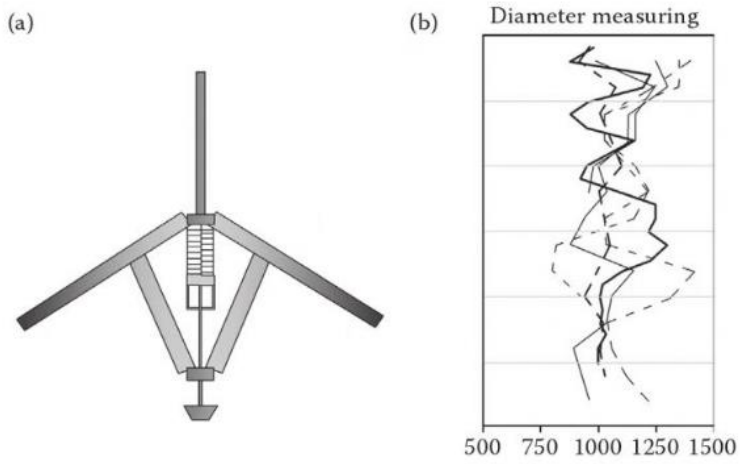

Figure 7 (a) Illustration of a calliper. (b) Deviations caused from the pressure and volume in the jack chamber (Croce, et al., 2014)

3.2 Indirect quality control methods

3.2.1 Sonic logging tests

An indirect method of estimating the diameter and homogeneity of a column is the sonic logging tests. Different versions of this method have been adapted by companies and jet grouting practitioners. But the principle of this control is performed inserting a measuring device through a borehole drilled along the vertical axis of a hardened column. The measuring device consists of a source and receivers which are separated by an offset distance. The source generates sonic waves which will consequently hit the boundary of the column's treated and untreated soil and reflect off this surface to transport to the receivers via time intervals. The time intervals can determine the diameter of the column with a relation of the sonic waves' distance travelled and the velocity in which the wave travels through the treated soil (Croce, et al., 2014). The wave velocity is compared with previously measured laboratory core samples while the distance and time intervals are measured before the diameter can be estimated.

To determine the homogeneity of the column, the sonic logging tests will record positive and negative half waves which are plotted in a time domain. The plot will highlight the homogeneity of the column by the shape of the half waves. Essentially the wave velocity is determined through this method which is applicant to the mechanical characteristics of the soilcrete. A constant shape of the half waves will result in a homogenous treatment while missing segments and irregular shapes can relate to defects of the treated soil (Croce, et al., 2014).

However, when applied to a freshly produced column, much of its water content is still present and little stability growth has been made in the column. This can result in the sonic waves' reflective action on the boundary between treated and untreated soil to be uncertain if groundwater is present in the subsurface soil. With a more stabilized column, the reflection from the boundary becomes much clearer, thereby this method is mostly performed when the column has hardened.

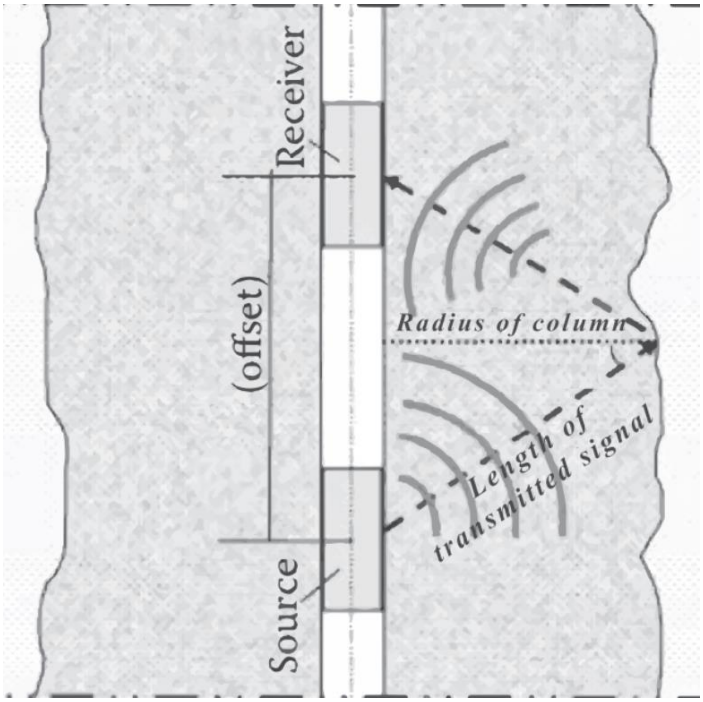

Figure 8 Sketch of the principle of sonic logging test modified from Croce, et al. (2014)

3.2.1.1 Acoustical Column Inspector (ACI®)

One example of an adaptation of the sonic logging tests is the Acoustical Column Inspector (ACI®) which is developed and patented by the geotechnical specialist contractor called Keller (Keller, 2022). This quality system assures the diameter of the column as well as the strength of the soilcrete during the jet grouting installation (Keller, 2015). The measuring process starts before the jet grouting procedure. Two pre-drilled boreholes will be positioned on each side of the expected column diameter. Once the boreholes have been measured for correct alignment, by measuring an inclinometer into the borehole, feeler pipes are inserted into each borehole using a special drill bit. These rods are then connected to highly sensitive piezo-sensors on the surface. As the column installation starts, the piezo-sensors will register the vibrations of the feeler pipes, certifying contact with the soilcrete. The data accumulated by the piezo-sensors is interpreted through an evaluation unit called the ACI®-Box, analysing the contact of the feeler pipes throughout the entire production of the column (see figure 9). Since the recording is performed during production it enables the operation parameters of the jet to be adjusted, adapting to changing soil layers.

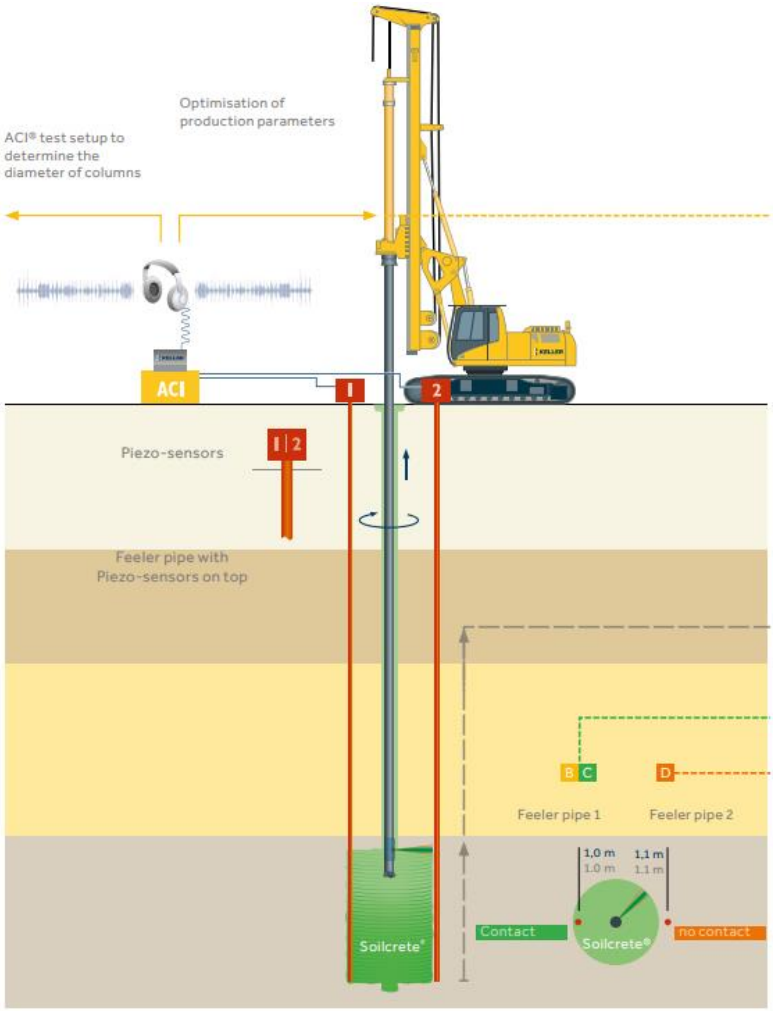

Figure 9 Schematic example of the Acoustic Column Inspector (Keller, 2015)

This method thereby quality assures the jet grout column simultaneously as production. Although, some miscalculations have been made using this technique, most of the attempts have been proved to correlate with the preliminary design geometry. However, the quality control can be time consuming as the right placement and angle of the feeler pipes before installation are essential to get the correct data. The installation procedure of the column is also slower due to constantly adjusting the injection parameters during production. And since it's time consuming, the control is not performed for every column but for a few columns within regions of the same expected soil conditions.

3.2.2 Thermochemical method

Assessing the diameter and cementation of the jet grout column, Brandstätter et al. (2005) investigated a thermochemical control. The theory of applying temperature measurements to a jet grouting column is based on the in-situ temperature and thermochemical analyses. Brandstätter et al. (2005) performed the measurements by inserting a temperature sensor at the vertical and horizontal centre of a freshly produced column. A second sensor was positioned at the surface to monitor the air temperature for reference. Starting from parameters of the expected properties of the cement content and column radius, a numerical analysis is applied with an iterative process to obtain acceptable errors between the measured and the calculated values and thereby find

suitable parameters with adjustments. The measurements displayed in figure 25 depicts an initial temperature of 20˚C, to rapidly increased to a maximum temperature of 70˚C for a 0.6-meter column radius with a cement (Portland cement PZ 275) content in the grout mixture of 15%. After the maximum temperature was reached an exponential decrease in temperature over the next 170 hours of curing to 40˚C was obtained. The results showed that the amount of cement in the grout mixture affects the heating period of the column at the beginning of the curing process, while a change in radius of the column influenced the decrease of temperature during cooling period. The control was verified by excavating the column, resulting in a promising correlation of the diameter.

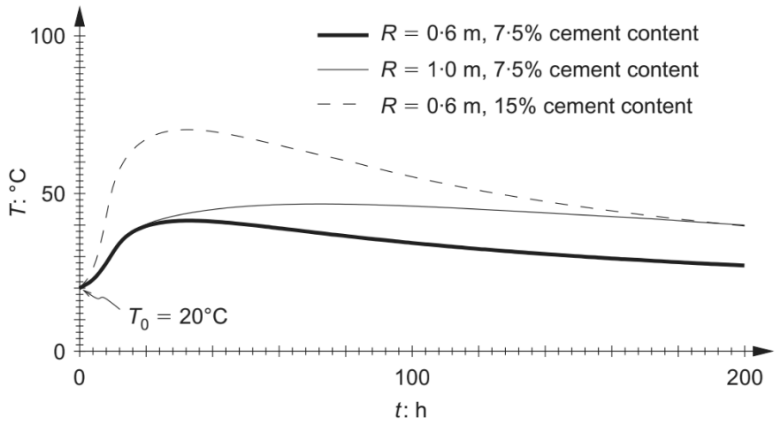

Figure 10 Temperature history obtained at the centre of jet grout columns for different radii and cement contents (Brandstätter et al., 2005)

Brandstätter et al. (2005) concluded that this method is strongly depended on the input parameters as well as executing thermal experiments of the binder to determine the chemical affinity. Moreover, the success of identifying the correct parameters is linked with the differing effects of the unknown parameters on the temperature history.

3.2.3 Spoil return

The calculations of volumes and densities of the spoil return could be used for estimating the diameter of a column. This indirect method was applied for a tunnel project in Taiwan by Ni & Cheng (2014). According to the theory of mass balance, the jet grouting volume should be equal to the volume of spoil return. But the volume of spoil return is larger than the jet grout volume in reality, and the ratio between these volumes are largely depended on the soil type of the site. To perform these measurements, the spoil return was used from a pit with a fixed volume where the spoil volume, flow rate and density were measured for each column before it was pumped to the ground surface to be shipped away. The ratios of volume of spoil returns to grout volumes were then measured for a unit length of the columns. Density measurements was also compared between the in-situ soil and grout mixture with the grout inheriting a lower density than the soil because of bleeding effects and consolidation of the soil. Therefore, Ni & Cheng (2014) suggested a desirable diameter of the column would be achieved if the density of spoil return was in between the values of grout and in-situ soil. If more in-situ soil was eroded and mixed with the grout, the spoil return should obtain a higher value of the density spectrum, otherwise the density will be less if the spoil volume is bigger than the jet grouting volume. This method can therefore give an indicator for undesired effects of the jet action if unexpected deviations from the spoil return are obtained.

The results would prove to be overestimates of the spoil density. An adjustable factor is thereby applied based on the ratio between the sum of total column volume and spoil volume over the sum of total column volume and grout volume. A 2,5% smaller diameter of each column was obtained compared to the design diameter for the specific site.

One important consideration of performing spoil return controls is to check if clogging in the borehole annulus can occur (Croce, et al., 2014). If clogging occurs the spoil return can give incorrect values, having the volume of injecting grout less than for normal conditions. The spoil return also needs to have a direct way of transporting to a storage where some losses of the volume will occur during the transportation. For larger jet grouting operations, the losses of spoil return will increase, obtaining more uncertainty for the volume measurement.

3.2.4 Electrical resistivity tomography

Quality control for determining column geometry and homogeneity via electrical resistivity imaging has been investigated by Bearce et al. (2016). Applying direct current (DC) electrical resistivity technique to jet grouting, a resistivity contrast between treated and untreated soil could be extracted. One commercially available resistivity method is the electric cylinder method (ECM) (Frappin & Morey, 2001). The method employed two different types of casings slotted in a borehole. The first casing involved an array casing with copper ring electrodes of equal spacing attached on a PVC pipe in direct contact with the soilcrete (see figure 11a). The second casing comprised of the same array casing but employing an external PVC casing with a larger inner diameter enfolding the array casing (see figure 11b). The gap between the inner and outer casing was filled with water for minimizing the resistance contact for each ring electrode. By measuring with ring electrodes, it enabled the electric field potential to be measured for full space conditions of a cylinder unlike the traditional half space conditions for electrical resistivity imaging.

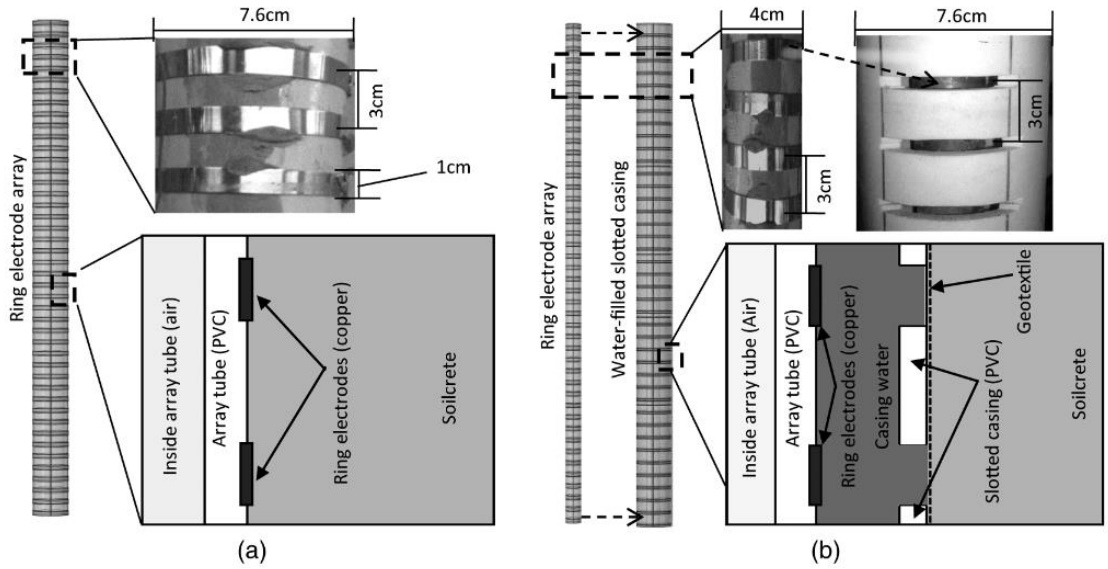

Figure 11 Illustration of the two different casing setups with ring electrode spacings. (a) Array casing in direct contact with the soilcrete. (b) Array casing with water filled slotted casing (Bearce et al., 2016)

The study was tested for electrode spacings of 3, 6, 9, and 12 centimetres in the laboratory, performing several measurements in the spam of 240 hours since column installation. The quality control then comprised of what resistivity contrast could be obtained from the different spacings combined with the different geometries of the jet grout specimen. Bearce et al. (2016) has construct a forward finite element model with similar geometries and resistivity properties of the laboratory measurements to assess a column prediction method (see figure 12).

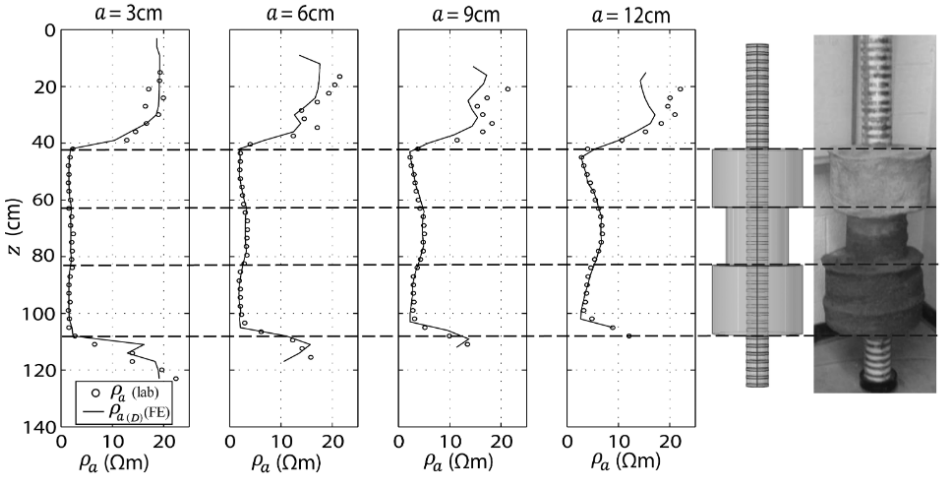

Figure 12 Quality control of electric resistivity imaging. Comparison of apparent resistivity for different spacings of a Wenner electrode configuration for laboratory measurements and estimations from FE-model. The lines represent the FE-model estimation while the dots represent the measured values

This quality control has not yet been established and a problem with this method is that larger error margin could be obtained if the geometry changes due to changing soil conditions. Bearce et al. (2016) refined the results by further finite element calculations to establish a more suitable geometric factor of the electrode configuration. This is because borehole resistivity has a variable geometric factor near surface which transitions from half-space to full-space conditions. Furthermore, the study was only applied for laboratory conditions with one electrode configuration for all measurements. Bearce et al. (2016) concluded that a $\pm 5\%$ difference correlation with the real column geometry could be achieved with the refinement of the geometric factor. The array casing with the electrodes being in direct contact with the soil proved to get the best results. The other setup left 40% of its injecting current to be lost in the casing fluid. To obtain the best resistivity contrast, the ERT-measuring should be conducted as soon as the soilcrete mixture is installed. With longer curing time, the resistivity growth showed a logarithmic behaviour with significant reduction between the resistivity contrast of treated and untreated soil as well as increased data uncertainty. The soilcrete resistivity after 1.5 hours was $\rho = 1.6\ \Omega m$ compared to $\rho = 8.5\ \Omega m$ after 10 days.

4 Electrical resistivity method

4.1 Background

Electrical resistivity methods have been used for geophysical investigations since the early 1900s, but it was not until the 1970s the method became popularised. Computers that could analyse the results from the measurement were the main reason for the increased practitioners during the 1970s (Reynolds, 2011). Currently the electrical resistivity methods are one of the most widely used geophysical techniques for subsurface investigations. By measuring the resistivity in the ground, it is possible to provide valuable information of earth properties (Binley & Slater, 2020).

The electrical resistivity measurements can be made at the surface and between boreholes or between a borehole and the surface. By using special cables, it is also possible to perform the measurements underwater in, for instance, lakes and rivers (Knödel, et al., 2007). Electrical resistivity methods can be used for several investigations. In the hydrological aspects the method can be applied to find groundwater or pollution in groundwater. For civil engineering purposes it is often used to find faults and fissures or for example to locate subsurface cavities (Reynolds, 2011).

4.2 Resistivity

Resistivity is a material property describing how resistant a material is to the flow of electric current. The reciprocal of resistivity is conductivity which describes the transport of electric charges in a medium. To understand resistivity, the resistance must first be understood. The resistance, R, describes an electric potential drop between opposite faces of a resistor and is measured in ohm (Ω). This phenomenon can be formulated using Ohm's law, denoted in equation 1 (Reynolds, 2011; Milsom, 2003):

$$R = \frac{V}{I} \tag{1}$$

where V is the potential drop between two faces of a resistor, I is the current passing through the resistor and R is the resistance. The resistance is also directly proportional to the length, L, and inversely proportional to the cross-sectional area, A, of a resistive media denoted in equation 2:

$$R \propto \frac{L}{A} \tag{2}$$

Combining these expressions, a product of resistance and distance can be formed, defining the resistivity:

$$\rho = \frac{A}{L} * \frac{V}{I} = K * \frac{V}{I} \quad (3)$$

With $K = \frac{A}{L}$ being the geometric factor.

Milsom (2003) defines resistivity as the resistance of a unit cube to current flowing between opposite faces, measured in ohm-metres (Ωm). Different materials inherit different resistivities, but the resistance can obtain the same potential drop between faces with the same material. What distinguishes the resistance to resistivity is the impact of a geometric factor, K. With longer shapes but smaller cross section of a medium, a higher resistance is obtained while lower resistances exhibited for shorter shapes and larger cross sections assuming the same material (Reynolds, 2011). The resistivity also depends on the anisotropy of a medium. Isotropic materials enable the same resistivity in all directions of the medium, while anisotropic materials resist electric charge for different directions.

4.2.1 Resistivity and conduction in soil and rock materials

The resistivity property varies immensely between different geological materials (Binley & Slater, 2020). For example, silver exhibits a resistivity of $1{,}6 * 10^{-8}\Omega$m while pure sulphur inherits $10^{16}\Omega$m (Reynolds, 2011). For different rock types, igneous rocks tend to have the highest resistivities, metamorphic rocks have intermediate, and sedimentary rocks inherits the lowest resistivity mainly due to its high pore fluid content. The age of the rock is also a relevant aspect since older rock have been exposed to mineralisation and compaction for a longer time, decreasing its porosity and permeability and thereby creating a more resistive material. Some resistivities and conductivities properties for common rocks, soils and ores are presented in figure 6 (Lowrie, 2007).

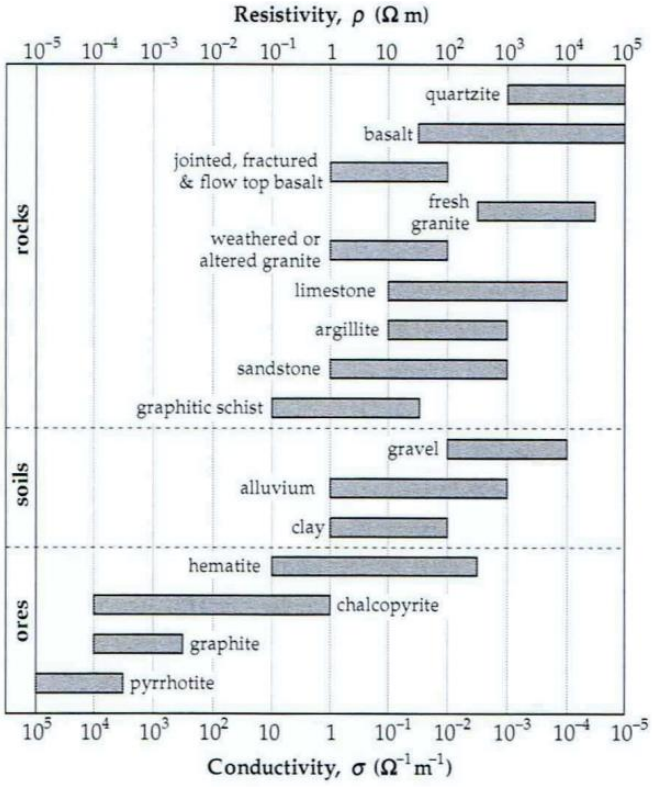

Figure 13 Resistivities and conductivities of common rocks, soils, and ores (Lowrie, 2007)

There are three different ways in which electric current is conducted through a rock: electrolytic, electronic, and dielectric conduction (Reynolds, 2011). The electrolytic conduction is the transport of ions in an electrolyte (a fluid containing ions which electrically conducts by the movement of ions when an electric field is present). Electronic conduction occurs when electrons transport through metals, carrying the charge. The dielectric conduction process occurs when atomic electrons slightly shift with respect to their nuclei in a resistive material if exposed to an external alternating current. The main conduction process through rocks and soils is the electrolytic conduction whilst electronic conduction can become significant for a high concentration of ore minerals. The dielectric conduction is more relevant in induced polarisation measuring which is negligible in this thesis.

Subsurface soil and rocks usually consist of a mix of different minerals of silicates, sulphurs, oxides, and carbonates which are mainly insulators (Binley & Slater, 2020). When pore fluids are present in the subsurface (generally groundwater) most of the conduction will be electrolytic (Knödel, et al., 2007), transporting the ions via interconnected voids between the grains. According to a table adapted by Knödel et al. (2007), dry clay can inherit a large resistivity value but very low when saturated, showing the great impact of the electrolytic conduction.

Table 1 Resistivity in different soil and rock materials (saturated and unsaturated) modified from Knödel et al. (2007)

Geological material	Minimum resisitvity (Ωm)	Maximum resistivity (Ωm)
Gravel	50 (water saturated)	$>10^4$ (dry)
Sand	50 (water saturated)	$>10^4$ (dry)
Silt	20	50
Clay (wet)	5	30
Clay (dry)		>1000
Igneous and metamorphic rock	<100 (weathered, wet)	$>10^6$ (compact)

For instance, saturated soil with highly mineralized water is a case in which the materials' resistivity will decrease (Reynolds, 2011). Binley & Slater (2020) found the electrolytic conduction is strongly linked with the mobility, concentration, and charge level the ions inherit in the electrolyte. As groundwater exhibits a complex ionic composition which can be difficult to measure, empirical formulae are applied depended on two measurable properties: temperature and salinity. The salinity impact can vary substantially for certain electrolyte compositions. Generally, for low salinity solutions (such as in-land groundwater), an increase of salinity decreases the resistivity (Binley & Slater, 2020). The temperature of the electrolyte is determined by the intrinsic electrical properties of the three physical phases (gas, liquid and solid) constructed in the porous medium. As groundwater exhibits liquid properties, the temperature-dependent impact (temperature between 0-100°C) is linked with the viscosity of the liquid. With increased temperature a decrease of viscosity is imminent (Fetter, Jr., 2014), allowing better mobility for ions in the electrolyte (Binley & Slater, 2020) and thereby, increasing the electrolytic conduction.

4.2.1.1 Archie's laws

Archie's laws have proved to be one of the most important petrophysical relationships used for estimating geophysical properties by correlating it with rock properties (Binley & Slater, 2020). The laws apply to rocks that are fully or partially saturated with saline brine. The laws are comprised of two parts where the first law applies to rocks fully saturated with saline brine which describes a relationship between the formation resistivity factor, F, and the porosity, ϕ, to the power of a cementation exponent, m (Archie, 1942). This relationship is denoted in equation 4.

$$F = \phi^{-m} \tag{4}$$

The second law applies to partly saturated rock with saline brine where a resistivity saturation index, I_r, (related to the resistivity of the rock, R, to the resistivity of a fully saturated rock, R_0) is equal to the degree of saturation, S_w, to the power of a saturation exponent, n. This is denoted in equation 5.

$$I_r = \frac{R}{R_0} = S_w^{-n} \tag{5}$$

4.3 Measurement of the electrical resistivity

In most electrical resistivity methods, a current is introduced through hardware into the ground via a four-electrode configuration consisting of two current electrodes (A and B) and two potential electrodes (M and N). The current electrodes apply current intensity into the ground, which can either be low frequency alternating current (AC) or direct current (DC) generating an electrical potential field. The potential electrodes will then measure the potential difference of the electric potential field which is illustrated as equipotential lines (lines of equal potential) intersecting the current lines (lines of equal currents) at perpendicular angels in figure 14. Here, the potential decreases in the direction of current flow assuming a medium has homogenous resistivity properties.

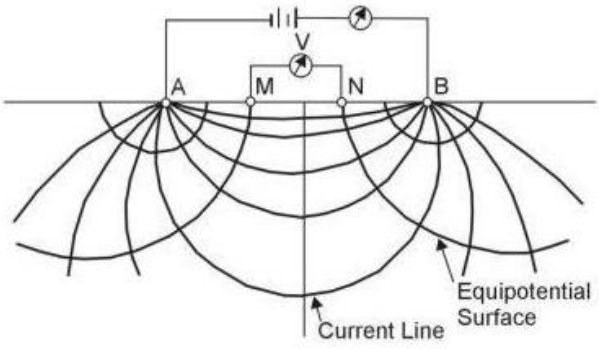

Figure 14 Illustration of equipotential lines and current lines of an electrode configuration in a medium of homogenous resistivity (Reynolds, 2011)

When measuring the electrical resistivity of the subsurface, the hardware measures the subsurface as a conductive environment while the space above the surface is non-conductive. This homogenous ground is referred to as the homogenous half space. Homogenous full space can also be applied. Here, the hardware sets a conductive environment in all surroundings. By measuring the applied current and the potential

difference, the hardware yields a relationship with the specific electrode arrangement to obtain the apparent resistivity for the homogenous half or full space. The difference between half space and full space is that the electrodes inject current and measure potential difference along two directions for half space, while full space inject current and measure potential difference for all directions. Important to note is that the "true" resistivity is not the apparent resistivity since the homogenous space is not a true reflection of the ground, which usually exhibits heterogenic properties (Reynolds, 2011).

4.3.1 Calculation of resistivity

The geometric factor applied for measuring the apparent resistivity relates with the electrode configuration. When determining the resistivity of the ground for a specific electrode configuration, the potential generated from the current electrodes is needed. This potential is denoted as V_P, which is defined at any position in the ground to be equal to the sum of the voltages from the current electrodes: $V_P = V_A + V_B$, where V_A and V_B are the potential contributions from these electrodes (Reynolds, 2011). Determining the potentials at electrodes M and N (see figure 15), the distances from the current and potential electrodes need to be known. The following expression can then be derived.

$$V_M = \frac{\rho I}{2\pi}\left[\frac{1}{AM} - \frac{1}{MB}\right] \quad ; \quad V_N = \frac{\rho I}{2\pi}\left[\frac{1}{AN} - \frac{1}{NB}\right] \tag{6}$$

For a homogenous half-space with resistivity ρ, the potential is given by:

$$\Delta V = \frac{\rho I}{2\pi r} \tag{7}$$

with r, being the distance and I is the current. The potential difference, ΔV, between the electrodes follows then to:

$$\Delta \mathrm{V} = V_M - V_N = \frac{\rho I}{2\pi}\left\{\left[\frac{1}{AM} - \frac{1}{MB}\right] - \left[\frac{1}{AN} - \frac{1}{NB}\right]\right\} \tag{8}$$

Reformulating the equation to denote the resistivity, ρ:

$$\rho = \frac{V_{MN}}{I} * 2\pi\left\{\left[\frac{1}{AM} - \frac{1}{MB}\right] - \left[\frac{1}{AN} - \frac{1}{NB}\right]\right\}^{-1} = K * \frac{\Delta \mathrm{V}}{I} \tag{9}$$

with $K = 2\pi\{\ldots\}^{-1}$ as the geometric factor for a specific array. As the distances between the current electrodes and potential electrodes vary with different arrays, the geometric factor will therefore also vary. Different geometric factors for specific electrode arrays can be found in table 3.

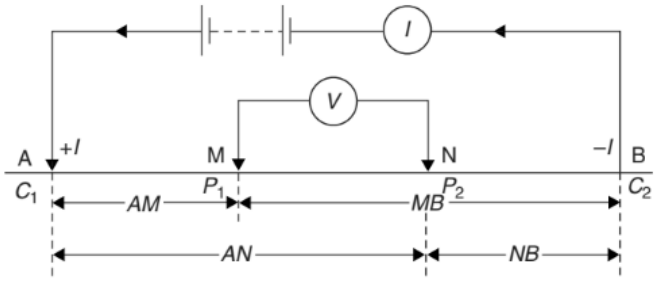

Figure 15 Generalized schematic of an electrode array in electrical resistivity surveying (Reynolds, 2011)

4.3.2 Electrode configurations

There are different types of electrode arrays exhibiting different advantages, disadvantages, and sensitivities. The factors of choosing a suitable electrode array are depended on the desired resolution and depth, the sensitivity and signal-to-noise ratios (Reynolds, 2011).

The sensitivity of the array is used to link the observed electrical resistivity data with the interpreted data during the inversion process, later described in section 3.4.4. It extracts the potential changes in relation to the resistivity changes of a region (Okpoli, 2013). So, the higher the value of the sensitivity, the greater the influence of the region will be on the measured potential difference. Sensitivity-values can vary in positive and negative values, telling also how the measurement will be influenced. With increasing data density relative to the grid size of the electrodes, increased sensitivity is obtained. Thereby, with more lateral data coverage of a configuration, sensitivities will exhibit higher values. The penetration depth is also a relevant aspect of the sensitivity, with larger penetration depth of the measured space obtaining decreased sensitivity. Sensitivities of the most common electrode configurations are presented in figure 18.

The signal-to-noise ratios depends on the placement of current electrodes and potential electrodes, with different ratios if the potential electrodes are placed inside or outside the current electrodes (Okpoli, 2013). For potential electrodes placed inside the current electrodes, a higher signal strength is achieved than for potential electrodes placed outside. Here, the geometric factor is also indirectly linked to the signal strength as it reflects the ranges of the potential difference of a configuration. With low values of geometric factors, a higher potential difference could be observed, thereby achieving higher signal-to-noise ratios. If a configuration exhibits higher values of the geometric factor, applied with low voltage when measuring, the risk of noise affecting the measurements is high.

Depth of investigation is a term defined as: "that depth at which a thin horizontal layer of ground contributes to the maximum amount of the total measured signal at the ground surface" (Roy & Apparao, 1971). The depth of investigation should not be confused with the depth of the total measured signal as contributions to the measured signal come from all depths, but rather at which depth the contribution is the largest. The conventional way of presenting the depth of investigation was to define each measured values' position by intersecting lines of 45-degree angles through the centre of each electrode pair illustrated in figure 8 (Hallof, 1957). The horizontal space between the electrode pairs, na (where n is the number of electrodes apart and a is the electrode spacing) then relates to the depth of investigation. Larger spaces will obtain larger depths of investigation and vice versa for smaller spaces.

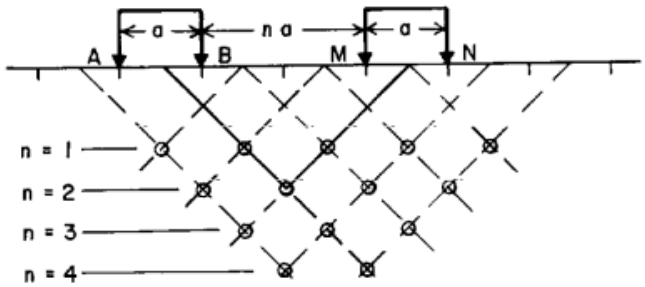

Figure 16 Illustration of the conventional way of presenting the depth of investigation (Edwards, 1977)

The most common four-electrode configurations are: Wenner-, Schlumberger- and dipole-dipole arrays. A less common array is the multi-electrode configuration known as multiple gradient arrays which will also be described (Dahlin & Zhou, 2006). A figure of these arrays can be seen in figure 17.

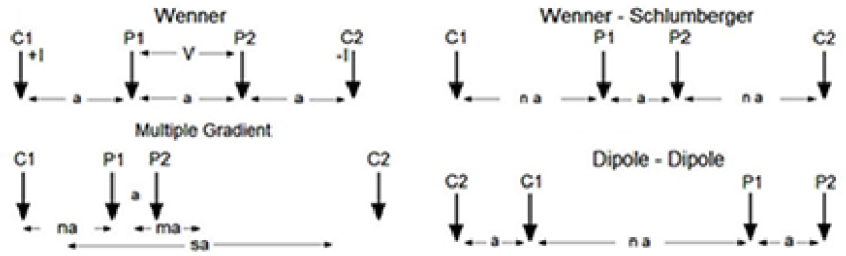

Figure 17 Illustration of different four-electrode configurations for electrical resistivity methods (Okpoli, 2013)

The Wenner array uses electrodes of equal spacing, a, where the current electrodes, $C1$ and $C2$, are placed outside of the potential electrodes, $P1$ and $P2$, enabling good signal strength (Dahlin & Zhou, 2006). It is performed by the current electrodes inducing current into the ground with the potential electrodes measuring the potential field between the current electrodes. To achieve readings of further depth, the spacing between every electrode will increase evenly for each measurement. For detecting horizontal resistivity readings, the electrodes are moved to the adjacent electrode and the process repeats until all combinations of electrodes are obtained. This configuration is most commonly used for profiling or vertical electrical sounding (VES) due to obtaining a high vertical resolution of the investigation area but achieving a lower investigation depth of the ground. It inherits a moderate signal-to noise ratio due to having moderate geometric factors of the arrays according to Dahlin & Zhou (2006). The Wenner array exhibits a moderate sensitivity as the investigation depth of this type of array is generally lower compared to the other configurations seen in figure 18a.

The Schlumberger array is similar to the Wenner where the spacing varies but always centred in the middle of the current dipole. This configuration is also suitable for vertical soundings as it has similar penetration depth and almost the same vertical resolution as the Wenner array. Since only one pair of electrodes is moved separately, it also proves a practical advantage. Sensitivity-values and resolution are also generally the same as Wenner shown in figure 18b.

In the dipole-dipole configuration, the current electrodes pair and the potential dipole electrodes pair are separated from each other. When measuring starts the current electrode pair will induce current and the potential pair will measure the potential difference at the midpoint between the electrode pairs. Once the reading is obtained, the potential pair will be moved further away from the current pair for each measurement enabling further penetration depth for the measurements until the signal-to-noise ratio is too low or you reach the end of the cable. The current pair will then change position to the adjacent electrodes and the process repeats until all positions along the electrode array have obtained a measurement. This will enable a weaker signal strength, but a higher lateral resolution compared to Wenner and Schlumberger. It will obtain a better depth penetration, making it suitable for profiling. The dipole-dipole inherits one of the largest sensitivities near the ends of the layout, but little sensitivity at the centre where the data

is normally plotted for a pseudosection (Dahlin & Zhou, 2006). Signal-to-noise ratio is low due to large values of a, (spacing in electrode pairs).

For the multiple or moving gradient array, the potential electrode pairs are first placed between the current electrode pair closer to one current electrode than the other (Dahlin & Zhou, 2006). When measurements start, the separation (defined as the separation factor, s, multiplied with the potential electrode spacing, a) between the electrode pairs sequentially moves closer from the smallest distance between the potential and the current electrode, na, to the furthest current electrode, ma. During each stage the potential pair acquire electric potential differences along each distance. Here the n-factor is defined as the smallest relative spacing between the current and potential electrode, whilst the m-factor is the midpoint factor of the configuration. For traditional gradient surveying, the measurements are often performed for current electrodes as fixed points, but the multi-electrode gradient survey executes many different combinations of the electrode layout with different spacings and separations obtaining as good or even better resolution than the Wenner array. The sensitivities and signal-to-noise ratios will however vary depending on the combination due to variation in geometric factor.

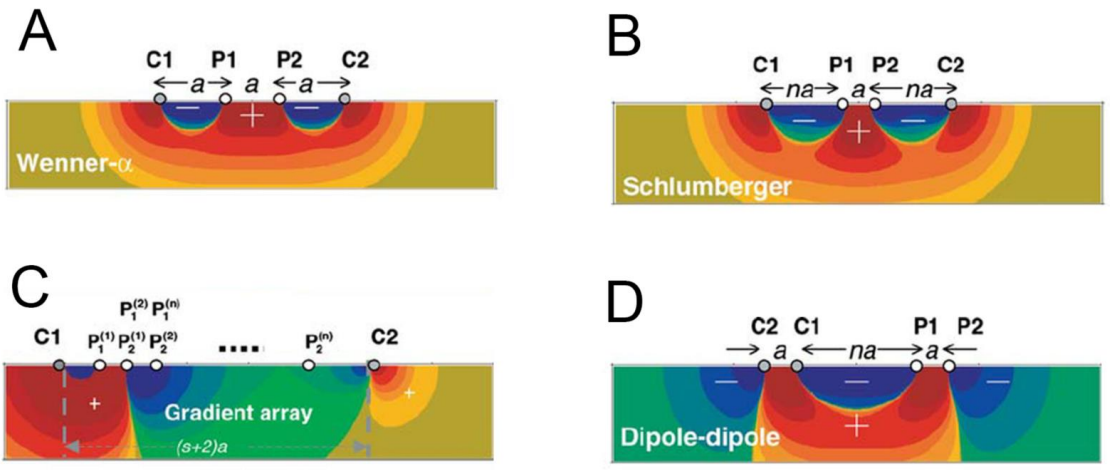

Figure 18 Sensitivity and resolution diagrams of electrode arrays modified from (Dahlin & Zhou, 2004). Regions of (+) are positive sensitivities and regions of (-) are negative sensitivities

The geometric factors of the different electrode configurations are presented in table 2.

Table 2 Geometric factors of different four-electrode arrays (Dahlin & Zhou, 2006)

Electrode array	Geometric factor, K
Wenner	$2\pi a$
Schlumberger	$\frac{\pi a^2}{b}\left(1-\frac{b^2}{4a^2}\right)\ if\ a \geq 5b$
Dipole-dipole	$\pi an(n+1)(n+2)$

4.4 Electrical resistivity tomography (ERT)

Electrical resistivity tomography is a method used to measure and depict the resistivity distribution of the underground in 2D or 3D images (Koh, et al., 1997). It is often the lithological nature of terrains and water content variations that contributes to the contrast in resistivity in the 2D or 3D images (Perrone, et al., 2014).

The ERT-process includes a multi-electrode cable that is laid out on the ground, which is connected to an instrument (Reynolds, 2011). A number of electrodes are connected to the cables at a fixed distance according to a specific electrode configuration. In the ERT-method, current is injected in the subsoil through the electrodes, and via the electrodes it is also possible to measure the voltage (Perrone, et al., 2014). To allow for sufficient injection of the current, a low resistance contact between the electrode surface and the subsurface soil is preferred. With larger resistance contact, the injecting current would be smaller in the soil which can decrease the signal strength to the measuring potential electrodes. To prevent large resistance contact, water can be poured along the electrode surface, enabling better conduction between the electrode and the soil. The ERT-survey is illustrated in figure 19.

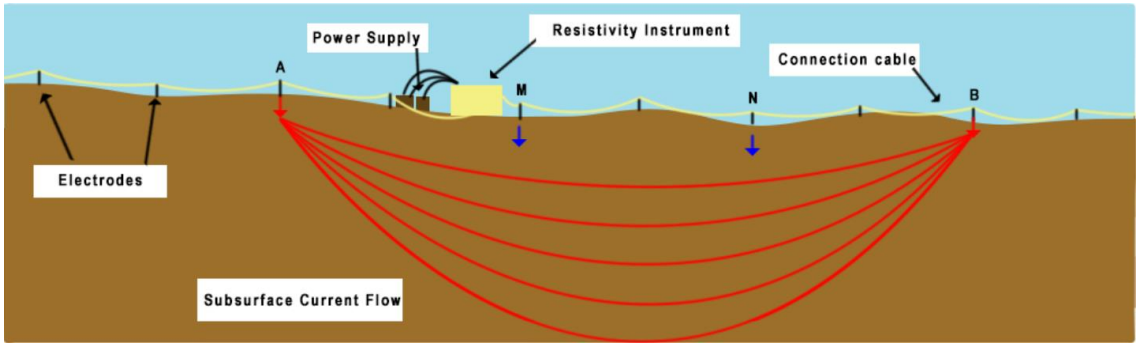

Figure 19 Illustration of an ERT instruments set up (Pierce, et al., 2012)

The vertical and horizontal resolution depends on the electrode spacing as well as the chosen electrode array (Reynolds, 2011). Longer distances between the electrodes increase the depth of investigation but will also result in a lower data resolution. The max length of quadripoles is related to the depth of the investigation (Knödel, et al., 2007) (see chapter 4.3.2).

ERT can also be performed in boreholes, shown in figure 20. The boreholes should have a casing of non-conductive material since conductive material will cause anomalies in the ERT-data (Tsourlos, et al., 2007). ERT-measurement in boreholes can be performed in different ways. The most common way of measuring ERT in boreholes is to place the current injection and the potential electrodes within the same borehole as illustrated in figure 20 (b) (see section 3.2.4) (Bearce, et al., 2016). In the so-called "cross-borehole method" in figure 20 (a) a common way of measuring the electric potential distribution between the underground space of the boreholes is to use the source electrode (current injection point) and the potential electrode (measuring point) to be placed in two separate boreholes (Zhou & Greenhalgh, 2001). Other electrode combinations can also be employed.

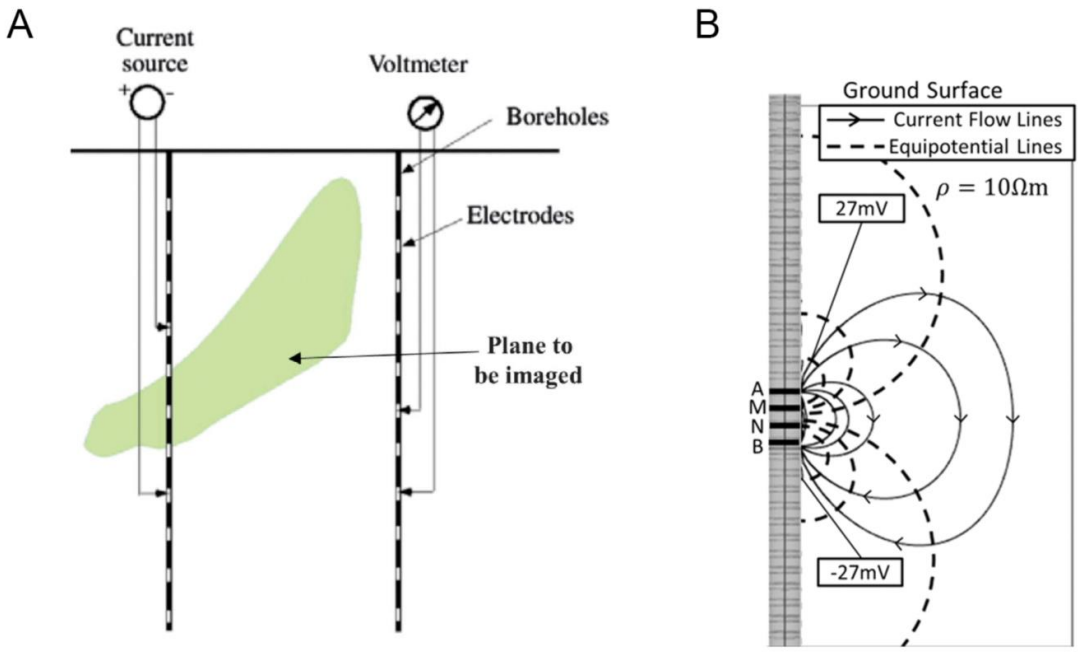

Figure 20 Illustrations of different ERT borehole measurements. A: Schematic of cross-borehole ERT-measuring (Daily, et al., 2000). B: ERT-measuring with a single borehole (Bearce et al., 2016)

4.4.1 Influence of noise

The ERT-signals can be disturbed by various noise sources in the ground. There are two types of noises, coherent noise and incoherent noise. Coherent noise often occurs with a definable frequency and is therefore possible to reduce or remove it with filters (Reynolds, 2011). These type of noise sources can be grounded metal fences, underground metal pipes and cables, power lines, electric corrosion protection for pipelines or leakage currents generated by industrial facilities, streetcars and trains. Especially metal pipes can disturb the resistivity measurements and influence the interpretation (Knödel, et al., 2007). The other type of noise, incoherent noise, comes from natural sources such as wind, rain, waves and electrical or magnetic storms and cannot easily be filtered. Though the influence of incoherent noise is usually negligible (Reynolds, 2011).

When electrical resistivity tomography is performed in boreholes that are deviated from complete verticality, the deviation can provide a source of noise in the data. Nevertheless, this type of noise still allows an accurate and successful experiment and will not affect the subsequent data interpretation severly. However, the errors in position of electrodes can affect the ability to construct a trustworthy resistivity image during inversion development (Myeong-Jong, et al., 2009).

4.4.2 Reciprocal measurements

To estimate the error of the resistivity measurements, a comparison of reciprocal measurements can be performed (Dahlin & Zhou, 2004). The reciprocal measurements compare the differences regarding the directionality of the measurement by swapping functions between the current electrodes and the potential dipole electrodes. According to the reciprocity principle, by swapping the functions of the electrodes the same apparent

resistivity should be obtained if the same geometry-related noise characteristics are applied. If the reciprocal measurements obtain a different result, an error can be estimated for the precision of the resistivity measurement (Parsekian, et al., 2017). The calculation of reciprocal analysis can be presented in a software called Erigraph (ABEM & MALÅ, 2007). A dipole-dipole configuration example of the reciprocal measurement is displayed in figure 21.

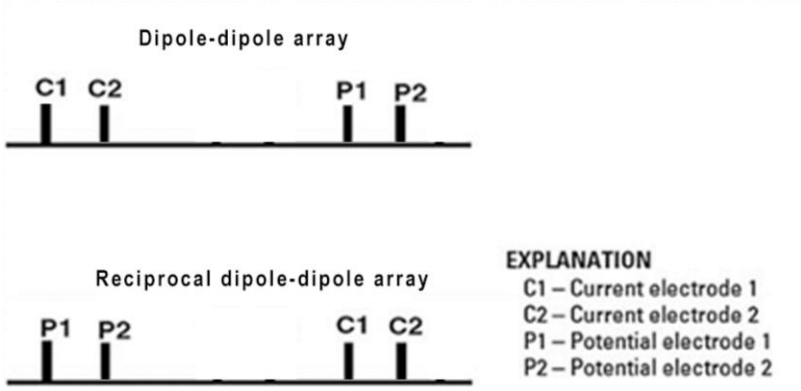

Figure 21 Reciprocal electrode scheme of a dipole-dipole array adapted from (Dahlin & Zhou, 2004)

4.4.3 Pseudosection

A pseudosection is a graphical presentation of the measured apparent resistivity data that provides an initial model of the subsurface geology. The measured apparent resistivity data values presents as a function of location and electrode spacing (Knödel, et al., 2007). A pseudosection shows a rough visual impression of the way in which resistivity varies with depth (Milsom, 2003). Anomalies will be displayed if a mass inherits a resistivity contrast in relation to the surrounding soil. Pseudosections should not be used for interpretations of the resistivity of the subsurface as different electrode configurations will display different anomalies of the apparent resistivity when measuring the same area (see figure 22). This is due to varying depths of investigation, sensitivities and signal-to-noise ratios of the arrays, described in section 4.3.2. To get the true resistivity distribution of the underground, an inversion process needs to be performed.

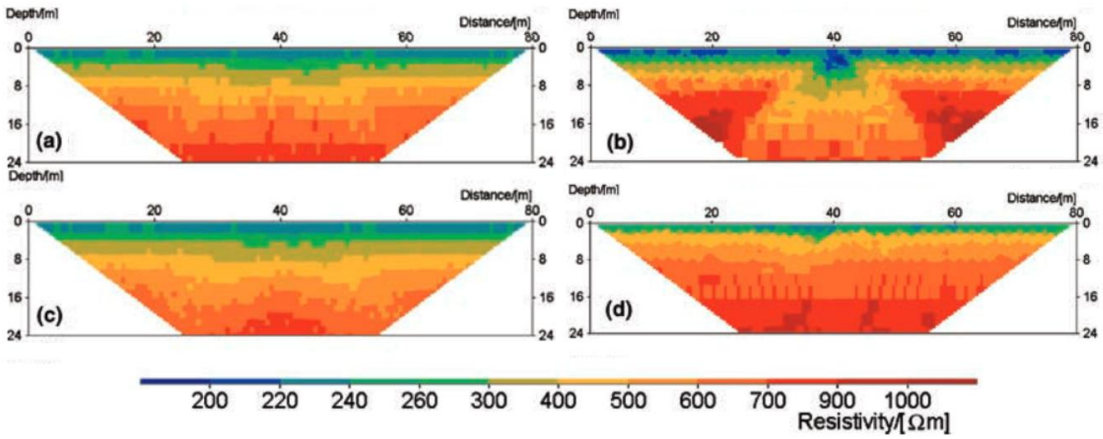

Figure 22 Pseudosections of apparent resistivity generated from the same synthetic model for different electrode arrays modified from (Dahlin & Zhou, 2004): (a) Wenner-alpha, (b) Dipole-dipole, (c) Schlumberger, (d) Multi-gradient

4.4.4 Inversion

To get the resistivity distribution of the underground, the apparent resistivity values must be inverted (Dahlin & Zhou, 2004). An inversion gives an estimate of the true resistivity properties of the subsurface due to consideration of the heterogenous underground and the different electrode arrays. The inversion process can be performed using different software, but the general steps of the inversions are the same.

In the first step a starting model needs to be chosen. Either the start model is determined by the program or defined by the user. Consequently, the program will calculate the values of the model and compare them to the measured data i.e., the model response. The software will then change the model to better adapt to the measured apparent resistivity values, called the optimization method (iteration). This iterative process will continue either until the values calculated from the model are sufficiently similar to the measured values i.e., until the selected deviations are reached, or until the maximum number of iterations have been reached. The software defines the difference between measured and calculated apparent resistivity with the root-mean-squared-error (RMS-error). Important to note, is that sometimes a very low RMS-error does not mean it is the "best" model from a geological perspective as it can give unrealistic values. The RMS-error should instead be very similar to each respective iteration after a few iterations have been performed. (Knödel, et al., 2007). Figure 23 displays a generalized inversion scheme. The result is a model that provides a better estimation of the resistivities from the measured data (Scales, 1988).

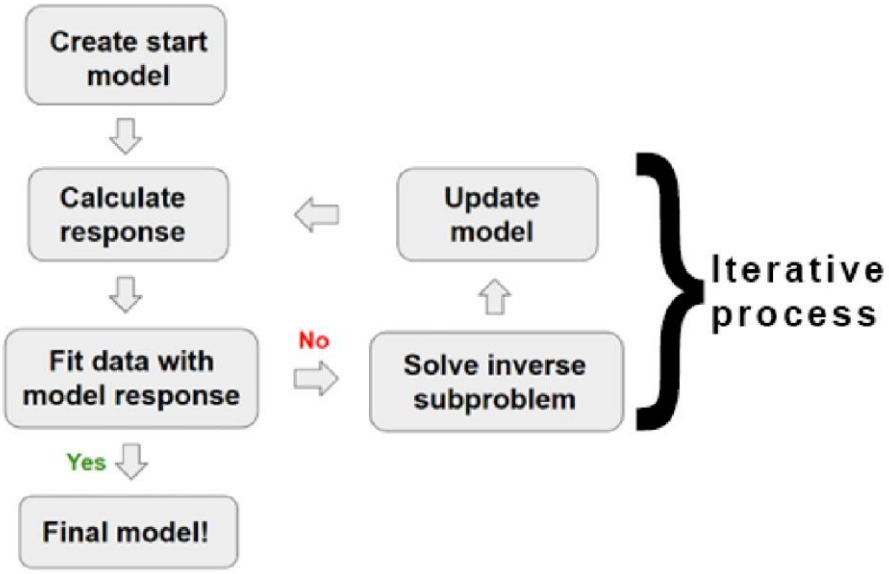

Figure 23 Generalized inversion scheme, modified from Scales (1988)

4.4.4.1 Res2DInv

One often commercially used software for inversion is Res2Dinv (Geotomo Software, 2010). The measured data of the apparent resistivity is inverted in the program and transforms into a 2-D model. The inversion model consists of rectangular cells, which size is determined either automatically as a function of the electrode spacing or manually. In general, the size increases with depth since the spatial sensitivities decreases with depth (Knödel, et al., 2007). The theory used by this software is based on Ohm's law with calculations of the Gauss-Newton algorithm applied on a smoothness-constrained least-

squares inversion denoted in equation 10 (Loke, et al., 2003). This produces two-dimensional sections through finite differences or finite elements computations by minimizing the difference between the modelled and the measured data (Perrone, et al., 2014). This function is called the objective function and an estimation of the true resistivities are calculated based on apparent resistivity data.

$$(J^T J + uF)d = J^T g \qquad (10)$$

Here, the Jacobian matrix, J, is employed, containing the sensitivities of the measurements with consideration of the model parameters. u, is the damping factor weighting the damping between the disturbance of the data and the inverse model through each iteration. d, is the model perturbation vector modifying the previous model, g, is the data misfit vector comparing and relating each iteration, T, is the transpose and, F, is the flatness filter considering topography effects between the electrode spacings in both horizontal and vertical directions (Lekmine, et al., 2012).

Within Res2DInv, most of the inversion is performed automatically with the "Ridge regularization", $L2$ norm. The regularization is essentially a penalty term which prohibits overfitting of each model iteration. This means that the parameters for each model iteration will decrease and simplify the model, streamlining the iteration procedure. The most common method of regularization is the damping least squares, but this method can sometimes force the solution to be smoother than it is. An alternative inversion method is the robust inversion which is based on the least-absolute deviation of each model iteration and can give more representative inversions.

Some settings can be adjusted depending on the suitability from the data, such as the damping factor and the flatness filter (Geotomo Software, 2010). For an acceptable inverse model, the number of iterations should not exceed 5-7 times with an RMS-error below 5% as it can otherwise obtain unrealistic results. An example of an inverse model based on measured apparent resistivity is presented in figure 24 below.

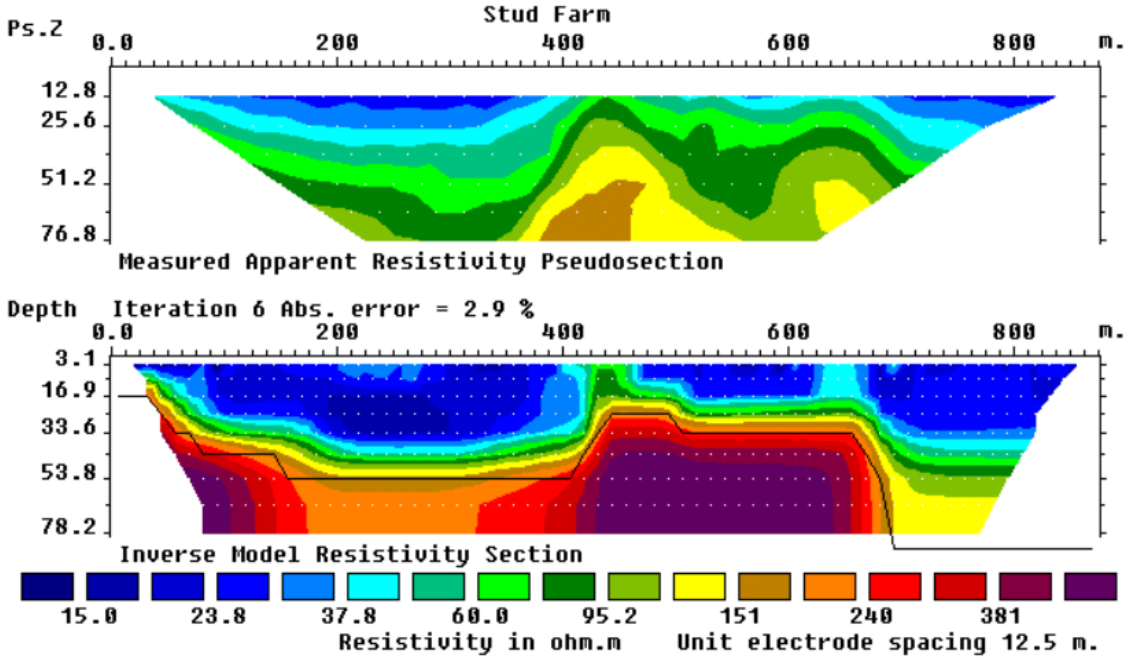

Figure 24 Inverse model based on apparent resistivity measurements modified from Geotomo Software (2010)

4.4.4.2 pyGIMLi

Another recently developed inversion software is “pyGIMLi”. This software is an open-source library used for modelling and inverting in geophysics based on the general-purpose programming language “Python” (Rücker, et al., 2017). The inversion procedure is comprised of finite element toolboxes and method managers extended within the “Python” programming language with common cell shape functions for up to three dimensions. The method managers represent a full set of actions to run all tasks within a certain geophysical discipline which are preconfigured for generalized inversion procedure. Thereby, the method managers combine subsequent levels to solve geophysical problems with a specific dataset.

The default inversion is a modified version of the Gauss-Newton algorithm with flexible regularization. The algorithm represents the inversion problem to minimize the objective function (similar function to Res2DInv) between the data misfit and model constraints.

The objective function compares with a misfit criterion denoted “χ^2”, which is another way of quantifying the distance between vectors. The misfit criterion is the mean value of the squared error-weighted misfit compared between the inversion model and the original data. The smaller misfit, the better chance of the data not containing any systematic errors and thereby giving better inversions. A good inversion model should inherit a χ^2- value around 1. A scheme of the pyGIMLi inversion process is illustrated in figure 25. With a desired inversion model obtained, the software can export the inversion results to different data-files and toolkits for detailed interpretations.

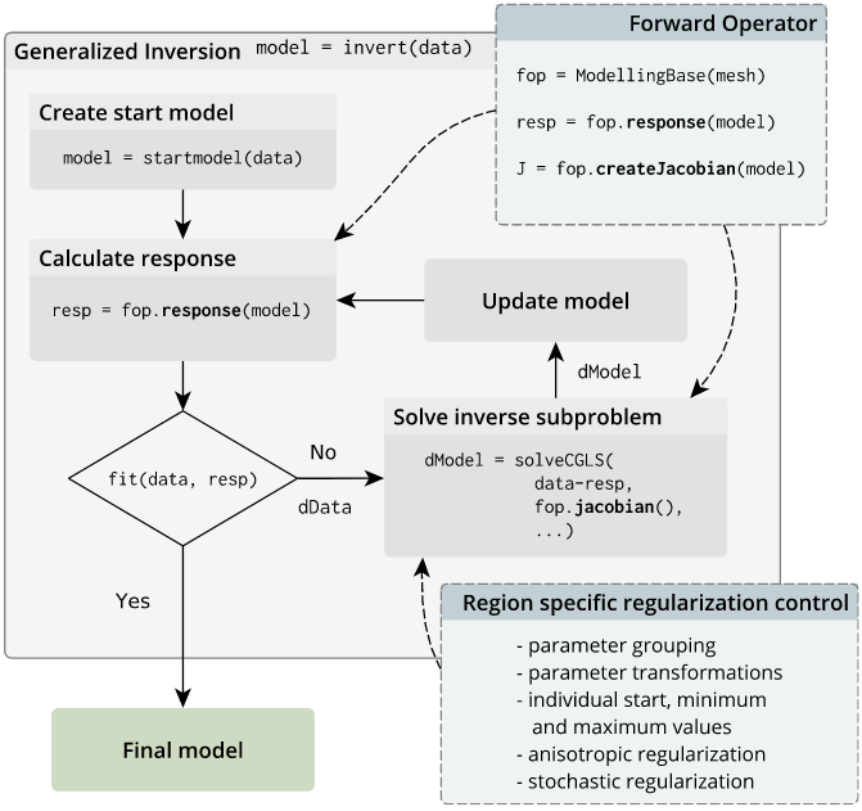

Figure 25 pyGIMLi inversion scheme (Rücker, et al. 2017)

5 Site: Moss

5.1 Construction site

The construction site is located in Moss in the south of Norway presented in figure 26. Here is build a new double track railway, a tunnel and a new station. The construction started in 2019 and planned to be complete in 2022. The work involves deep dry soil mixing, jet grouting and rock grouting (Keller, 2019).

To improve the ground stabilization in the area jet grouting ribs are planned to be established. The jet grouting ribs will be installed in the slopes or at the end of the slopes that currently have low geotechnical stability, to increased safety on the slopes. The jet grouting ribs will be installed to stabilize the ground in a few places along the construction area (Safetec Nordic, 2022).

Figure 26 Map showing the location of the construction site (Google, 2022)

5.1.1 Location

The area where the project will be established starts in north of Moss close to Sandbukta, where the existing double tracks end. The new tracks will be laid above the ground for approximately 800 meters until it reaches the North entrance to the Moss tunnel. The tunnel will go through Moss to the station area where the south entrance is located. From the south entrance a 400-meter-long loose material culvert up to the station will be established. The loose material culvert is established in a sheet pile construction pit and is founded partly directly on blasted rock and partly on piles to rock. The station area, including the platforms, technical culvert, station building, and bridges will remain in the port area. South of the station, the railway continues into the Carlberg tunnel and comes out again northeast of Carlberg farm. The railway will then go in a loose mass culvert and environmental culvert with a total length of approximately 500 meters. The loose mass culvert is partly founded directly on rock, piled to rock and partly directly on lime cement stabilized loose materials (Jernbaneverket, 2016). Figure 27 shows the location of the existing railway and the new railway.

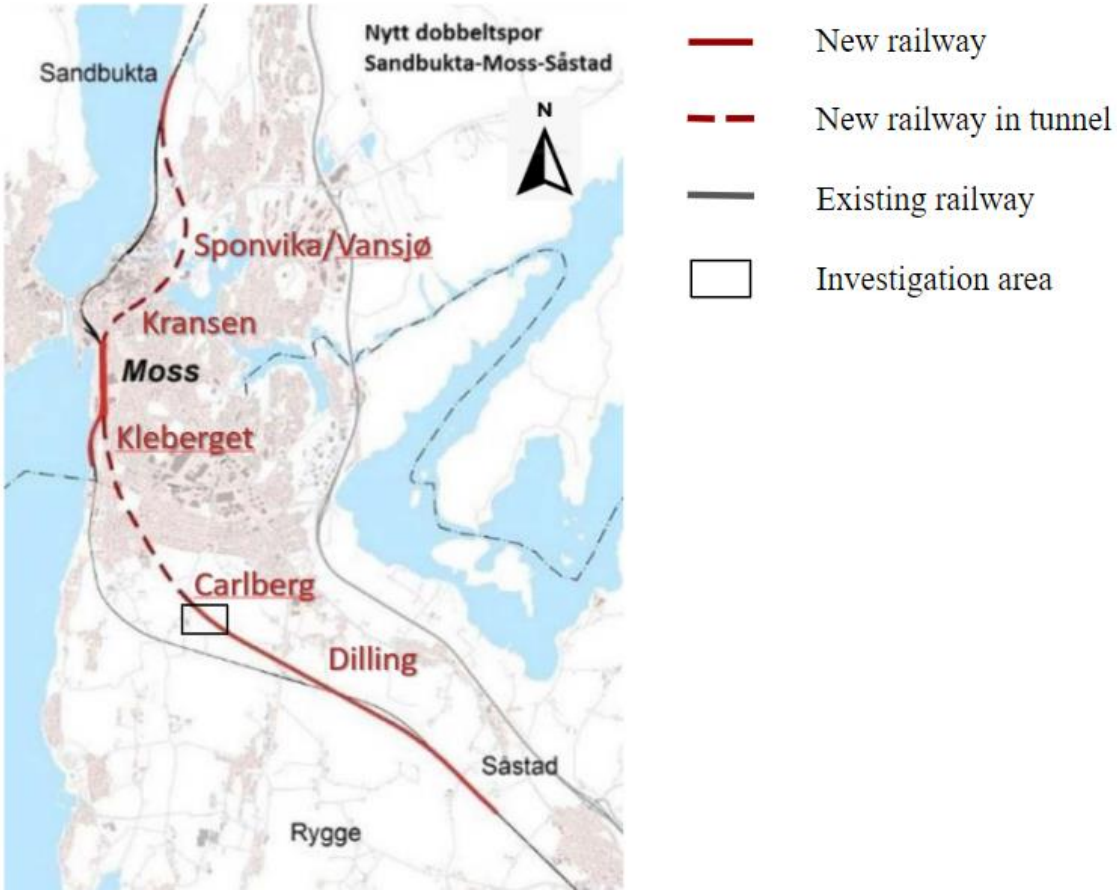

Figure 27 Map of the location of the existing railway and the new railway (Jernbaneverket, 2016)

5.1.2 Geotechnics

The terrain along the route varies from approximately +2 m above sea level by the current station area at Moss harbour to approximately +50 m at "Verket" in the north and "Carlbergåsen" in the south. To the west of the station area is "Verlebukta" with a seabed depth of approximately 5-10 m just outside the quays. From the harbour in Moss the terrain is rising in all directions. In some places the terrain is sloping 1:3 and in other

areas the sloping is 1:15 which is enough to start a landslide. In general, there is great variation in depths to bedrock along the route. The largest depths to bedrock (up to 50 m) is registered down by the harbour area, as well as between Carlbergåsen and Larkollveien. North of Sponvika / Vansjø, near Kleberget and near Carlbergåsen the rocks are close to the surface. In Dilling the depths to rocks is about 45 m and in Kransen the depths to rocks are deeper than 50 m (NGI, 2021).

The soil along the route mainly remains of fill masses, as well as marine beach and sea deposit. North of "Sponvika / Vansjø", "Kleberget" and "Carlbergåsen", a number of soil types are also found. Down by Moss harbour, the loose masses mainly consist of fill masses and sandy, gravelly masses over clay. In the south the soil is characterized by a high clay content, while in the north the soil has a significantly higher content of silt and sand. South of Carlbergåsen, the loose materials consist of an upper layer of 1-3 m with sandy clay and dry crust clay with underlying layers of slightly over consolidated clay that have locally high content of silt, sand and gravel (NGI, 2021). Figure 28 shows the soil in the area around Moss.

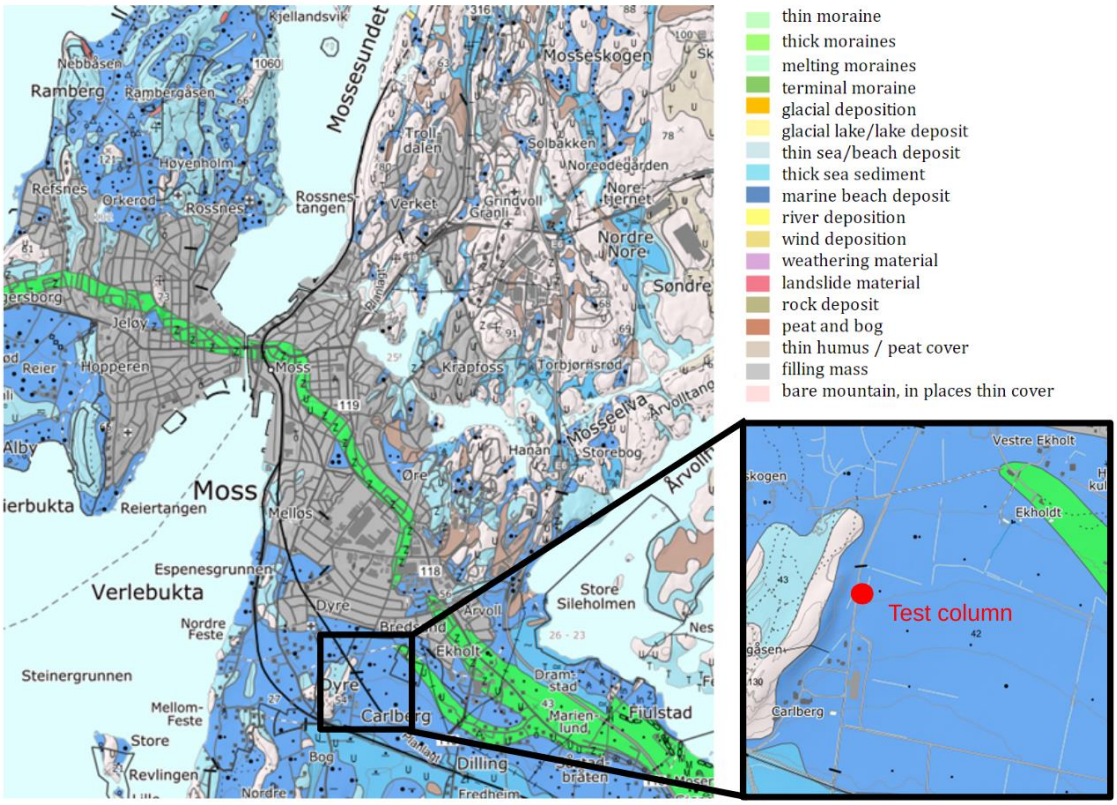

Figure 28 The soil in Moss presented in a map with color coordination. (NGI, 2021)

5.1.3 Jet grouting in investigated area

The jet column where the resistivity measurements was performed is located nearby the south entrance of the Carlberg tunnel, next to Carlberg farm (se figure 29). According to Keller the purpose of the jet columns in this project is stabilization, internal bracing and water cut-off. The jet grouting system used was double fluid system with water and cement slurry. The average diameter of the jet column was set to 1.2 meters. The cement used for the jet grouting is a type of CEM II compound. The grout mixture inherited 12% cement content with a water to cement ratio (W/C) of 1.2.

According to NGU (2022) the bedrock in the area where the measurements were performed consists of granitic gneiss. The soil in the area is shown in figure 29. Most of the area consists of marine beach deposit, but there is also sea/beach deposit and sea sediments. Northeast of the location of the measurements consists of thick moraines. The jet grout columns are established in the marine beach deposit (NGU, 2022). The groundwater level in the area is between 0.5 to 1.5 meters below the surface (Keller, 2022).

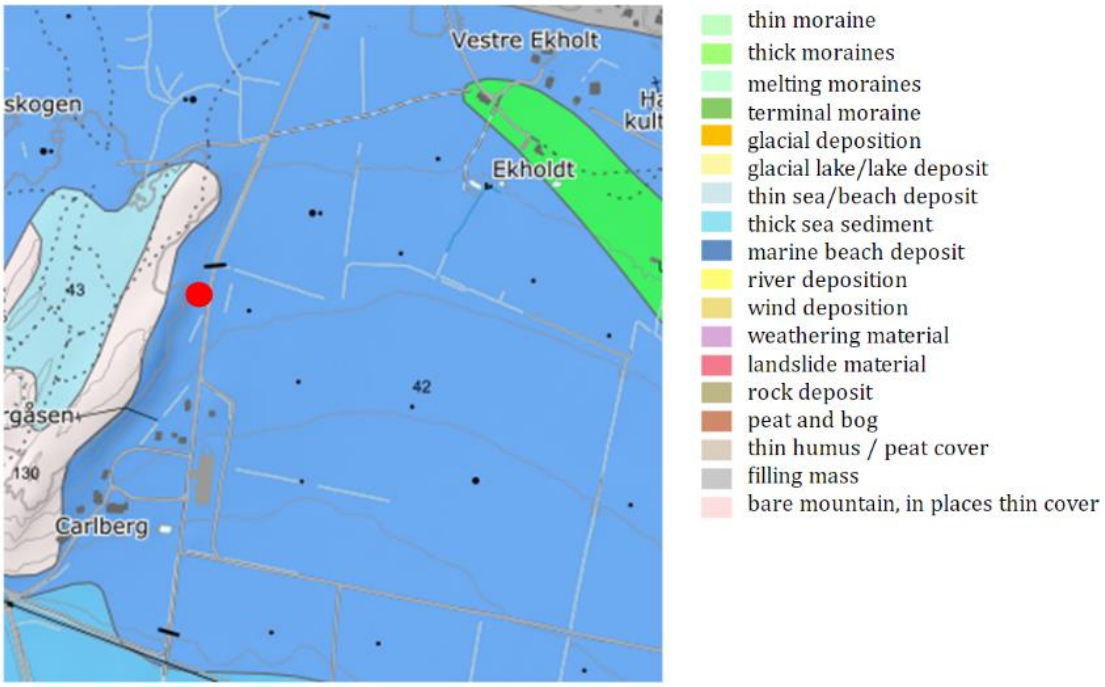

Figure 29 The soil in the site where the measurements were performed presented in a map with color coordination. Location of studied column is illustrated with a red dot (NGI, 2021)

The soil in the area where the measurements are performed mostly consists of clay and quick clay. Closes to the surface is a layer of topsoil and in some places, there is a thin layer of sand, gravel or stone above the bedrock. The depth to rock is between 3 to 27 meters (see figure 30). The location of the boreholes is shown in figure 31. The jet column in which the ERT measurements is performed in is placed a few meters north of the borehole 11-015C-T. The depth to rock in the place where the jet column is established is approximately 15 meters.

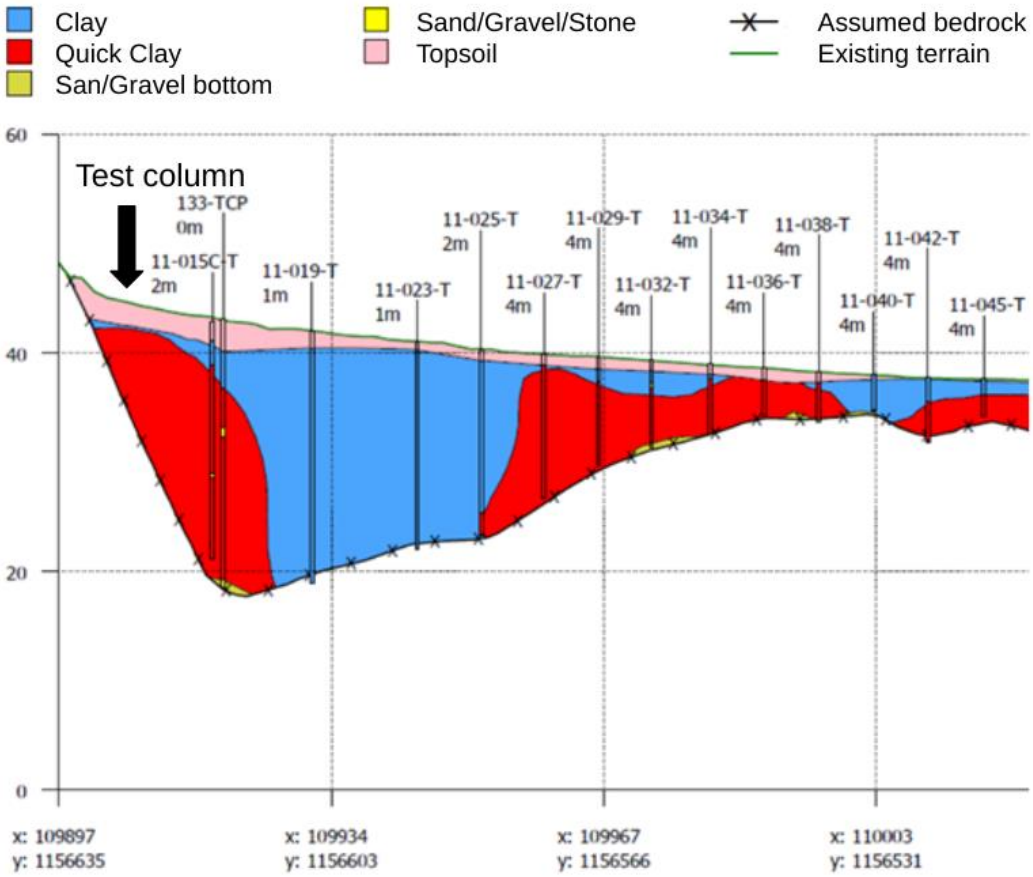

Figure 30 Diagram showing the soil in the site where the measurement was performed (Keller, 2022)

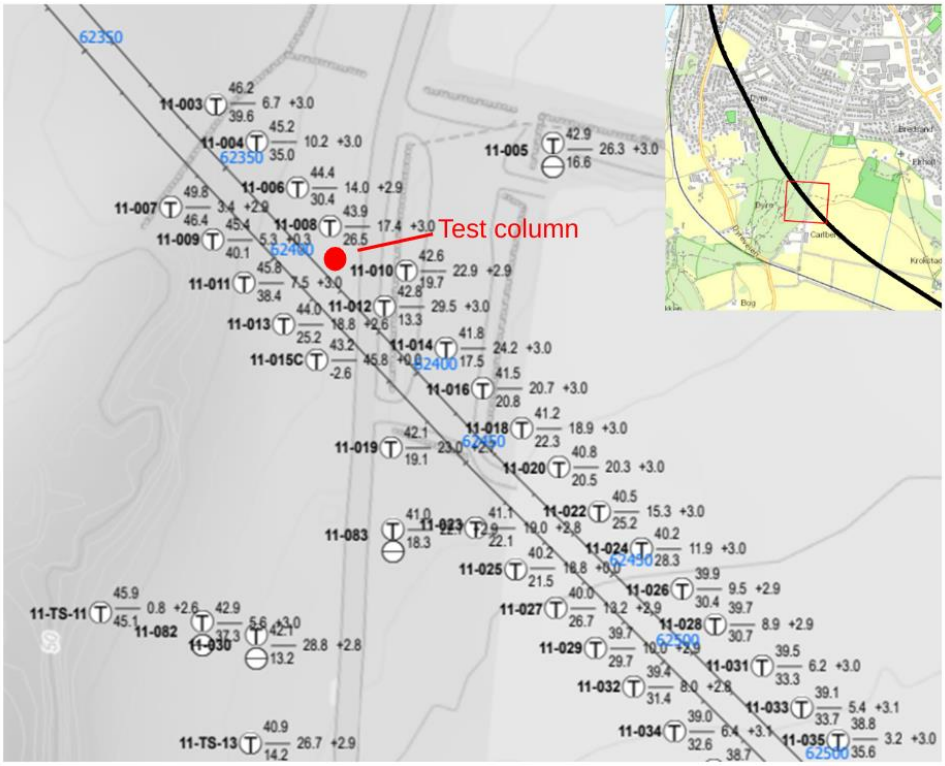

Figure 31 Map of the locations of the boreholes and the placement of the measured test column (Keller, 2022)

Figure 32 shows a soil profile from the position of the jet column based on the information given on site and the information given in figure 30. Closes to the surface is a layer of topsoil which is approximately 2.5 meters deep. Under the topsoil is a thin, about 0.5 meters, layer of clay. Most of the soil in the area where the jet column is placed consists of quick clay. This layer is below the clay layer down to bedrock and is approximately 12 meters thick.

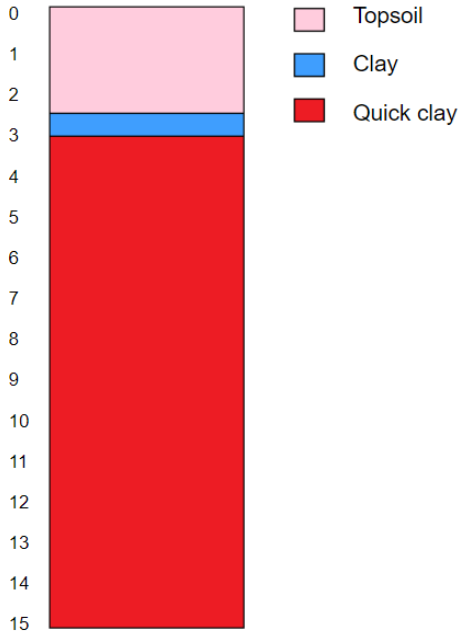

Figure 32 *Soil profile from the location of the measurements interpret by the soil profile in figure 30*

6 ERT measurement and inversion setup

6.1 ERT-measurements

To perform the ERT-measurements, preparation for establishing the necessary components was done at LTH, Lund. The equipment was tested, and the installation process simulated. The equipment used for the ERT-measurements are listed below.

6.1.1 Equipment

The equipment used for the survey is listed for a composed cable and the measuring devices.

Composed cable

- Four electrode cables of stainless steel with total measuring lengths of 3,5 meters (0,5 meter spacing)
- Four temperature sensors (one wire of 5 meters, two wires of 10 meters and one wire of 15 meters)
- Steel wire covered with polyurethane (20 meters length)
- Fibre glass rod (20 meters in length)
- Anchorage (Steel pipe of 1 meter in length and 4 steel nails)
- Duct tape

Measuring devices

- ABEM Terrameter LS 2
- GSM-logger with 4 channels
- 12-volt, 75-ampere hour battery

6.1.1.1 Composed cable

To perform resistivity measurements, electrode cables were used with a spacing of 0.5 meters apart. Previous information regarding the depth of the jet grouting column was estimated to be around 15 meters. Each electrode cable comprised of 8 electrodes enabling the measuring length for every cable to be 3.5 meters. Thereby, by attaching four electrode cables consecutively a 15,5-meter total measuring length could be achieved. Each cables had an 8-pin connector at the upper end for connecting it to an adapter that mated with the 32-pin connectors of the measuring device, hence an additional length (lead-in) for every cable was needed to line up the end connectors to the Terrameter.

For studying the curing process, the temperature history of the soilcrete curing needed to be measured. Four temperature sensors were mounted on the electrode string with a

spacing of four meters starting from between the first and second electrode of the composed cable. An important consideration for the placement of the sensors was to avoid being too close to an electrode as current is conducting through the metal cap of the temperature sensors, potentially disturbing the measurements of the electrode. By placing the sensors in between the electrode spacing, the disturbance minimizes.

Another component of the composed cable was the attachment of a steel wire to prevent tensile stresses occurring during installation to damage the electrode cables as these cables are sensitive in strength. The wire is covered with polyurethan, functioning as a current isolator to prevent further measurement disturbances of the electrodes. Figure 33a and b presents how the different components are attached. The anchorage is shown in figure 33c.

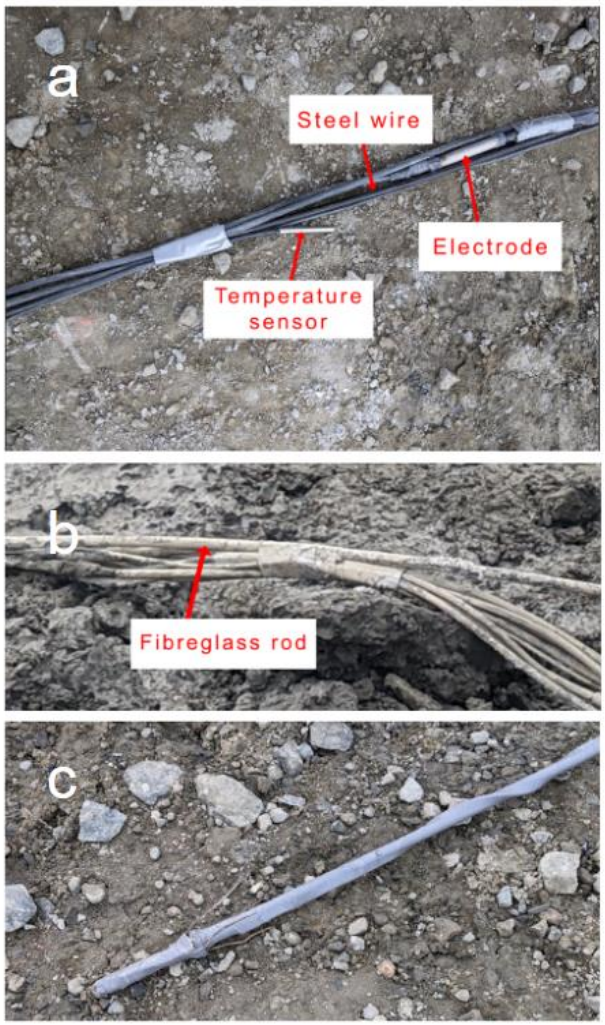

Figure 33 Composed cable comprised of temperature sensors, electrode cables, fiberglass rod, anchorage and a steel wire

A fibreglass rod is also employed to enable sufficiently high stiffness of the composed cable when inserted into the soilcrete seen in figure 33b. This material is also non-conductive for minimizing measuring disturbance. Lastly the anchorage is mounted at the bottom comprised of a steel pipe with nails seen in figure 33c. All components of the composed cable were attached with duct tape.

6.1.1.2 Measuring devices

To measure the apparent resistivity of the soilcrete an ABEM Terrameter LS2 was employed. This device measured and saved the data to later be processed for interpretation. Each input connector from the electrode cables was connected through an adapter to enable the Terrameter of measuring. A 12-volt, 75-ampere hour battery was used as power supply of the device.

The temperature sensors were connected to a Comet U0141M temperature logger with built-in GSM modem. This device measured the temperature with a 10-minute time interval and uploaded data automatically to a web platfrom called “Comet Cloud”. This enabled measurements to be performed without being present at the site.

6.1.2 Methodology

6.1.2.1 Installation

After a freshly produced column is made by the jet grouting machine, the monitor is replaced with a type of nozzle which is hollow. This nozzle attaches the steel casing and the driver then submerges the steel casing into the column seen in figure 34a. The residual casing which is not submerged is separated and lifted upwards to enable insertion of the cables into the column (see figure 34b). The anchorage was inserted first (see figure 34c), followed by the composed cable until the anchorage reached the bottom of the column The cables were then pulled back to ensure that the anchorage was fixed at the bottom (see figure 34d). The residual cable length which is not submerged was inserted onto the residual casing above (see figure 34e). Both casing components were then mounted together to be withdrawn from the jet grout column (see figure 34f). This resulted in the cables installed at the centre of the soilcrete mixture ready for measuring. A plastic bag and duct tape were used to cover the input connectors of the electrodes and temperature-sensors, protecting them from slurry and moisture during the installation. Figure 35 displays a jet grouting machine inserting a steal casing into the soil to install a new jet grout column.

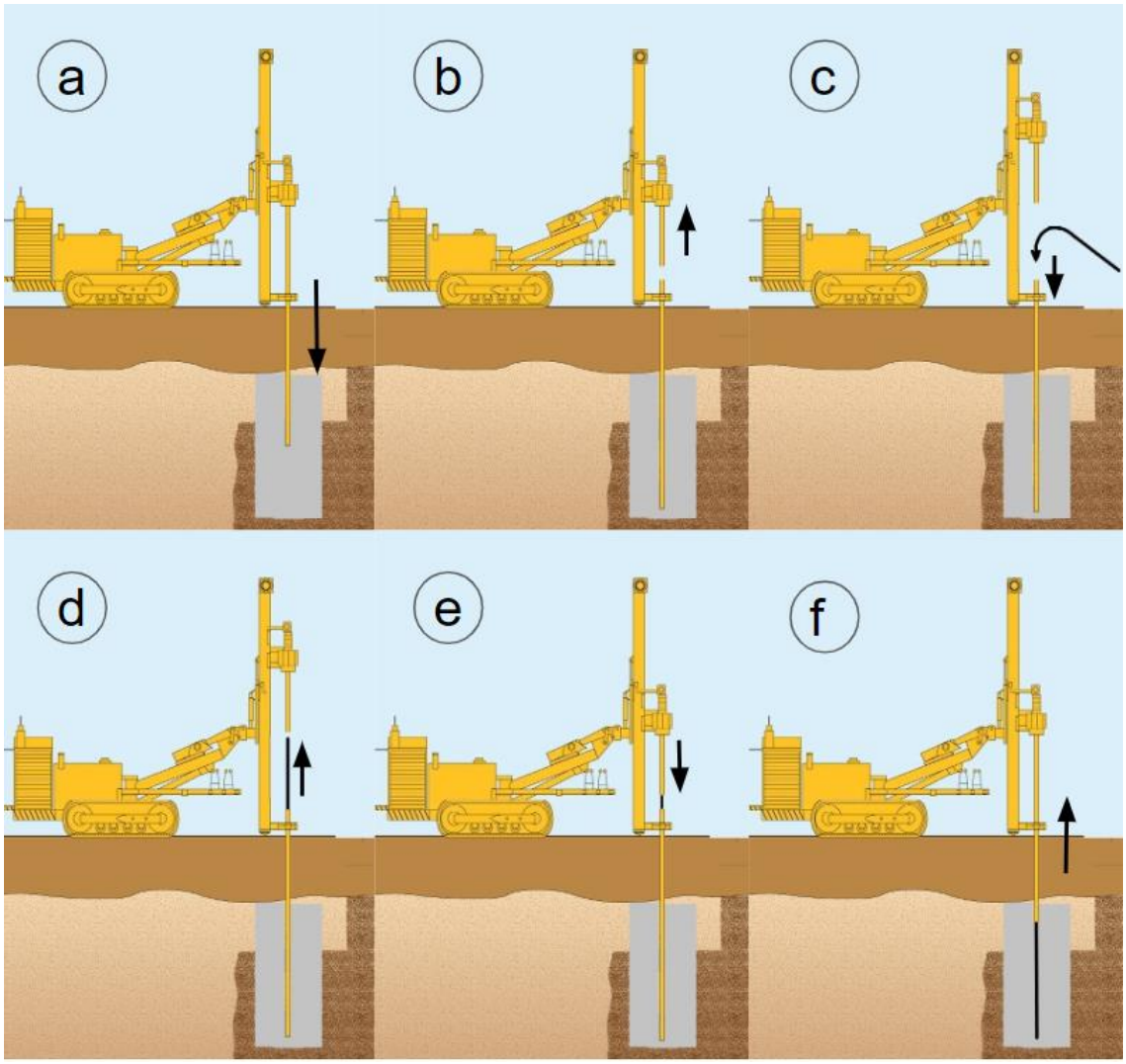

Figure 34 Illustration of the installation procedure of the electrodes in the jet grouting column

Figure 35 Jet grouting machine inserting steel casing

6.1.2.2 Measurements

The input connectors of the electrode cables were uncovered and inserted into an adapter to enable measurements. The measurements were checked for different electrode configurations for comparison with a specific spread file adapted for the specific electrode layout called “1X32”. The specific spread file tells the instrument that the electrodes are placed in a line of 32 electrodes with an input value of 0.5 meters in X-axis. Y-axis and Z-axis are set to 1 meter but can be negligible as electrodes are not present in Y- and Z-axis for this electrode layout.

The used electrode arrays were dipole-dipole (forward and reciprocal) having 248 datapoints respectively, as well as multi-gradient with 430 datapoints. The settings of the instrument are presented in table 3. The acquired data are then transferred from the instrument to a computer for the processing and interpretation.

Table 3 Measuring and transmitter settings for ABEM Terrameter LS2 for all electrode configurations (Measure mode: IP 100%)

Setting	Intensity
Minimum number of stackings	4
Maximum number of stackings	4
Error limit	1,0%
Delay Time	1,4 seconds
Acqusition time	0,6 seconds
Number of IP Windows	10
Record Full Wave Form	Yes
Power Line frequency	50Hz
Sample rate	3750/4500Hz
Minimum Current	1mA
Maximum Current	200mA
Maximum Power	250W
Maximum output voltage	600V
Electrode test	Focus One
Bad electrode	1KΩ
Fail electrode	300KΩ
Electrode test current	20mA
Load variation margin (10%)	20%

6.2 Development of ERT-model

The extracted data from the site measurements are used for the processing and inversion with the aim to establish the boundary between the treated and the untreated soil. This was made possible using the two software “Res2DInv” and “pyGIMLi”. Since the ERT-measurements were performed in a vertical electrode layout with surrounding mass covering the electrodes (instead of the usual measuring of a horizontal electrode layout on top of the ground surface), the data interpreted would be incorrect. To account for the different geometry, a translation of the raw data applied to the correct geometry has been considered in the software.

6.2.1 Res2DInv

To perform inversion in Res2DInv, the correct format for the data needs to be exported from a software called “Terrameter LS Toolbox”. The data which contained outliers and errors were filtered in the Res2DInv software before further processing. The standard format for Res2DInv is “.dat”-files, however when performing an inversion in the software the data will be set to the wrong geometry. Res2DInv will interpret the data as electrodes being placed on the ground surface, as for a traditional ERT-measurement. Thereby, the data were imported into a cross-borehole model where the electrodes’ position coordinates needed to be swapped in direction as well as mirroring the data in opposite direction before inversion. Therefore, a conversion from the exported “.dat”-file to a cross-borehole “.dat”-file had to be performed.

This is first executed by simulating the ground surface by defining fictious surface electrodes, which are placed at positions of 0; 0.5; 1.0; 1.5; 2.0; 2.5; 3.0; 3.5 meters in both positive and negative x-direction since the borehole will be placed at the centre. The positions of the surface electrodes are based on the expected radii which the grout will penetrate through the soil in radial direction (x-direction), with an expected radius of 0,6

meters. Some margin was implemented to detect the resistivity contrast. With the topography defined, two boreholes are created: one fictious and the actual borehole used for the measurements. The fictious borehole is created due to the software interpreting the data as traditional cross-borehole ERT measurements (see section 4.4). The fictious electrode is placed at 3 meters in x-direction while the actual borehole containing the data is placed at the centre (0 meters in x-direction). Consequently, the electrodes' placement in depth (z-direction) for both boreholes are determined, having 28 electrodes with a spacing of 0.5 meters. Since the first electrode closest to the ground surface was not levelled with the ground surface, an estimation of 0.05 meters offset in positive z-direction (downwards) was applied to the electrodes for a more accurate inversion. Since the electrodes' position was offset in z-direction, the same offset was applied to the data to correlate with the previously defined electrode positions.

Before the inversion is performed, some settings are set to establish a better inversion interpretation. The damping factor is set as flexible depending on each iteration with an initial value of 0.15 and minimum value of 0.02. "L1" regularization norm is also applied while the RMS-error criteria is set to less than 2%. The inversion will be executed as robust inversion for minimizing the risk of oversmoothing between each model iteration and to be more robust against noise in the data.

After running the inversion, it is displayed using certain logarithmic contour values. This enables the inversion to be displayed in a higher resolution by having more interpolations between each data cell. It also presents the same spectrum of resistivity values for every inversion for better comparison. The inversion is saved into an "inv"-file which was also used to examine the resistivity change in the column. Here, the resistivity change was calculated by the relative difference between the resistivity obtained in the inversion after one hour of curing to each consecutive inversion model's resistivity values for the time after curing. Thereafter, a new "inv"-file is created containing the relative resistivity change which can be plotted in the Res2DInv software.

6.2.2 pyGIMLi

The pyGIMLi-inversion comprised of first importing the necessary method managers from the pyGIMLi library, as well as the classes from the Python programming language (see appendix 1). Consequently, the data files from the measurements are called separately for the software to process. The data files were extracted from a software used for exporting the rawdata called "Terrameter LS Toolbox" to ".dat" files (same as for Res2DInv), here potential outliers found in the data were also filtered before exporting. This format is the standard format for inversion of Res2DInv, which pyGIMLi can manage as well. For streamlining the data-handling, both software uses the same data format. With the data called for process, an initial pseudosection of the data was created for reference to the inversion later.

The vectors of the ".dat"-files consist of the position of the current and potential electrodes in each axis for the respective apparent resistivity measurement. pyGIMLi uses the resistance values of the data to perform the inversion process, why a geometric factor and a resistance vector was added to the data file. Here, the geometric factor is calculated using a pre-programmed manager imported from the pyGIMLi library based on the electrode positions for each measurement and the electrode configuration. The resistance vector could then be determined by dividing the apparent resistivity vector with the geometric factor vector according to equation 9.

As the electrode cable was submerged in the subsurface soil, four electrodes were on top of the surface since the actual depth of the column turned out to be smaller than expected. These electrodes were thereby excluded in the measurements. However, the first electrode closest to the surface was not levelled at the surface, why an estimation of five centimetres offset in z-axis was defined for the respective electrodes. With the positions redefined, a new geometric factor was calculated multiplied with the previously calculated resistance to obtain a calculated apparent resistivity vector. An error estimation retrieved from reciprocal analysis was implemented in the data matrix consisting of a relative error assumed for a typical value of 3% as well as an absolute voltage error for a typical value of 100µV. This was performed to simulate the errors for the pyGIMLi software to consider before inversion. Plotting the error estimation can identify if any data inherited some sort of errors.

The next step was to create the correct geometry which the data can be employed into. A 3D mesh is thereby created, exhibiting a cylindrical shape expected from the jet grout column. This is first defined by creating a circle area consisting of five different layers with respective radii set to 0.25; 0.5; 0.8 and 2 meters on a total circle area of 4 meters in radius. This was performed to define the expected and relevant boundaries showcasing how the grout material will penetrate radially in the column (see figure 36).

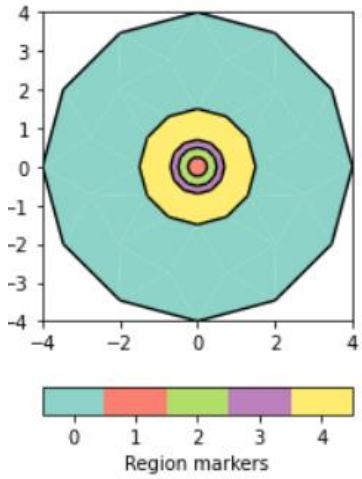

Figure 36 2D circle mesh with boundaries and regions

The depth of the 3D mesh was thereafter defined. Here, the amount of elements is defined in relation to the number of electrodes (sensors), with two elements between adjacent electrodes, to increase the inversion interpolations in depth. Matching of the original position for each electrode is thereafter performed for a more accurate inversion. The first element of the depth vector is redefined to simulate the ground surface while the two last elements of the vector is increased in depth due to having margin, minimizing the risk of losing any inversion from the data. Consequently, the mesh is extruded with inputs from the circle mesh and the depth vector. An illustration of the 3D-mesh is shown in figure 37.

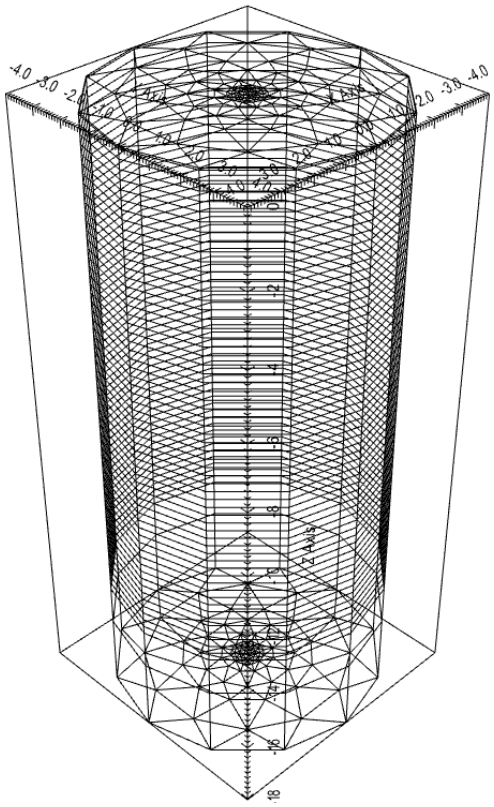

Figure 37 3D mesh of the cylindrical body which the data were imported into

Before exporting the 3D mesh, an easier approach of interpreting in three dimensions is to mark the different regions in depth. Functions comprised of the layers and the different circle areas of the boundaries are called to match the 3D-mesh with the appropriate markers previously performed in the circle mesh.

With the correct geometry applied, the inversion process can be performed. This is done by calling and defining the ERT method manager from the pyGIMLi library with the data as input value. The manager then applies the data to the appropriate geometry (mesh) previously created. The regularization is performed for the standard first order smoothness constraints with "L2 norm". This smoothness constrain is usually performed between individual cells but in this case the smoothness is performed between regions i.e., several cells are defined within the same marker. Therefore, every region is programmed to be treated as a single region, but smoothness occurs between the regions (which are otherwise decoupled) since the inversion in radial direction is of interest.

The inversion is set to a robust inversion with a damping factor of 0.20. Comparing the data to the performed inversion a "showfit" function is performed as well as a "misfit" function. The "showfit" function plots the original data with the inverted one while the misfit can identify if the original data contains systematic errors. With the inversion completed, the results are saved and exported to a "vtk."-file. The results will show a 2D-inversion being translated into 3D by applying the resistivity in radial direction to a cylindrical shape for each layer.

To examine the relative resistivity change in the column the resistivity values from the "vtk"-files were used. Here, the relative resistivity change was calculated by the difference between the resistivity obtained in the inversion after one hour of curing to each consecutive inversion model's resistivity values for the time after curing. The

difference was then divided by the resistivity values from the one hour inversion. Thereafter, a new “vtk”-file is created which can be interpret in the software “Paraview” in three dimensions.

Having the electrodes measuring from the centreline of the column out in radial direction, the actual inversion should also be showcased in the same way. Therefore, a 2D format of the figure is also programmed for presenting the inversion.

6.2.3 Error estimation

For interpreting where and how the electrodes could potentially give uncertainty in its data, an error estimation based on reciprocal analysis (see section 4.4.2) from the dipole-dipole measurements was performed. It was executed by matching the electrode positions of the respective dipole-dipole measurement and comparing the apparent resistivity values to then estimate the error in percentage.

$$error\ estimation = \frac{|\rho_{a,F} - \rho_{a,R}|}{\rho_{a,mean}} * 100\ [\%] \qquad (11)$$

Where $\rho_{a,F}$, is the apparent resistivity value for the forward dipole-dipole measurement and $\rho_{a,R}$, is the apparent resistivity value for the reciprocal measurement. $\rho_{a,mean}$ is the mean apparent resistivity value of both measurements. Multiplying with 100 obtains the error estimation in percentage. After each error estimation value for every electrode position is determined, a pseudosection of the error estimation could be viewed in the software Erigraph for evalution.

7 Results

The results will be arranged for first presenting the temperature history of the column for verifying the curing process, then pseudosections from the first measurements and the last measurements presenting the unfiltered data (the remaining pseudosections for each measurement occasion is attached in appendix 2), thereafter the inverse models based on the Res2DInv and pyGIMLi software are shown followed by the error estimation which is based on reciprocal analysis from the dipole-dipole measurements.

Since the inversion results from the dipole-dipole configurations obtained large errors in Res2DInv, the inversion results of the multigradient configuration are only presented. However, the pyGIMLi inversions are presented with all three configurations. The dipole-dipole Res2DInv inversions can be found in appendix 3.

The ERT-measurements for all electrode configurations were performed on five separate occasions, whilst the temperatures were measured continuously throughout the curing process. A table presenting each ERT-measurement occasion and the time after curing started is shown in table 4 below.

Table 4 Measurement occasions with the respective dates, times after curing and configurations

Occasion	Date	Time after curing (h)	Configuration
1	2022-04-06	1	Multigradient
		2	Dipole-dipole (forward)
		2.5	Dipole-dipole (reciprocal)
2	2022-04-07	15	Dipole-dipole (forward)
		16	Dipole-dipole (reciprocal)
		17	Multigradient
3	2022-04-07	24	Dipole-dipole (forward)
		25	Dipole-dipole (reciprocal)
		26	Multigradient
4	2022-04-08	39	Dipole-dipole (forward)
		40	Dipole-dipole (reciprocal)
		41	Multigradient
5	2022-05-09	789	Multigradient
		790	Dipole-dipole (forward)
		790	Dipole-dipole (reciprocal)

7.1 Temperature history of the column

Figure 38 show graphs of the temperature history for different depths in the centre of the soilcrete column during the curing process. The y-axis displays the temperature values whilst the x-axis displays the time in hours. The measurements started directly after the insertion of the composed cable into the column. An initial temperature from all the sensors varied between 25-29˚C with a steep increase in the first few hours. The highest temperature recorded was for the sensor placed at 9 meters in depth measuring 60.1˚C after 11 hours of curing. The sensors placed at 5 and 13 meters in depth inherit the same maximum temperature of 59.2˚C after 16 hours of curing. The sensor placed at 1 meter below surface recorded a maximum temperature of 52˚C after 19 hours of curing. When the maximum temperature for each recorded depth was reached an exponential decline in temperature occurred until 470 hours. Note here, after 40, 75 and 175 hours the measurements stopped due to a connection failure to the measuring device.

The lowest temperature recorded for the sensors at 5, 9, and 13-meters depth after 456 hours of curing was 19˚C whilst the sensor placed at 1 meter in depth was 15.9˚C. An increase in temperature occurred right after 470 hours for all sensors with varying temperatures between 25-31˚C after 620 hours with a linear decline thereafter. The final temperature recordings just before the last ERT-measurement was 23˚C for T1, 29.2˚C for T2, 28.2˚C for T3 and 24.7˚C for T4 after 789 hours.

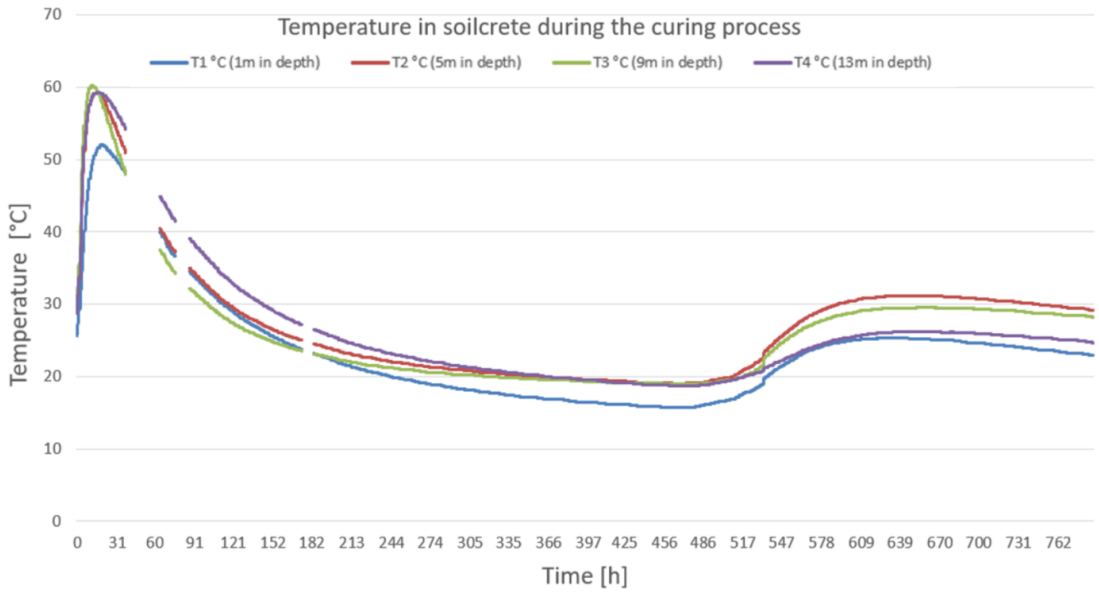

Figure 38 Temperature history at the centre of the soilcrete column for different depths

7.2 Pseudosections

The pseudosections displayed in figure 39 and 40 are acquired from the unfiltered data of the first and last measurement occasion in the software Terrameter LS Toolbox from the multigradient, dipole-dipole forward and reciprocal configurations. These pseudosections are lateral pseudosections, where the depth below the surface is presented in horizontal direction and the radial direction from the centre of the column is presented vertically. This is due to the Terrameter interpreting the measurements to be performed for a traditional ERT surface measuring and thereby interprets the surface to be present along the centreline of the column where the electrodes are placed.

The pseudosection based on measurements performed after one hour of curing of the multigradient configuration in figure 39 (a) show the first electrode to be present at 4 meters in horizontal direction, why this distance should be subtracted when evaluating the pseudosection. The pseudosection depicts an apparent resistivity contrast in the form of a boundary along the surface of the pseudosection. This boundary varies between 0.9 Ωm closest to the surface to 4.2 Ωm in the outer region of the boundary. The transition zone, found at 0.4-0.6 meters, shows an increase of apparent resistivity to 7.8 Ωm which gradually increases with depth to around 27 Ωm. Two anomalies can be identified at 4.5 meters and 12 meters along horizontal direction at the surface, ranging from 0.6-0.9 Ωm with a diagonal anomaly extending in depth from the 4.5-meter anomaly.

The pseudosections from the dipole-dipole measurement in figure 39 (b) and (c) also indicate an apparent resistivity contrast as a boundary on top of the pseudosection in table 9. Note here the electrode closest to the surface is instead found at 3 meters in horizontal direction and should also be subtracted when evaluating the pseudosection. The apparent resistivity varies from approximately 0.3 Ωm on the surface of the pseudosection to 2.2 Ωm in the bottom of the boundary. The transition zone varies between 0.2-0.5 meters in depth. In the dipole-dipole forward pseudosection, three anomalies appear between 12.5-14 meters along horizontal direction at the surface of the section, inheriting very low apparent resistivity values in contrast to the surrounding apparent resistivities. The reciprocal dipole-dipole pseudosection exhibit similar anomalies at the same location as the forward pseudosection.

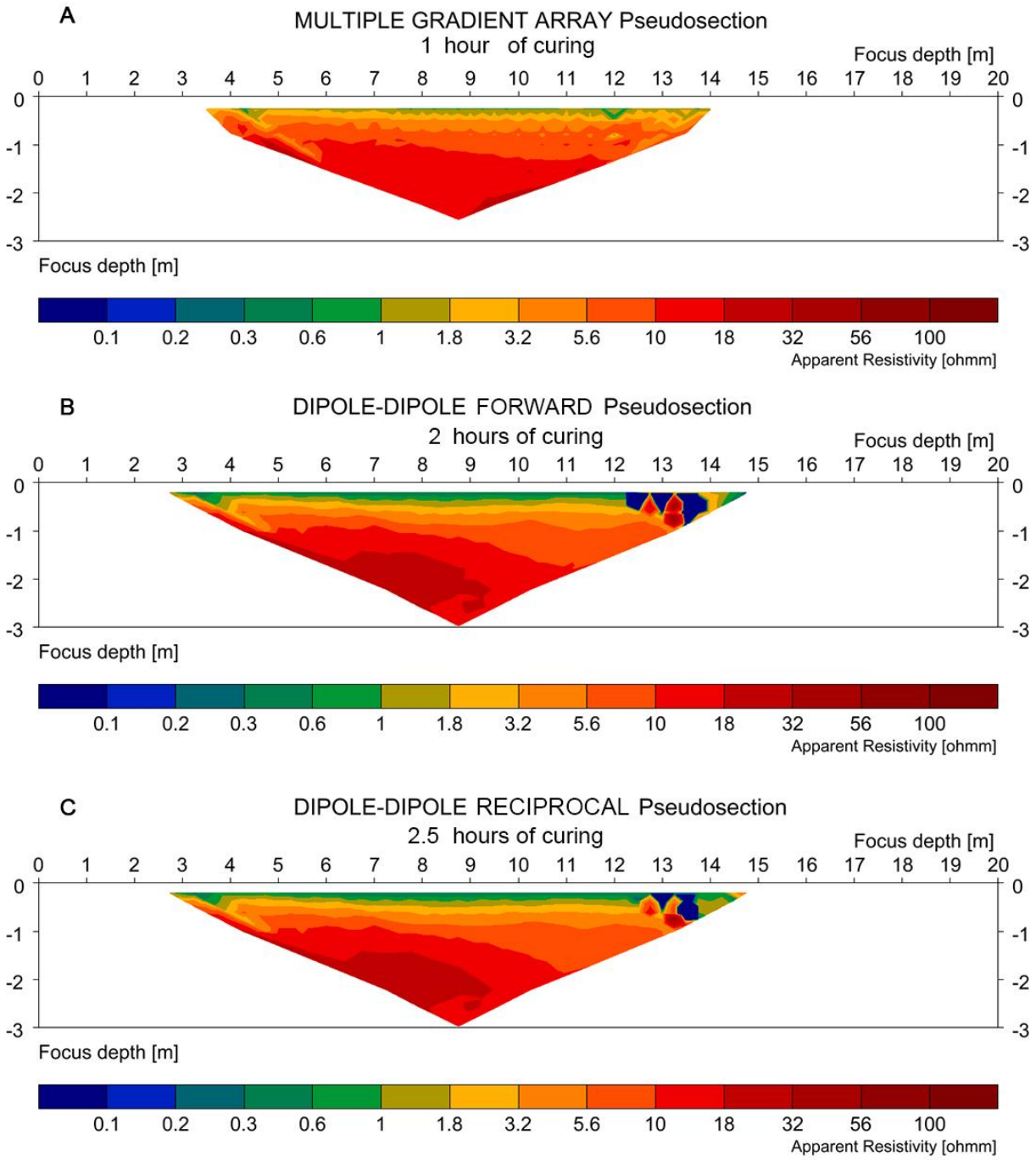

Figure 39 Pseudosections based on the first measurement occasion (1-2.5 hours of curing) with the multigradient (A) and the dipole-dipole configurations (B: Forward, C:Reciprocal)

The pseudosections acquired from the unfiltered data for the last measurement occasion (789-790 hours of curing) in figure 40 show much less continuity of the apparent resistivity boundary along the surface in horizontal direction. The multigradient configuration after 789 hours in figure 40 (a) depicts a smaller variation of apparent resistivity contrast compared to the 1-hour multigradient measurement in figure 39 (a). The apparent resistivity contrast boundary is less distinguished but a region between 8.5-11 meters in horizontal direction is relatively continuous extending to 0.6 meters in vertical direction with apparent resistivities of 3 Ωm. Several anomalies of lower apparent resistivities can be found at 8 meters as well as 11.5-12 meters in horizontal direction. Similar anomalies also appear in some regions at 1 meter in vertical direction. At 4 meters in horizontal direction where the electrode closest to the surface is present, an area of larger resistivity values of 110 Ωm is found at the surface of the pseudosection.

The pseudosections acquired from the dipole-dipole configurations after 790 hours of curing in figure 40 (b) and (c) show a clearer apparent resistivity contrast compared to the multigradient configuration in figure 40 (a). However, the contrast boundary along the horizontal direction varies more in vertical direction compared to the pseudosections from 1-2.5 hours of curing in figure 39. Apparent resistivities between 0.7-2.6 Ωm are found closest to the surface of the pseudosection and increases to 5-11 Ωm further away from the surface. There is however, a region at the surface with larger apparent resistivities between 5-7 meters in horizontal direction for both dipole-dipole configurations. This region also contains large contrasts at around 1 meter in vertical direction. The dipole-dipole configurations have similar appearance, however the reciprocal configuration exhibit more anomalies than the forward at the same areas.

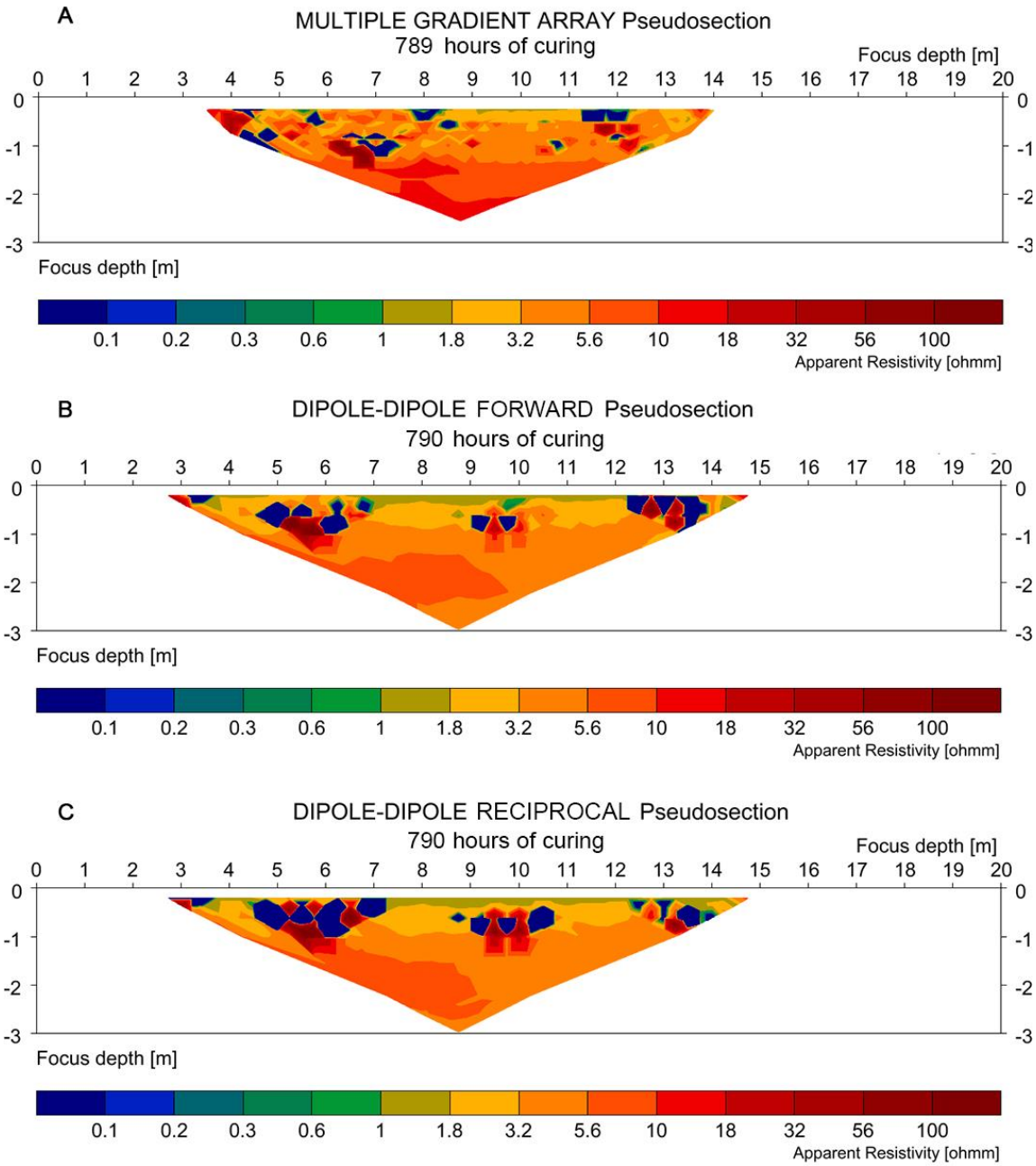

Figure 40 Pseudosections based on the last measurement occasion (789-790 hours of curing) with the multigradient (A) and the dipole-dipole configurations (B: Forward, C: Reciprocal)

7.3 Res2DInv Inversions

The cross-borehole inversions in Res2DInv based on the multigradient measurements for different curing times are presented in figure 41 and 42. Here, the electrodes' placement are represented as black dots that form a vertical line in the centre of the inversion models which is also the centreline of the jet grout column. The vertical axis represent the depth below the surface and the horizontal axis represent the radial distance from the centre of the column. The resistivity scale is logarithmic as can be seen below the models whilst

the number of iterations as well as difference in model response until the RMS-criteria of less than 2% was reached is presented above the models.

Regarding the first multigradient inversion after one hour of curing in figure 41 (a) the inversion resulted in three iterations with a difference in model response of 53.7%. A vertical resistivity contrast boundary can be seen from a radial distance with resistivity values between 1.5 Ωm and 4.4 Ωm in the centre which extends to 8.8 Ωm at 0.4-0.7 meters in radial direction. The transition zone is mainly consistent from 3.8-9.8 meters in depth with slightly larger zones from 10.3-12.8 meters while slightly smaller at 1.3 meters in depth. The resistivity at 3 meters in depth show a value of 15 Ωm in the centre which decouples the transition zone.

The inversion of the multiple gradient measurement after 17 hours of curing is shown in figure 41 (b). Three iterations were made during the inversion which resulted in a difference in model response of 52.3%. The centre of the column exhibit resistivities of 1-4 Ωm. Approximately 0.5-0.7 meters in radial direction from the centre of the electrodes, vertical resistivity boundaries are found. These are relatively homogenous apart from 2.8-4.3 meters in depth where the vertical resistivity boundary extends to 1 meter. The resistivity between the boundaries, close to the electrodes, is between 4.0-17.6 Ωm. The surroundings show a variation of resistivity, between 17.6 Ωm in some parts to more than 80 Ωm at 2.3-5.8 meters in depth. From 8-10.3 meters depths the resistivity value is approximately 35 Ωm.

Inversion model of multigradient measurement after 26 hours of curing is presented in figure 41 (c). Similar to the previous Res2DInv inversion, the vertical resistivity boundaries are found between 0.5-1.0 meters from the electrodes in radial direction. The centreline of the electrodes exhibits low resistivities of 1-5 Ωm. The resistivity in between the vertical resistivity boundaries is about 2.2-17.6 Ωm. The surroundings show a higher resistivity, between 35.2 Ωm at 8.3-10.8 meters below the surface, and up to 15-35 Ωm in most of the top region. The vertical boundary in this inversion is more homogenous than the previous inversions obtained from measurements after 17 hours of curing. Three iterations were performed with a difference in model response of 49.7%.

The Res2DInv inversion for measurements after 41 hours of curing presented in figure 41 (d) shows different results than the other inversions. The centreline of the column has decreased in resistivity with more areas showing 1-2 Ωm than 5 Ωm. The boundary is relatively homogenous of 0.5-0.7 meters in radial direction until a depth 2.3-2.8 meters as well as below 12.3 meters where thicker zones are shown of 1 meters in radial direction. The surroundings show a substantially larger resistivity compared to the centreline of the column with more than 80 Ωm. The inversion was performed for four iterations with a difference in model response of 42.9%.

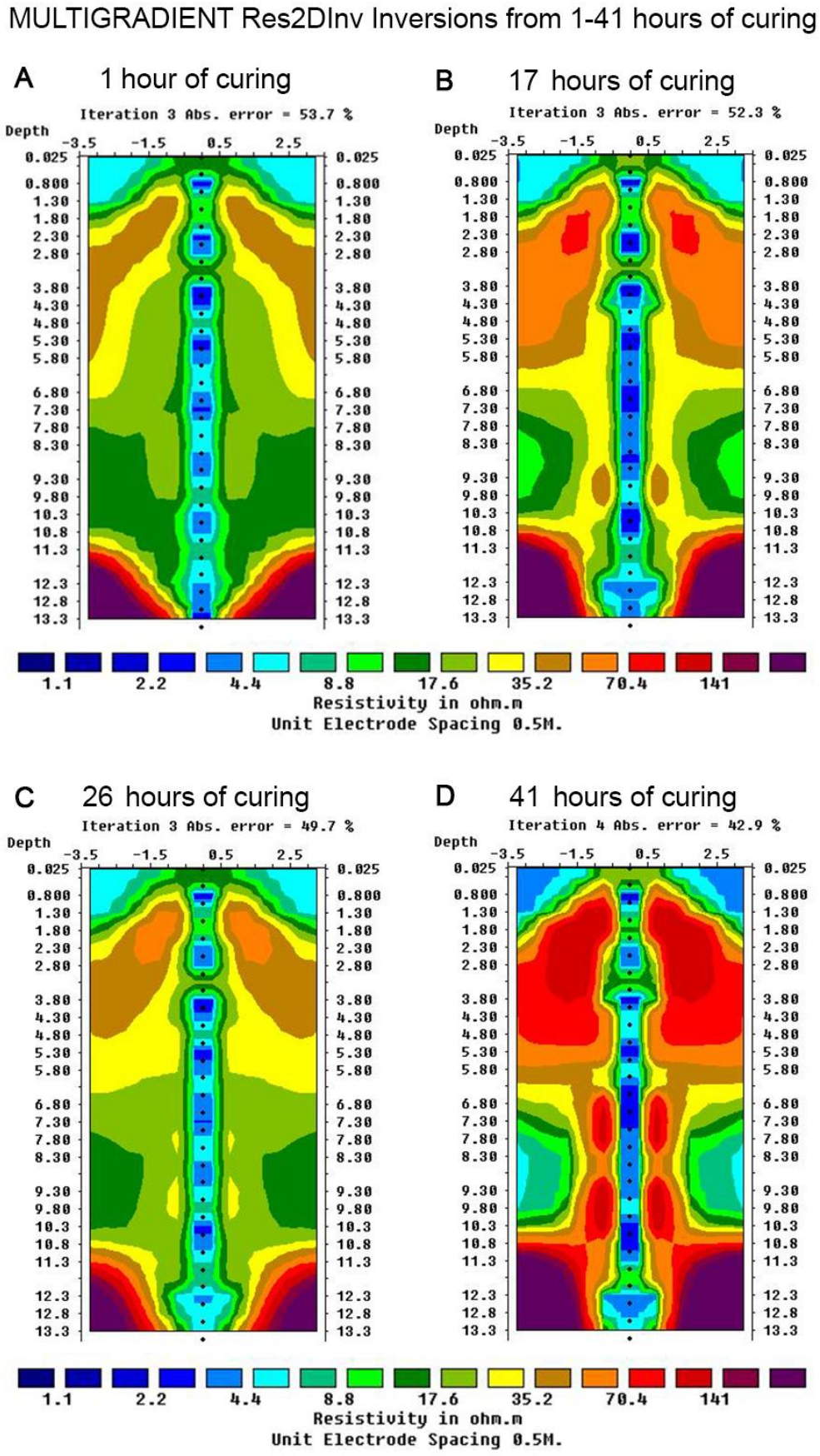

Figure 41 Res2DInv inversion models based on the multigradient configuration between 1-41 hours of curing

The Res2DInv inversion acquired from measurements after 789 hours of curing is presented in figure 42. The resistivity distribution is very different compared to the previous measurements. The resistivity contrast boundary can hardly be determined as most of the column inherits similar resistivities to the surroundings. Several regions of 5-18 Ωm are present throughout the column and the surrounding soil. Three iterations were performed with a difference in model response of 49.9%.

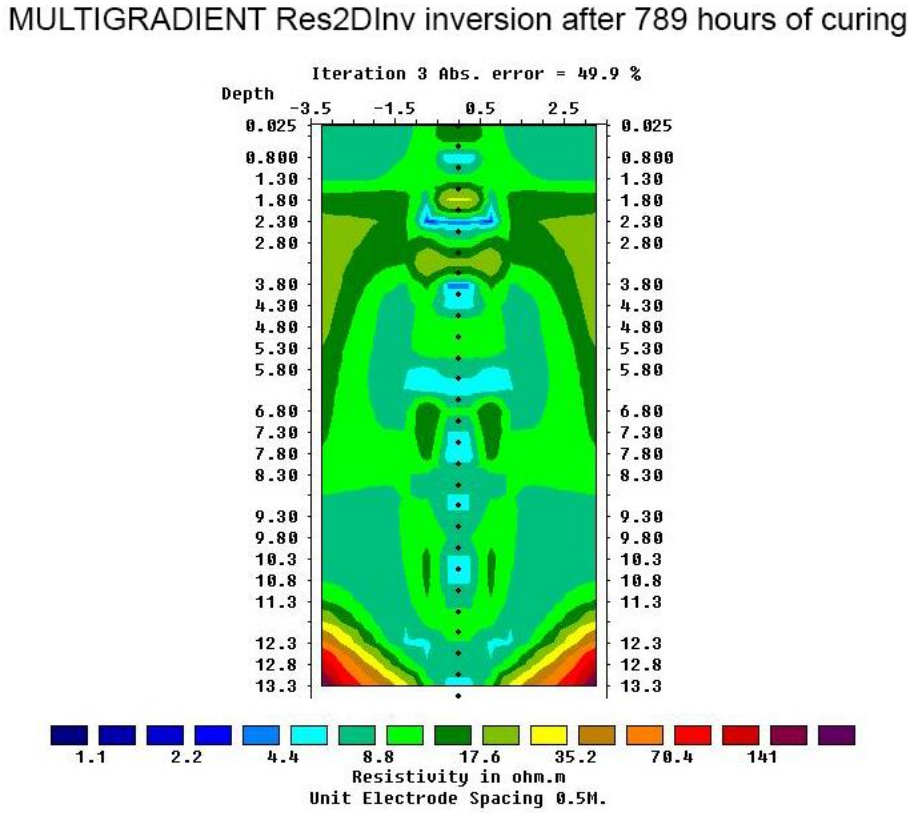

Figure 42 Res2DInv inversion model based on the multigradient configuration after 789 hours of curing

7.4 pyGIMLi Inverisons

2D-pyGIMLi inversions applied to the correct geometry is shown on the left side in figure 43 to 47 while a comparison between the original data and the inverted data is shown on the right side. The 2D-model show cell blocks placed 0.25; 0.5; and 0.8 meters in horizontal direction from the centre of the electrode array as well as the depth below the surface in vertical direction with the inverted resistivities in logarithmic scale. Thereby, the 2D-model only depicts one half of the column unlike the Res2DInv inversions. The right figures also present the resistivities in logarithmic scale with the different quadripoles measured by the ABEM Terrameter LS2. Some outliers and errors were found in the measured data which were mostly filtered. The filtered datapoints are illustrated as white cell blocks in the original data and the inverted data on the right side of figures 43 to 47.

The inversion of the multigradient configuration after one hour of curing in figure 43 (a) resulted in a difference in model response of 30.06% and χ^2-value of 2.60 with four

iterations. An outlier line was found for the electrode closest to the surface and a region at the bottom which were filtered. The inversion applied to the correct geometry, show a resistivity value varying between 1-3 Ωm along the centre of the borehole extending radially to approximately 0.5 meters in radial direction. There is also an outer boundary of 8 Ωm from 0.5 to 0.8 meters in radial direction. The edges of the electrode array seem to be more resistive than the middle section with large resistivity at the bottom of the borehole.

The pyGIMLi inversions of the dipole-dipole configurations after 2 hours of curing gave largely different results in figure 43 (b). Both datasets exhibited more outliers than the multi gradient configuration. The inversion obtained from the forward configuration presented larger resistivities of 3-4 Ωm between 1-2 meters below surface and 5-10 Ωm from 11-14 meters below surface. The centreline of the electrodes showed a low homogenous resistivity of 1-2 Ωm between 2-11 meters in depth which extends to 0.5 meters in radial direction. An outer boundary of larger resistivity of 3-5 Ωm is found between 0.5-0.8 meters in radial direction. The difference in model response was 43.84% and a χ^2-value of 4.09.

The reciprocal configuration in figure 43 (c) obtained similar results regarding the resistivities near the centreline of the electrodes and the contrast boundary extended in radial direction. However, the homogenous region of low resistivities starts from 2.5-12 meters in depth. The reciprocal also obtained larger resistivities near the surface and lower resistivities in the bottom region. The difference in model response was 43.11% and a χ^2-value of 2.88, correlating better with original data than the forward configuration.

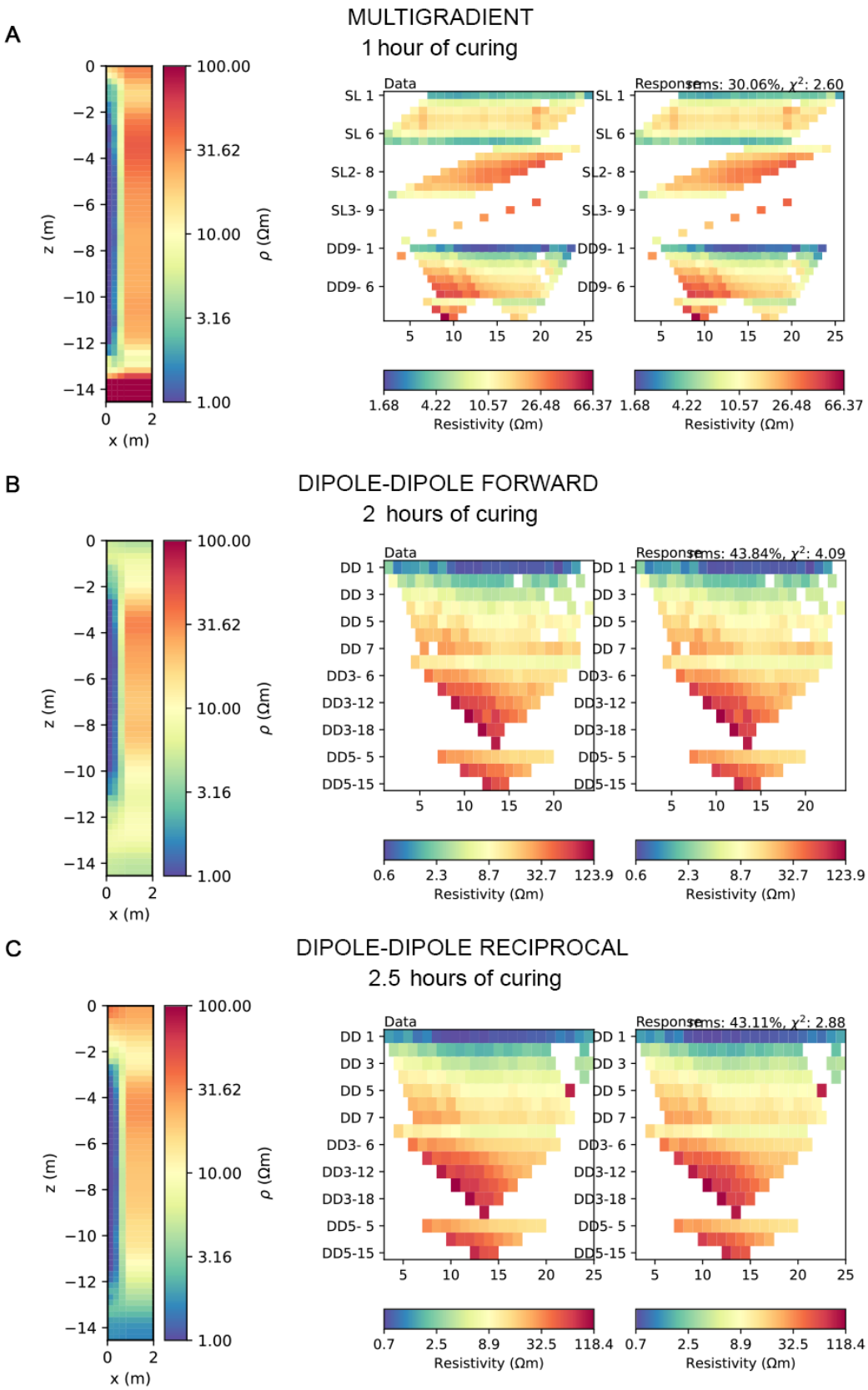

Figure 43 pyGIMLi inversion models based on the first measurement occasion (1-2.5 hours of curing) with the multigradient and the dipole-dipole configurations. Left figures show the inversion applied to the correct geometry. Right figures show the original data compared to the inversion with the difference in model response

The 2D-pyGIMLi inversions of dipole-dipole and multigradient configurations after 15-17 hours of curing differ in appearance shown in figure 44. The dipole-dipole forward and reciprocal configuration in figure 44 (a) and (b) exhibits larger resistivity values between 3-5 Ωm from 0-2.5 meters in depth. Lower resistivities of 1-2 Ωm are still obtained in the centre of the electrode array between 2.5-9.5 meters in depth. There is however a slightly larger resistivity found between 9.5-11 meters in depth in the forward inversion in figure 44 (a). Additional outliers were also contained in the data in the top region of the column which were filtered. The difference in model response for the dipole-dipole forward was 60.65% with a χ^2-value of 3.65 whilst the reciprocal configuration inherited a difference in model response of 81.80% and a χ^2-value of 3.85. The multigradient configuration showed a clearer distinction of resistivity contrast throughout the whole column. Much of the resistivity is largely unchanged compared to the previous multigradient inversion. The difference in model response was 32.26% with a χ^2-value of 4.34.

Regarding the inversions after 24 to 26 hours as well as 39 to 41 hours of curing in figures 45 and 46, the resistivities have only increased a few decimals in the centre of the column since the previous measurements' inversions for all configurations. The multigradient configurations in figure 45 and 46 (c) exhibits a lower difference in model response and χ^2-value to the measured data compared to the dipole-dipole configurations in figure 45 and 46 (a) and (b). This also applies for the amount of outliers and errors found in the data, where more datapoints were filtered for the dipole-dipole measurements.

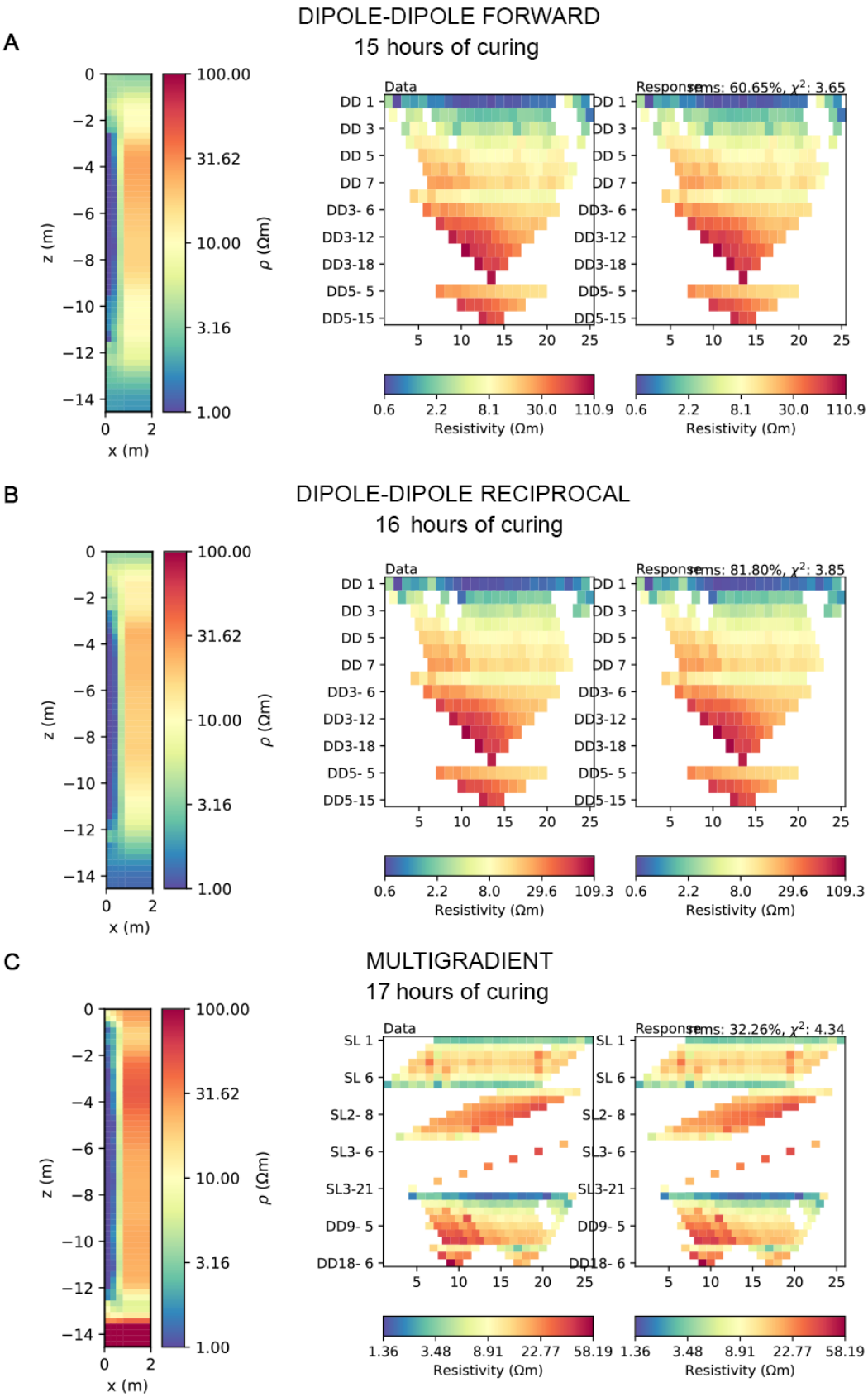

Figure 44 pyGIMLi inversion models based on the second measurement occasion (15-17 hours of curing) with the multigradient and the dipole-dipole configurations. Left figures show the inversion applied to the correct geometry. Right figures show the original data compared to the inversion with the difference in model response

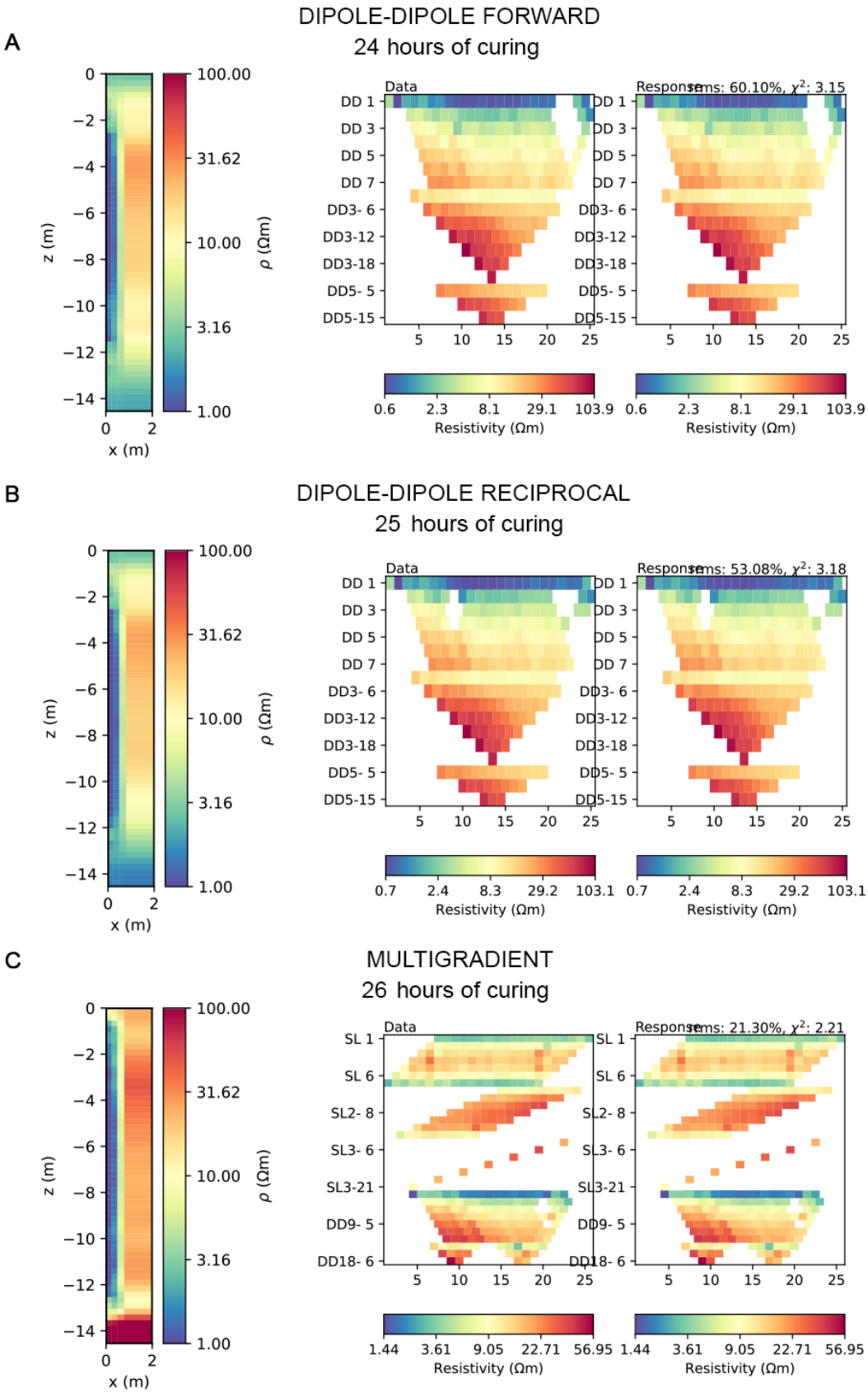

Figure 45 pyGIMLi inversion models based on the third measurement occasion (24-26 hours of curing) with the multigradient and the dipole-dipole configurations. Left figures show the inversion applied to the correct geometry. Right figures show the original data compared to the inversion with the difference in model response

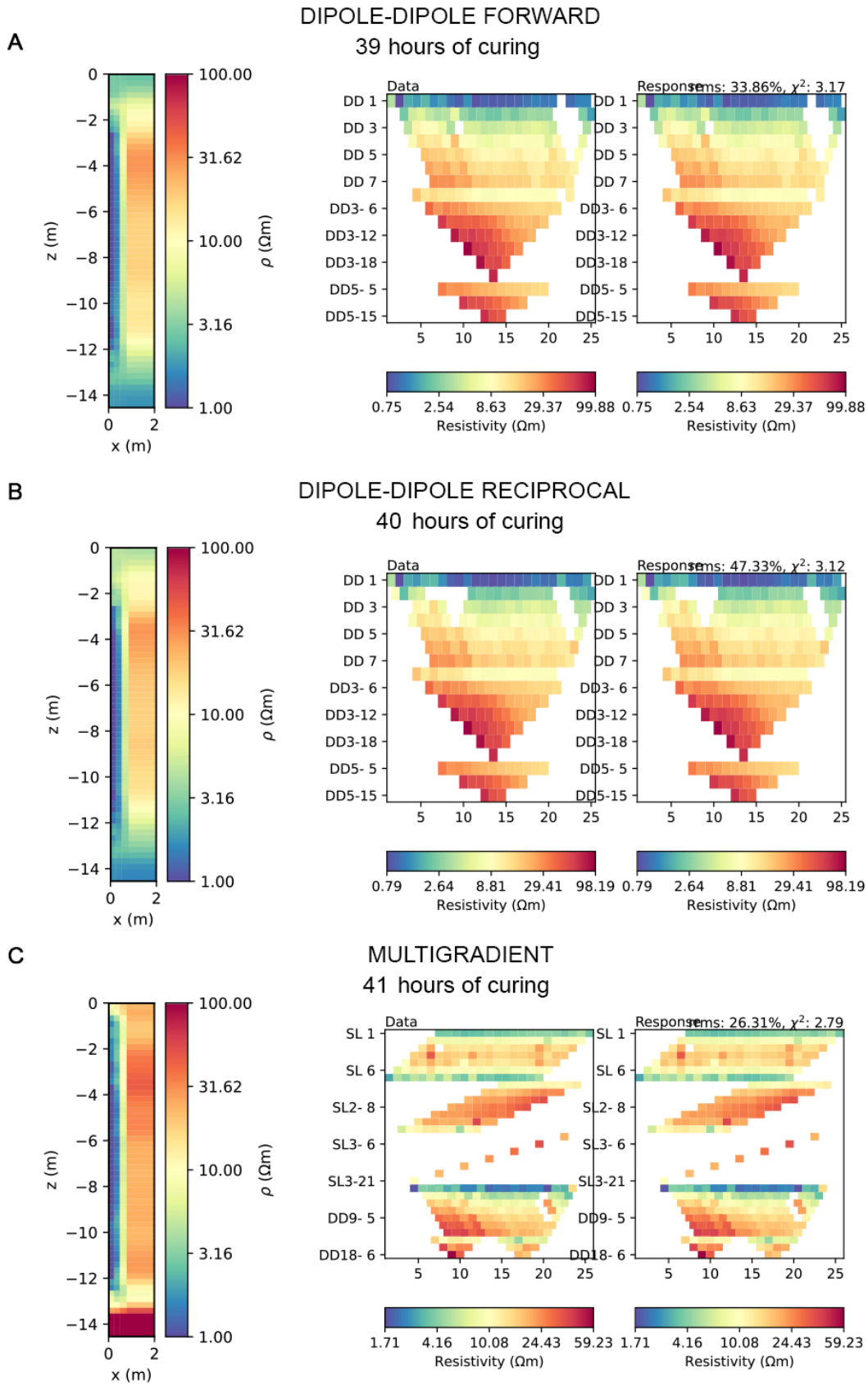

Figure 46 pyGIMLi inversion models based on the fourth measurement occasion (39-41 hours of curing) with the multigradient and the dipole-dipole configurations. Left figures show the inversion applied to the correct geometry. Right figures show the original data compared to the inversion with the difference in model response

The 2D-pyGIMLi inversions of the dipole-dipole and multigradient 789 hours and 790 hours of curing are presented in figure 47. Major differences are obtained compared to the previous inversions as well as comparing the configurations. The multigradient inversion in figure 47 (a) show an inhomogeneous contrast boundary. Regions of 0.25 meters in radial direction are found at depths of 3-4 meters as well as a point located at 5.5 meters in depth. The outer boundary region of 8 Ωm previously homogenous at 0.8 meters in radial direction has now decreased in resistivity of 5 Ωm along some regions of the column. The resistivity has generally increased since the multigradient inversion after 41 hours of curing in figure 46 (c) with a few points along the centreline of the electrode to still inherit low resistivities of 2 Ωm.

The dipole-dipole configurations in figure 47 (b) and (c) obtained a more homogenous contrast boundary with a region along 2.5-3.5 meters in depth which decouples the continuity of the boundary. A resistivity increase has occurred since the previous inversion, exhibiting resistivities of 5-8 Ωm along all boundaries in the forward configuration whilst 3-5 Ωm for the reciprocal configuration. The data inherited many outliers which were filtered out as can be seen on the right side in figure 47 (b) and (c). A 25.96% difference in model response and a χ^2-value of 10.48 after four iterations was achieved with the multigradient configuration while the dipole-dipole reciprocal obtained a lower difference in model response of 21.74% and a χ^2-value of 1.91 after four iterations. The forward dipole-dipole configuration resulted in a larger difference in model response of 39.58% but a lower χ^2-value of 3.73 compared to the multigradient inversion after four iterations.

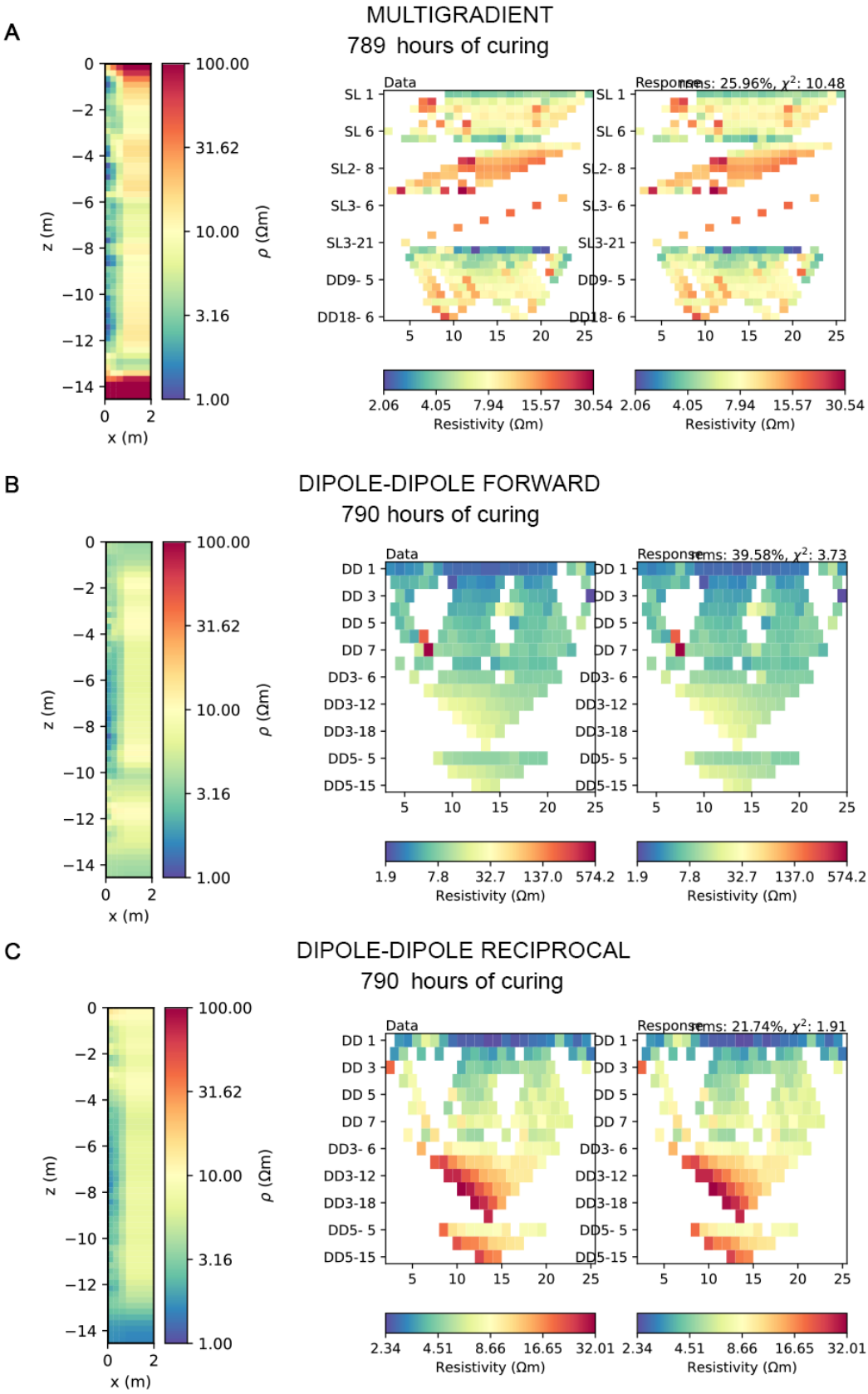

Figure 47 pyGIMLi inversion models based on the fifth measurement occasion (789-790 hours of curing) with the multigradient and the dipole-dipole configurations. Left figures show the inversion applied to the correct geometry. Right figures show the original data compared to the inversion with the difference in model response

7.5 Error estimation

The error estimation is presented as a lateral pseudosection similar to the pseudosections in section 7.2 where the same principle of the horizontal and vertical directions apply. The error estimation is acquired from the software Erigraph.

Figure 48 and 49 displays the apparent resistivity errors between the dipole-dipole measurements. Note here the first electrode is present at 1.5 meters in the pseudosection and should therefore be subtracted when evaluating the apparent resistivity errors. Regarding the error estimation based on the dipole-dipole measurements after 2 hours of curing in figure 48 (a), most of the pseudosection inherit an apparent resistivity error between 1% to 8%. Although, some major errors (larger than 20%) are found for the electrodes closest to the ground surface as well as a region starting from 10.5 meters in depth to the bottom of the array.

The error between the dipole-dipole measurements after 16 hours of curing is shown in figure 48 (b). Most of the pseudosection exhibit an apparent resistivity error between 0 % to 8 %. The upper part of the pseudosection, close to the electrodes, the apparent resistivity error is high, between 18% to 20%. From 3-5.5 meters in depth, and from 10.5 meters to the bottom of the array the area with high resistivity error remains.

The apparent resistivity error for the dipole-dipole after 25 hours is shown in figure 48 (c). Similar to the previous error estimation, the apparent resistivity error is relatively low in most part of the section, but there are areas close to some of the electrodes that have a higher apparent resistivity error. From two to five meters is an area, bigger than in the first measurement but smaller than the second measurement, that have an apparent resistivity that is approximately 18 % to 20%. There is also an area from ten meters to the bottom, where the apparent resistivity also is about 18% to 20 %.

Figure 48 (d) displays the apparent resistivity error based on the dipole-dipole measurements after 40 hours. Similar to the previous measurements error estimation, most of the section shows a relatively low error between 0% to 10%. Closest to the electrodes located at a depth of 1.5 meters, 2.5 meters to 5.5 meters and 10 meters to 12 meters below the surface the apparent resistivity error is high, approximately between 18 % to 20 %.

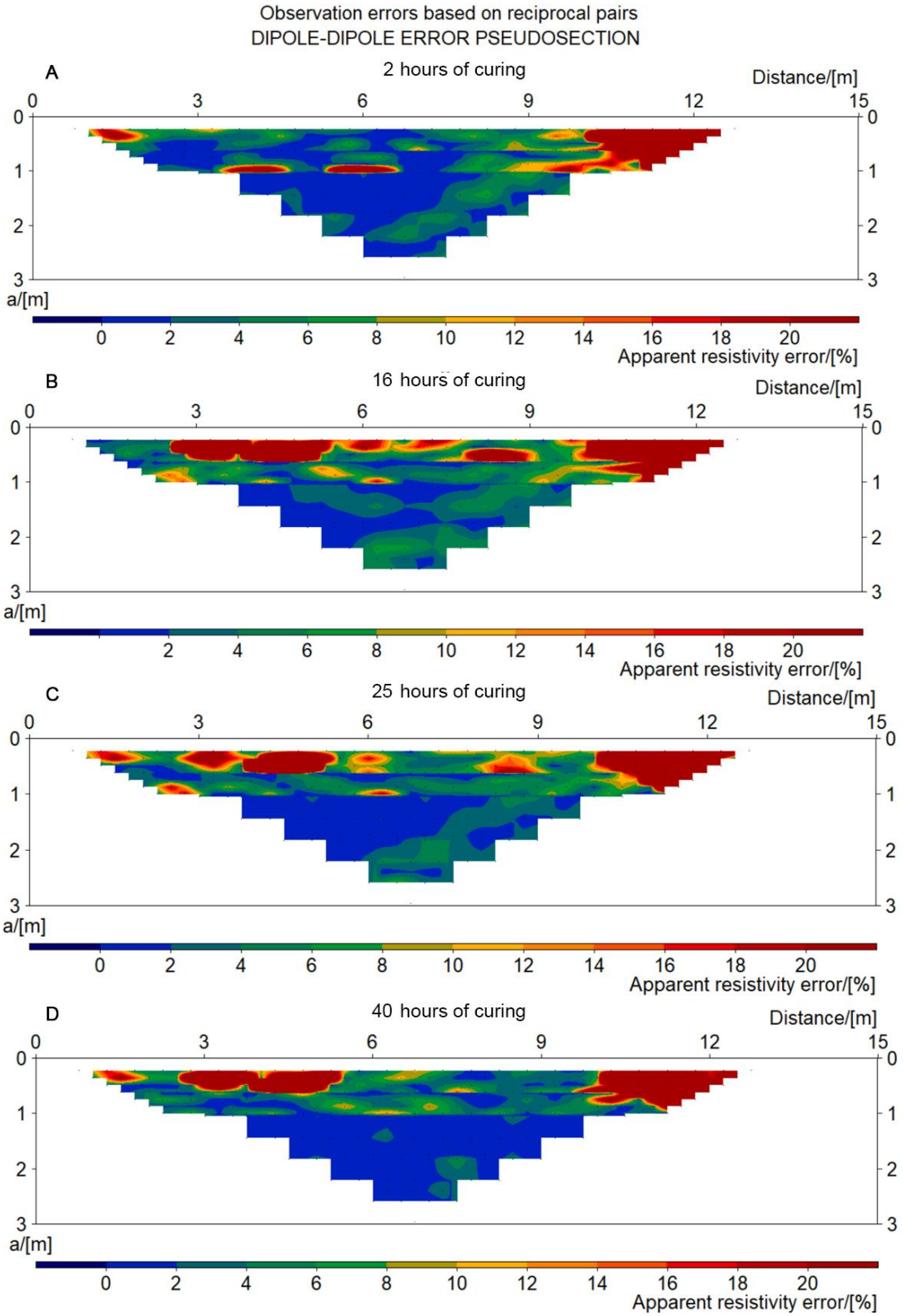

Figure 48 Apparent resistivity error estimation based on reciprocal analysis of dipole-dipole measurements after between 2-40 hours of curing

The apparent resistivity error estimation based on reciprocal analysis of the dipole-dipole configurations after 790 hours of curing is presented in figure 49. A large increase of errors has occurred since the fourth measurements. The major error region in between 1-4 meters of depth has increased radially from the electrodes. The errors obtained in the bottom of the electrode array are largely unchanged. However, an additional error at 6.5 meters in depth has appeared. Increases of errors are also appearing in the furthest regions from the column with 6-20%.

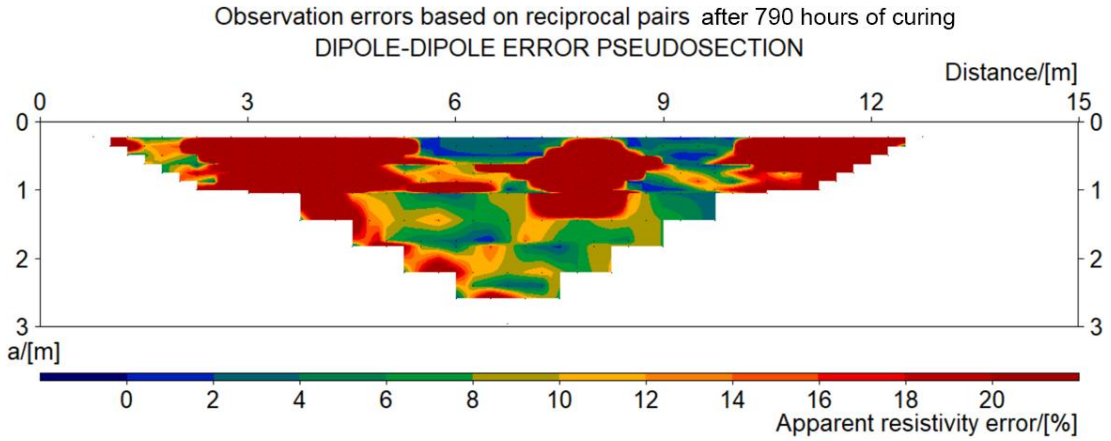

Figure 49 Apparent resistivity error estimation based on reciprocal analysis of dipole-dipole measurements after 790 hours of curing

8 Analysis and discussion

8.1 Results analysis and discussion

8.1.1 Temperature history during the curing process

The curing process of the soilcrete is interpreted via the measured temperature history. As can be seen from the graphs in figure 38, a steep incline from the initial stages of curing occurs. The overall behaviour of the curing correlates well with the data Brandstätter et al. (2005) have. However, the maximum temperature documented from this thesis displayed around 60°C compared to 70°C from the study. Brandstätter et al. (2005) used 15% cement content for a 0.6-meter column radius while this thesis used 12% cement content of the same radius. The cement type used for the grout mixture was also different which can explain the difference in maximum temperature.

The maximum temperature recorded from the depths of 5, 9 and 13 meters reached similar values around 60°C while the temperature at 1 meter below surface rose to 50°C. A probable motive for these differences is that the soilcrete closer to the surface is more exposed to surface conditions. The first measurements were performed in April with an air temperature between 5-10°C. Due to such temperature contrast, the heat from the soilcrete can be transferred faster to the surface during the heating period than for soilcrete placed deeper in the ground due to less surface exposure.

The exponential decrease that follows after maximum temperature was reached is similar for all depths but differ slightly. The temperature at 13 meters of depth shows the slowest decrease which is probably due to having the least surface exposure with the most grouting material on top and more compact soil in its surrounding. Surface conditions allow for evaporation from the water content in the grout mixture as well as being less insulated and thereby retaining less heat. This would mean that the bottom temperature retains the heat the longest with less heat retained closer to the surface. However, this is not true regarding the temperature decrease at 9 meters as it exhibits the fastest decrease in temperature. Plausible explanations for this can be that a region along the column consists of less soilcrete and thereby has a smaller diameter than the rest of the column. This correlates with the conclusion Brandstätter et al. (2005) presented, with smaller diameter of the column show a steeper decrease in temperature. The temperature distribution was not recorded for the subsurface soil, which could otherwise give a better explanation of the difference in temperatures at the measured depths of the column.

The lowest recorded temperature occurred after 470 hours where the temperature was steadily setting in the hours before and the temperature changes were very small between each measurement. This could mean that the curing process was completed at this time. The temperature at 1 meter below surface show a 3°C-difference compared to the rest of the sensors which show a setting temperature of 19°C. Since this sensor is closest to the surface, the surface temperature would give a greater impact on the soilcrete temperature at this depth than further down the column.

After the curing sets at 470 hours the temperature increased again. It was informed that new columns were installed at 1.5 meters from the centrelines of the studied column. The heat generated from the adjacent columns' curing seems to affect the temperature in the studied column. The sudden increase of the temperature would probably not affect the curing process of the column as the temperature history before the new installation indicated that a setting temperature was reached. However, the renewed increase in temperature will affect the resistivity measurements.

Some temperature measurements could not be recorded at 40, 75 and 175 hours after curing due to the connection failure to the measuring device. But, as can be seen between the last recorded temperatures before the abrupt stops and restarts of measuring, a clear exponential decrease in temperature occurs between these measuring points. Therefore, the connection failure had little effect when evaluating the curing process.

8.1.2 Res2DInv inversions

All borehole inversion results presented from the Res2DInv software indicate a resistivity contrast boundary along the vertical axis apart from the measurements performed after 789 hours of curing. This vertical contrast boundary could represent the soilcrete interaction in the subsurface soil, telling how much the soilcrete extends in radial direction to the soil and the radius of the column could be interpreted based on this boundary. The resistivity contrast in regard to the multigradient measurement after one hour of curing in figure 41 (a) can be explained due to the soilcrete containing high water content as well as having material with higher ion concentration than the subsurface soil which allows for a better conduction environment than the soil. The multigradient inversion show a relatively low resistivity of 1.1-4.4 Ωm which is similar to the values Bearce et al. (2016) presented after 1.5 hours. The resistivity increases slightly in radial direction to the contrast boundary varying between 0.5-0.8 meters in radius. The set radius of the column was aimed towards achieving a 0.6-meter radius which is slightly larger compared to the one-hour inversion model. As this measurement was performed one hour after curing started, the soilcrete might still be setting into the soil and the interaction between the treated and untreated soil could be incomplete or the outer regions of the column have already adapted to the soil conditions. It could also be that the interaction is completed, but a larger resistance contact of the electrode can be present in the regions of thicker resistivity zones.

Based on the soil profile around the investigated area in figure 32, most of the surrounding soil consisted of quick clay. The surrounding soil shows a resistivity between 17-20 Ωm from measurements after 1 hour of curing which correlates to the resistivity spectrum of which clay exhibits according to Lowrie (2007) and Knödel et al. (2007). It is thereby considered reasonable values for the surrounding soil. The groundwater level was expected to be in the range of 0.5-1.5 meters in depth. With groundwater present, a resistivity contrast would be expected due to the water enabling better conduction through wet clay compared to dry clay. It was however difficult to determine where this contrast occurred based on the inversions which is possibly due to the high resistance contact for the electrode at 1.5 meters in depth, why the inversions show a higher resistivity along this region for a majority of the measurements. Therefore, the groundwater impact on the column could not be evaluated.

The Res2DInv inversions from the following measurements after 17 to 41 hours of curing in figure 41 (b-d) show relatively small radii difference. The interaction from the soilcrete

to the surrounding soil seems to have been completed already after the first hours. The resistivity contrast in the most outer regions of the column can be explained by the soilcrete reaching its eroding distance where the soil content is larger than the grout mix and thereby depicting larger resistivities. The radius obtained from the inversions is also slightly larger than what was intended for the column (0.6 meters). It could be due to the inversion being interpreted with a 2D assumption of the geometry of geological structures, that can overestimate the radius of the column (later discussed in more detail in section 8.2.3). A region of smaller radius is found at a depth of 9 meters for the measurements between 17 to 41 hours of curing, correlating with the steeper temperature decrease at this depth seen in figure 38. The shadow effect could have an impact on this, meaning a larger soil particle which the injecting grout could not erode, leaving a section of the column to have a smaller radius than the rest of the column. It could also be due to a layer of larger soil resistance to be present at this depth which can be more difficult for the grout to penetrate through. This suggests that a smaller region is present at this depth and the inversion models could therefore detect possible inhomogeneities of the column radius.

The relative difference in resistivities in linear scale compared to one hour of curing to each consecutive inversion result is shown in figure 50. The resistivities shown in the inversions between 17 to 789 hours of curing suggest a slow resistivity increase of the soilcrete with curing time. The outer regions in radial direction of the column seems to increase more rapidly than the centre of the column. This is most likely due to the water content to be contained for a longer time within the centre since it has the least exposure to the surrounding soil which can allow for a better drying environment. The large positive resistivity changes in the surrounding soil seen in figure 50 (c) can be due to outliers in the measured data as it does not coincide with the previous measurements. It can also be that large resistivity changes are created by the mismatch of the actual geometry compared to the assumed 2D geometry which in Res2DInv is based on. This can also be reflected when seeing the resistivity decreasing slightly between 1 to 41 hours of curing in figure 50 (c) with around -50-0 % in the centre of the column. However, the relative resistivity change after 789 hours of curing in figure 50 (d) does show a great relative increase of resistivity along the centreline of the column between 50-200 %.

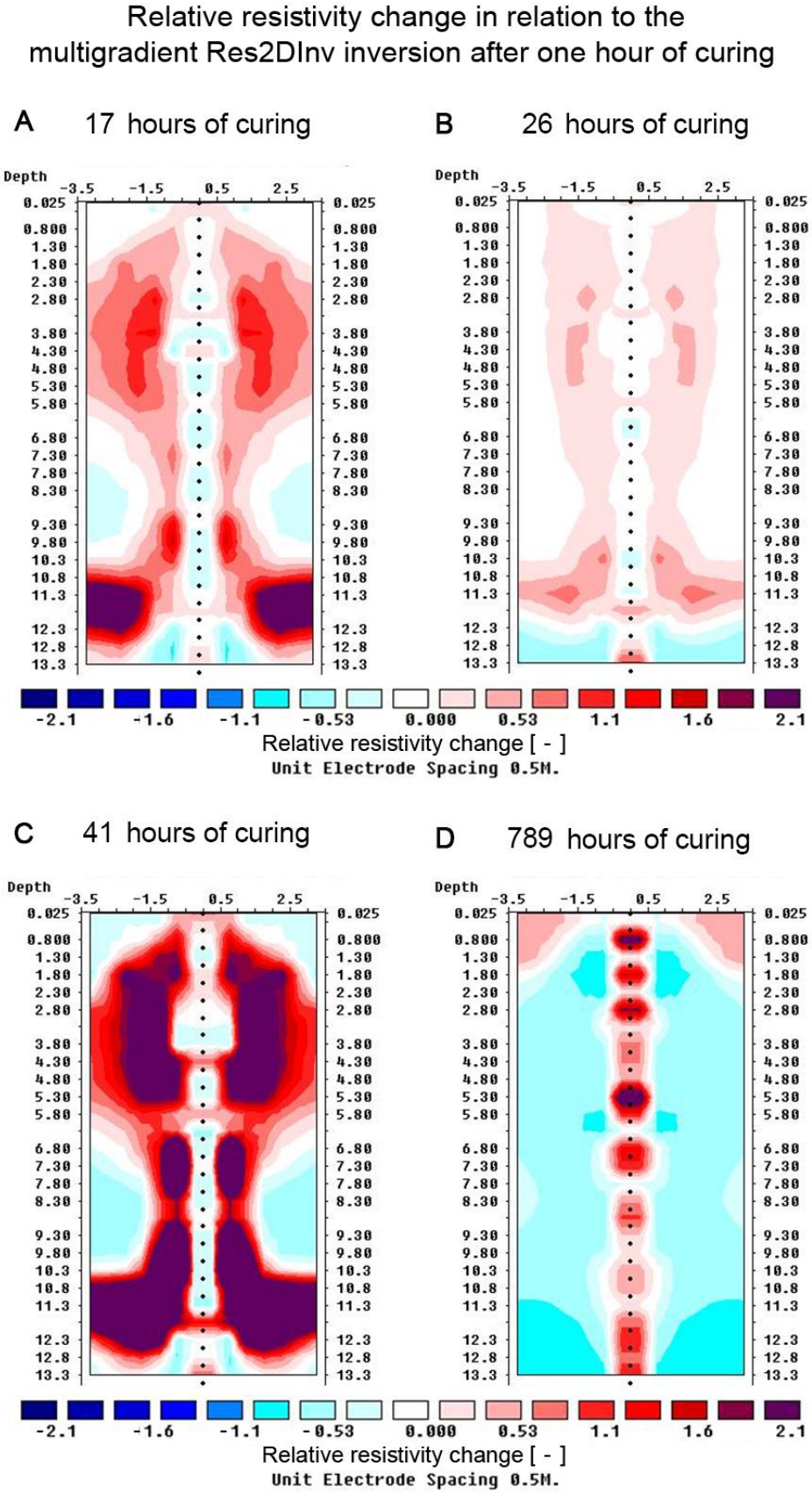

Figure 50 Relative resistivity change in relation to the multigradient Res2DInv inversion after one hour of curing. Red regions are positive changes, blue regions are negative changes

Regarding the inversion results from measurements after 789 hours in figure 42, the resistivities coincided with the surrounding soil, suggesting that the curing process in the column has advance, although it might be possible that the resistivity could continue to rise above that of the original soil. However, this made the vertical resistivity boundary impossible to determine and the quality control could not determine the column geometry based on inverted dataset. But as can be seen from figure 50 (d), the relative resistivity change could be an alternative to determining the geometry and homogeneity after curing is complete as a clear homogenous area along the centreline of the column has increased in resistivity.

As previously mentioned, only the Res2DInv inversion results from the multi-gradient configurations were presented. The inversions obtained from the dipole-dipole configurations showed unreasonably large resistivities in the surrounding soil seen in appendix 3 with very low resistivity in the centreline of the electrodes which did not extend more than 0.2 meters in radial direction. One possible theory could be that the dipole-dipole measurements are more sensitive towards the loss of signal strength compared to multigradient. Dipole-dipole places the potential pair outside of the current pair which for each measurement places the potential pair further away from the current pair, and thereby less signal strength is obtained at the potential pair. As a large contact resistance was found at 0.5 meters below the surface, the loss of signal strength is imminent which explains the inversions to show large resistivities at this region.

All inversions obtained relatively high inversion errors (between 42.9% to 53.7%). A probable explanation for this is the quality of the dataset. With more outliers in the dataset, the inversion can amplify the errors and outliers for each iteration due to the sensitivity and depth of investigation factors. Some outliers were filtered from the datasets which decreased the model response difference significantly, however the model response differences were still large. Another explanation is the original data needed to be applied to an assumed 2D geometry, since Res2DInv is based on the assumption that all structures have an infinite extension in the direction perpendicular to the modelled plane, which is further discussed in section 8.2.3. All inversion models are probable depictions of the actual column, but with risk of inaccurate resistivity contrast and diameter due to the 2D assumption enforced on a 3D structure. Therefore, it could potentially mean that the Res2DInv-method is an uncertain way for quality assuring jet grouting columns.

8.1.3 pyGIMLi inversions

The pyGIMLi inversion results show a resistivity contrast boundary along the Z-axis which extends in radial direction and can therefore be interpreted as the soilcrete interacting with the surrounding soil. For the multigradient and dipole-dipole configurations from the first measurement in table 8 and 11, a low resistivity of 1-2 Ωm in the centreline of the electrodes is obtained which extends to 0.5 meters in radial direction and an outer boundary of larger resistivities of 8-9 Ωm at 0.8 meters. A mean radius can then be interpreted between these boundaries which correlates with the set column radius of 0.6 meters. The resistivity in the column also correlates with the values presented from Bearce et al. (2016). The resistivity of the surrounding soil varies between 10-30 Ωm which is similar to the clay resistivity spectrum presented from Lowrie (2007) and Knödel et al. (2007).

The 3D-inversion results based on the relative resistivity difference between the multigradient measurement after 1 hour of curing compared to each consecutive multigradient measurement is presented in figure 51 for a linear scale in percentage. The difference in resistivity is largely unchanged for the first 41 hours when compared to the measurement after 1 hour of curing seen in figure 51 (a-c). Resistivity increase is mostly found in the outer region of the column with an increase between 100-200 % after 41 hours of curing in figure 51 (c) but little to no difference in the centre. Resistivity along the centreline of the electrode array should expect to increase with curing time due to less water content and ionic concentration in the soilcrete which is mainly not the case. However, due to the high temperatures in the soilcrete between 17-41 hours of curing, it could explain why the resistivities are low. But the temperature difference between the 17 to 41 measurements is around 10-15 ˚C and could therefore still result in larger resistivity changes between these measurements. Only in the inversion results obtained from the last measurements in figure 51 (d) increased resistivity values of 200-400 % is found throughout the column. It might be due to the pyGIMLi software interpreting the apparent resistivities with high regularization and damping factor in the inversion, which thereby changes the inversion models less for each iteration. But to fully understand this, more data from different test subjects need to be taken into consideration when evaluating the inversion models. Furthermore, numerical simulations could contribute to a better understanding.

The resistivity contrast boundary looks relatively homogenous for the inversion results based on the measurements between 1 to 41 hours in figures 43-46, where the radius seems to be continuous in between 0.5-0.8 meters. It does however differ in homogeneity regarding the last measurements in figure 47, where the boundary varies between regions much more. At 3 to 4 meters below the surface a larger resistivity is obtained, decoupling the continuity of the column. This is most likely due to the high contact resistance of some electrodes exhibit at these depths which can cause large apparent resistivity values.

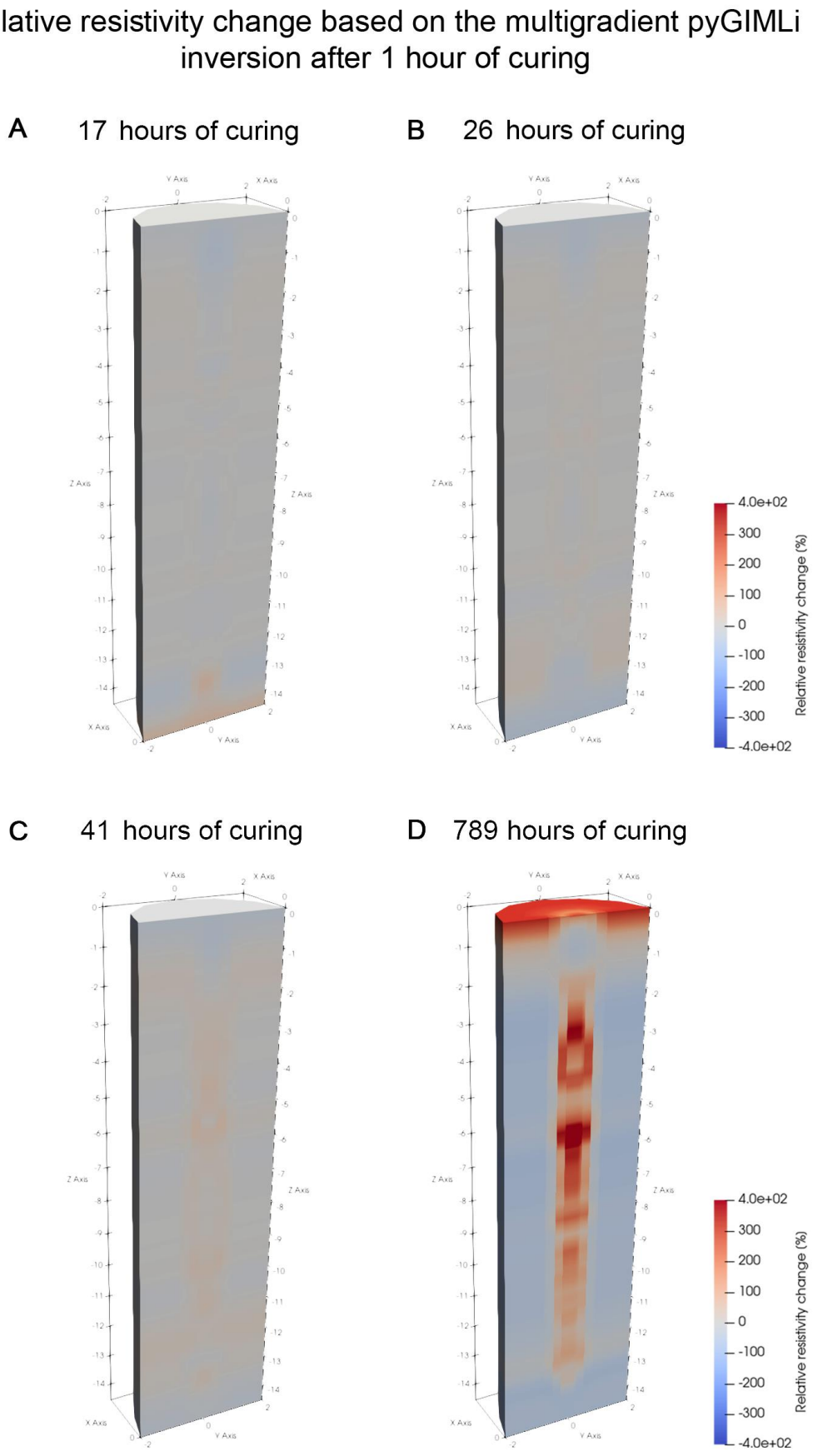

Figure 51 Relative resistivity change in relation to the multigradient pyGIMLi inversion after one hour of curing

The inversions from the multigradient and dipole-dipole configurations differ in appearance especially at the top and bottom regions. Plausible explanation to this can be that more outliers were filtered at these regions for the dipole-dipole configuration compared to the multigradient as the dipole-dipole contained more uncertain data. The inversion would then be based on less data points and therefore sets a mean resistivity value based on interpolation of adjacent data points. Why the dipole-dipole measurements contained more outliers can be due to this configuration being more sensitive in the loss of signal strength as discussed in section 8.1.2. A comparison of the sensitivity regions can also be seen in figure 18 (c) and (d).

The model response difference and χ^2-values were relatively high for the pyGIMLi inversion models. However, the multi gradient configuration did show better model responses compared to the dipole-dipole configuration for almost all inversions, suggesting the multi gradient is a more appropriate configuration for this application. As the datasets contained many errors and outliers, the same problems would occur for the pyGIMLi inversion as for Res2DInv. Attempts at filtering outliers also proved to significantly reduce the model response differences and χ^2-values. But it was still not possible to obtain better inversion models and that further development within the pyGIMLi-model needs to be performed. But due to time limitations for this thesis, the pyGIMLi-model could not be further developed.

8.1.4 Comparison between the software inversions

The pyGIMLi and Res2DInv software provided inversion models of varying credibility. The datasets contained large uncertainties which were attempted to be filtered and the software handled these uncertainties differently. Res2DInv provided inversion results with relatively homogenous contrast boundaries from the datasets after 1 to 41 hours. However, an area of large resistivity was present at the top region of the column based on the measurements performed between 17 to 41 hours of curing. This could be due to the L1-norm trying to fit the noise found from the measured data. The pyGIMLi inversions depicted a more continuous column along the same region and therefore handled the filtered outlier better than Res2DInv. This also occurred for the last measurements where the Res2DInv showed no resistivity contrast compared to the inversions from pyGIMLi. Both software did also identify a smaller radius around 9-10 meters in depth, suggesting both software to detect inhomogeneities of the column.

The Res2DInv inversions showed slightly larger radius from the vertical resistivity contrast boundary between treated and untreated soil than intended for the column compared to the pyGIMLi inversions which depicted contrast boundaries close to the intended column radius of 0.6 meters. Thereby, the pyGIMLi inversions suggested a more realistic figure of the column radius than Res2DInv.

Both software obtained large differences of model responses to the original data, however the pyGIMLi inversion generally resulted in less difference in model responses compared to Res2DInv. The model response difference obtained from the multigradient configuration was also generally lower than the dipole-dipole configuration for both software, suggesting that the multigradient configuration was better suited for this application. pyGIMLi inversions could also depict more realistic models from the dipole-dipole measurements than the Res2DInv inversion results.

Res2DInv obtained slightly larger resistivities in the centreline of the electrode array with more curing time compared to pyGIMLi but the resistivities in the centre of the column

for the inversion models from both software were largely unchanged after 41 hours of curing. Res2DInv did not show a resistivity contrast after 789 hours unlike the pyGIMLi-inversion. Overall, the Res2DInv resistivity values correlated better when compared to the values from Bearce et al (2016). The study also mentioned that a smaller resistivity contrast between treated and untreated was obtained with curing time, which occurred for our inversion models as well. However, Bearce et al. (2016) used a different grout mix with different soil conditions in a lab setting. Therefore, it is not for certain if the measured test column would show similar resistivities as Bearce et al. (2016).

Both software inherits different strengths and weaknesses. The Res2DInv inversions showed more realistic resistivity values, relative to expectation based on published data, but slightly overestimates in column radius. pyGIMLi depicts less realistic resistivity values but better column radius estimations. However, the chosen parameters in pyGIMLi did inherit lower resolution than Res2DInv and evaluating the column radius was therefore more difficult to determine. The pyGIMLi software would be preferred for this type of inversion but needs to be developed further with increased resolution as well as adjusted inversion settings.

8.1.5 Error analysis

The evaluation of the error estimation based on reciprocal analysis of the dipole-dipole apparent resistivity values from figures 48 and 49 indicated several zones with higher error values. As mentioned in section 4.4.2, forward and reciprocal measurements should obtain the same apparent resistivities in theory. That could not be observed as it was instead found that several regions exhibited errors of >20%.

In the first measurements obtained from figure 48 (a) after 2.5 hours of curing, the apparent resistivity errors are generally small along the column ranging from 1-8%. A small error at the top of the column was identified but a big zone with large errors were found at the bottom of the borehole. The small error at the top of the column could be that the electrodes at the top inherit noise in the measured data caused by the surface conditions. Bearce et al. (2016) mentioned that the measurements transitioned from full space to half space conditions at the surface and the geometric factor could be wrongly interpreted by the Terrameter. The large region of errors in the bottom of the column could be that the anchorage at the bottom was made of a steel pipe which is highly conductive and thereby expects to generate noise in the measurements.

Evaluating the error estimations based on the following measurements seen in figure 48 (b-d) as well as in figure 49, additional errors occur at depths between 2-5 meters which sequentially increased for each measurement. So far, the reasons are not known, but two plausible theories are discussed. The first theory involves the heat produced by the curing to potentially damage some of the electrodes at this region. The measurements after 17 hours of curing surpasses the time at which the maximum temperature in the soilcrete was reached. Therefore, the damage to the electrodes could have occurred during the heating period of the curing. The second theory involves corrosion taking place on the electrode surfaces. If current of high intensity is injected through the electrodes, an electrochemical reaction between the surface of the electrode and the soilcrete can occur, corroding the surface of the electrode. With corrosion on the surface of the electrode the resistance contact between the electrode and soilcrete could increase, which would lead to disturbances for the injecting current. Increased resistance contact generally means lower signal strength to the measuring potential electrodes, why the potential electrodes

could detect large variations in apparent resistivity. An indication for the corrosion theory was that the contact resistance for the electrode at 0.5 meters in depth was very large in relation to the rest of the electrodes. An apparent contradiction to this hypothesis is that the electrodes were made of stainless steel, but such steel may still corrode. For better understanding of what could have caused the additional errors, more systematic measurements with varying voltages of current injection for different material compositions in contact with the electrodes needs to be performed. A different electrode material could also provide information regarding this behaviour.

8.2 Evaluation of the measurements and inversions

8.2.1 Installation

The installation of the composed cable was made possible by inserting the composed cable into the steel casing via the jet grouting machine after production of the column. As this would assure the composed cable to be correctly aligned along the centre of the column, the data obtained from the first measurements suggests that some damage might have occurred during the installation. One plausible cause could be that it was subjected to strain during the lifting of the steel casing as well as the straightening of the cable. When the anchorage made contact with the bedrock, an inclined bedrock surface could have enabled the composed cable to be offset from the centreline in the bottom region of the column. Based on the geological model in figure 30, an inclined bedrock surface is present. When straightening the cable, the jet grouting machine exerts tension forces on the cable when pulled upwards. This could have enabled the anchorage to unfold the spikes in an inclination at the bottom, bending the composed cable at the bottom region. The fibreglass rod provided stiffness to the cables, but longer lengths allow for more flexibility of the rod why the bending could have occurred. This bending could also have amplified when the steel casing was removed due to the supportive walls provided by the steel casing diminishes. An anchorage more adaptive to inclination as well as a rod of higher stiffness might have provided better alignment of the electrodes.

Another theory could be that the composed cable was attached with duct tape where the tension forces could have exceeded the duct tape strength, detaching some cables from the fibreglass rod and thereby have electrodes misaligned from the centre. As the composed cable was not commercially produced, duct tape was found to be the best solution for attaching the electrode and temperature cables to the fibreglass rod. Maybe a suitable tool specified for these types of measurements would have been used, the attachment strength would obviously be much stronger.

Apart from the above-described misalignment cause, we believe that the installation method was plausible. Before the installation procedure, an evaluation with the workers at the site was made. Due to their great knowledge, experience and understanding of the jet grouting procedure, the installation procedure seemed reasonable with the set of used equipment. The problems that occurred were mainly due to the equipment not being perfectly adapted for the soilcrete conditions as well as the installation. A recommendation for future investigations is an improvement of cable equipment that is better suited for these conditions.

8.2.2 Measuring

The ERT-measurements were first performed for four separate occasions during the first three days of curing. This was performed to study the initial stages of the curing process where the most changes of the curing in the column were expected. The fifth measurement occasion was performed 33 days after curing which was 19 days after most of the soilcrete was cured according to the temperature history in figure 38. Due to the construction site being in Norway (see figure 26), significant planning had to be made before each site visit since the travel times to the site were long and necessary equipment had to be brought. As it was informed that new columns adjacent to the test column were going to be installed after 19 days of curing, the ideal measurement occasion would have been just before the new installation. But due to personal time schedules not aligning with Keller's schedule, it was unfortunately not possible to visit the site at this time. Therefore, a decision was made to wait for the adjacent columns to complete most of its curing before visiting the site once more. Initially, it was planned to leave the instrument connected to the electrodes and perform ERT-measurements automatically and wirelessly from Lund similar to the temperature measurements, but power to the instrument could not be supplied on the site, why the measurements had to be performed manually.

The data obtained from the measurements presented several outliers and errors, and it was discussed in section 8.1.2 if electrochemical reactions could have caused corrosion on the electrode surfaces due to high intensity of the injecting current from the electrodes. A lower intensity of the injecting current could have avoided this reaction resulting in more accurate data to be obtained. Another electrode material could have been another solution.

The electrode spacing of the composed cable was set to 0.5 meters. This enabled the inversion models to obtain a certain resolution. A shorter electrode spacing with more electrodes would have increase the resolution and the inversions could map the column in more detail as what Bearce et al. (2016) have performed. Configurations performed for the measurements were multigradient and dipole-dipole. The multigradient configuration seemed to be more suitable for these types of measurements, probably due to obtaining lower geometric factors and being less sensitive to the loss of signal strength than the dipole-dipole configurations. However, the dipole-dipole measurements did provide error estimations from reciprocal analysis and was therefore useful as well. Reciprocal analysis can be applied to different configurations such as the Wenner and Schlumberger configurations. As these configurations generally provide data of higher resolution but less depth of investigation than dipole-dipole, it might have been beneficial to test these configurations as well. This is because resolution was of more importance than the depth of investigation in these measurements, since the column's distance in radial direction was relatively short.

8.2.3 Inversion

The Res2DInv inversions were implemented into a 2D inversion model. This meant that one fictious borehole and the borehole containing the actual data was applied to the model. This made the software invert the data under the assumption that all geological structures have an infinite extent in the direction perpendicular to the modelled plane, when it is in fact extent in a three-dimensional space. Therefore, the applied geometry would be wrong.

The pyGIMLi inversion models showed too low resolutions making it difficult to determine where the contrast boundary was present. This is due to the regions in the mesh were set too wide. With more regions implemented in the model, a model of higher resolution could be obtained. But since more regions increases the number of cells in the model, more processing power from the computer is needed during the inversion process making the inversion process much more time consuming.

The estimation of where the first electrode below surface was positioned has also an affect on the geometry applied to the inversion. It was difficult to measure on site since it was not possible to be close to the curing soilcrete for safety reasons. However, the estimation seemed plausible when relating the distance from where the first non-submerged electrode was positioned.

The motive for why all inversion models obtained large differences in model response is most likely due to number of errors and outliers and how the ERT-data was measured. The electrode array measured the potential differences in full space conditions, which the geometry applied to the inversion was adapted for as well. Full space conditions mean the current lines are distributed through all directions in the medium, while half space conditions assume a conductive environment in one half of the electrode surface while the other half is non-conductive, eg. air. For this case, it would mean that for half space conditions the current injected in the soilcrete would only be distributed for one half of the column when it is in fact distributed through the whole column. Full space conditions were taking into consideration; however these 3D-measurements were translated to a 2D-inverse model under the assumption that the resistivity distribution is rotationally constant (meaning the resistivity varies only with depth). Considering that the column geometry varies for all directions in reality, this method is not entirely accurate to the real column as it cannot be said from the measurements how the resistivity distribution varies in all three directions. For that, a cross-borehole ERT-measuring (see section 4.4) could for example be performed, but this requires more space and equipment. The measurements could then be inverted in Res3DInv (instead of Res2DInv) or in a developed model adapted to these measurements in pyGIMLi. Improvements for the pyGIMLi inversion could certainly be made with the set of data used but due to a limited schedule for this thesis, further improvements of the pyGIMLi inversions were not made.

8.3 Comparison of existing quality controls

This quality control establishes a less invasive method of the soilcrete compared to excavation or callipers. This is because the composed cable contains a small area in relation to the column and should have little effect on the mechanical properties of the column as well as not intruding in the surrounding soil. It can therefore be considered as an indirect quality control. How less invasive it is compared to existing quality controls is still unclear. Much of the existing indirect quality controls consist of inserting an oblong rod into the soilcrete which is similar to this methodology. It is although clear that it is not less invasive than the spoil quality control due to no object interfering with the soilcrete for this control.

The ERT-methodology seems less time consuming compared to excavation but rather similar to ACI®. The column is produced in nominal lifting and rotational speed compared to ACI® which needs constant adjustments throughout the production. And the insertion procedure of the composed cable goes much quicker compared to the

installation of feeler pipes since alignment of the cable is performed with the jet grouting machine. However, the measuring procedure in ERT takes time as well as extracting the data to a computer and perform inversion. As the ERT-method lacks development in routine application, further development within this aspect can establish a less time-consuming methodology.

The quality of measurements in ERT could be better than sonic logging tests during the initial stages of curing, due to allowing a good electric conduction environment. The sonic logging tests would obtain more uncertain data at the initial stage of curing since little stability growth in the column is present. However, as the soilcrete cures the resistivity contrast between treated and untreated soil gets smaller whereas the sonic logging tests clearer distinguishes sonic velocities between the soilcrete and the soil. As the initial stages of the curing are of most importance when determining the geometry and homogeneity of the column, the ERT-method could provide better data than sonic logging tests. A beneficial control would be to combine these quality controls for when they acquire the best data during the curing process.

This ERT-method is not reusable for the same set of equipment unlike the ACI®-control which reuses the feeler pipes for the next column. The composed cable inserted into the soilcrete cannot be extracted from the soilcrete due to the anchorage being attached at the bottom making the cable fixed in the column. It is also not certain if the method is applicable to structural columns rather than test columns. Many existing quality controls demand a test column to be used. As this method should not interfere with the stability of the column, the excess wiring that is not submerged into the soilcrete could be cut off from the submerged electrode array when no more measuring is necessary.

The installation procedure can become a valid quality control with improvement of equipment, however as the inversion models presented uncertainties, the inversion methodology of this thesis needs to be further developed to be as accurate as the other indirect quality controls. Furthermore, the inversion models have not been validated by excavation of the test column and can therefore not be determined how accurate this quality control is. But the resistivity contrast between treated and untreated soil makes it clear that this would be the quality parameter for the ERT-method, why potential within this method exists in comparison to existing quality controls.

9 Conclusion

The installation procedure seemed viable to the set of equipment used and it proved to be much less invasive than direct quality controls. Therefore, this quality control can be categorized within the indirect quality controls potentially have a faster installation than some existing quality controls. However, the equipment proved to be less adaptive to the soilcrete conditions and the installation procedure which resulted in lack of data quality. The resistivity data contained many outliers and errors which was most likely due to a combination of misalignment of the electrode cable and corrosive action on the electrodes' surface.

The inversion models obtained in this thesis showed that a resistivity contrast between the treated and untreated soil was found. The resistivity contrast gets smaller with curing time but can present a distinction between the soilcrete and the subsurface soil in pyGIMLi (unlike Res2DInv). Thereby, the resistivity contrast can be a valid measurement parameter throughout the curing process of the column.

Large differences between model responses and original data were obtained from both software inversions. The pyGIMLi software obtained better model responses with better correlation to the intended column radius than the Res2DInv software making the pyGIMLi software to be more suitable for column inversions. Less resistivity increase was however found from the pyGIMLi inversions compared to the Res2DInv inversions and when comparing the resistivity values to Bearce et al. (2016), the Res2DInv inversions had better correlation. Due to the used lower resolution in the pyGIMLi inversions, the model also proved more difficult to determine the diameter of the column compared to the Res2DInv models.

The multigradient configuration acquired better data quality than the dipole-dipole configurations, suggesting the multigradient configuration to be more suitable for this application. Although, the dipole-dipole measurements provided necessary data to error analysis. For measuring the column, the resolution seemed to be of more importance than increased depth of investigation which is why a different configuration than the dipole-dipole configuration could have provided data of higher quality.

The conclusion of this thesis is that the ERT-method has potential to be applicable to quality assuring jet grouting columns. The quality parameter for determining the geometry and homogeneity of the column would be defined by the point of which the resistivity contrast between the treated and untreated soil is located in the inversion models or how the relative resistivity changes during the curing process. The ERT-method could potentially be a more time-effective and accurate quality control with development in routine application and inversion models compared to existing indirect quality controls. However, the inversion software used in this thesis are not ideally suited for this application but alternatives should be tested and probably adapted. As the ERT-method has not been validated it could not be compared with the accuracy of existing quality controls.

9.1 Recommendations

For improved data quality in the measurements, a lower injected current might reduce corrosive action on the electrode surface. On the other hand, lower current will reduce the signal levels, so a trade-off will be required. The electrodes should also be tested with different material compositions in contact with the electrodes as well as varying voltages, configurations, and different electrode materials to get a better understanding of the occurrence of faulty measurements. This can also enable the quality control to accumulate further data references.

A commercially available product specified for ERT-column measurements should be used for prohibiting misalignment or damage to the electrode layout. The measurements should also be performed right after the column's curing is completed, as well as an automatic ERT-measuring to study the curing process in more detail.

To obtain more accurate inversion models, refined settings within the pyGIMLi software should be made. The Res2DInv models are recommended to further refine the cross-borehole geometry. Other software should also be tested. A software which was not tested for this thesis was AarhusInv which includes support for inversion of cylindrically symmetrical geometries around boreholes which would be applicable to single stabilised columns.

The ERT-methodology has potential to be further developed in routine application, mostly regarding the inversion methodology. With a standardized inversion model that is user friendly, the inversion method could be streamlined and allow for a less time-consuming procedure.

10 References

ABEM & MALÅ, 2007. *Erigraph - User Guide,* Lund: ABEM & MALÅ - Guideline Geo.

Archie, G. E., 1942. *The Electrical Resistivity Log as an Aid in Determining Some Reservoir Characteristics.* Dallas, s.n.

Bearce, R. G., Mooney, M. A. & Kessouri, P., 2016. Electrical Resistivity Imaging of Laboratory Soilcrete Column Geometry. *Journal of Geotechnical and Geoenviromental Engineering,* 142(3), pp. 1-10.

Bellato, D., Schorr, J. & Spagnoli, G., 2018. Mathematical Analysis of Shadow Effect in Jet Grouting. *Journal of Geotechnical and Geoenviromental Engineering,* 144(12), pp. 1-10.

Binley, A. & Slater, L., 2020. *Resistivity and induced polarization: Theory and Applications to the Near-Surface Earth,* Camebridge: Cambridge University Press.

Brandstätter, C., Lackner, R. & Mang, H. A., 2005. In situ temperature measurements provide new insight into the performance of jet grouting. *Ground Improvement,* 9(4), pp. 163-167.

Brinck, M., Stigenius, K. & Beijer Lundberg, A., 2021. *Conference Series: Earth and Enviromental Science 710.* Stockholm, IOP Publishing.

Bruce, D., 1994. Jet Grouting. In: *Ground Control and Improvement.* New York: John Wiley & Sons, Inc., pp. 580-683.

Burke, G. K., 2004. *Jet grouting systems: Advantages and disadvantages In: Geosupport 2004.* s.l., s.n., pp. 1-12.

Croce, P. & Flora, A., 2000. Analysis of single-fluid jet grouting. *Géotechnique,* 50(6), pp. 739-748.

Croce, P., Flora, A. & Modoni, G., 2014. Jet Grouting. In: *Jet Grouting: Technology, Design and Control.* s.l.:s.n., pp. 1-3.

Dahlin, T. & Zhou, B., 2004. A numerical comparison of 2D resistivity imaging with 10 electrode arrays. *Geophysical Prospecting,* 52(5), pp. 379-398.

Dahlin, T. & Zhou, B., 2006. Mulitple-gradient array measurements for multichannel 2D resistivity imaging. *Near Surface Geophysics,* 4(2), pp. 113-123.

Daily, W., Ramirez, A., Binley, A. & LaBrecque, D., 2000. Electrical Resistance Tomography - Theory and Practice. *The Leading Edge,* 23(5), pp. 573-598.

Edwards, L., 1977. A modified pseudosection for resisitvity and ip. *Geophysics,* 42(5), pp. 939-1087.

Essler, R. & Yoshida, H., 2004. *Ground Improvement.* 2:a ed. Abingdon: Spon Press.

Fetter, Jr., C., 2014. Principles of Ground-Water Flow. In: *Applied Hydrogeology.* Harlow, England: Pearson Education Limited, p. 171.

Fetter, Jr., C., 2014. Soil Moisture and Ground-Water Recharge. In: *Applied Hydrogeology.* Harlow, England: Pearson Education Limited, p. 266.

Frappin, P. & Morey, J., 2001. *Jet grouted column diamter emasuremnet using the electric cylinder method,* France: Soletanche Bachy. Internal Publication.

Geotomo Software, 2010. *geoelectrical.* [Online]
Available at: epsc.wustl.edu/~epsc454/instruction-sheets/Res2dinv03.59.pdf
[Accessed 16 Maj 2022].

Google, 2022. *Google maps.* [Online]
Available at:

https://www.google.com/maps/place/Moss,+Norway/@58.2202143,9.8579748,5.89z/data=!4m5!3m4!1s0x46414d6141a68625:0xaf141a7a20c83738!8m2!3d59.4340914!4d10.6583833
[Accessed 14 Mars 2022].

Günther, T., Rücker, C. & Spitzer, K., 2006. Three-dimensional modelling and inversion of dc resitivity data incporporating tomography. *Geophysical Journal International,* 166(2), pp. 506-517.

Hallof, P. G., 1957. *On the interpretation of resistivity and induced polarization measurements,* Camebridge: Camebridge-MIT.

Hislam, J. & Smith, N., 2019. Jet Grouting. In: P. Pallett & R. Filip, eds. *Temporary Works: Principles of design and construction, Second Edition.* London: ICE Publishing, pp. 109-115.

Jernbaneverket, 2016. *Østfoldbanen VL(SKI-) Moss-Sandbukta-Moss-Såstad,* Oslo: Jernbaneverket.

Keller, 2015. *Acoustic Column Inspector - ACI,* Wien: Keller.

Keller, 2019. *Keller Geoteknikk lands €42m Norway contract.* [Online]
Available at: https://www.keller-geoteknikk.no/en/news/keller-geoteknikk-lands-eu42m-norway-contract
[Accessed 14 Mars 2022].

Keller, 2022. *Jet Grouting.* [Online]
Available at: https://www.keller.co.uk/expertise/techniques/jet-grouting
[Accessed 31 01 2022].

Knödel, K., Lange, G. & Voigt, H. -J., 2007. *Enviromental Geology: Handbook of Field Methods and Case Studies.* Hannover: Springer.

Koh, C. et al., 1997. Electric Resistivity Tomography for Geophysical Inverse Problems. *Transactions on Magnetics,* 33(2), pp. 1852-1856.

Lekmine, G., Pessel, M. & Auradou, H., 2012. Experimental Study of ERT Monitoring Ability to Measure Solute Dispersion. *Groundwater,* 50(2), pp. 285-295.

Loke, M., Acworth, I. & Dahlin, T., 2003. A comparison of smooth and blocky inversion methods in 2D electrical imaging surveys. *Exploration Geophysics,* 182(3), pp. 182-187.

Meinhard, K. et al., 2016. Extending chem-thermal quality assessment for jet grouting. *Proceedings of the Institution of Civil Engineers - Ground Improvement,* 169(4), pp. 264-274.

Milsom, J., 2003. Electric Current Methods - General Considerations. In: *Field Geophysics: Third edition.* Chichester: John Wiley & Sons Ltd,, pp. 83-91.

Modoni, G., Croce, P. & Mongiovi, L., 2006. Theortical modelling of jet grouting. *Géotechnique,* 56(5), pp. 335-347.

Myeong-Jong, Y., Jong-Ho, K. & Jeong-Sul , S., 2009. Borehole deviation effect in electrical resistivity tomography. *Geosciences Journal,* 13(1), pp. 87-102.

Nakanishi, W., 1974. *Method for forming an underground wall comprising a plurality of columns in the earth and soil formation.* United States, Patent No. 3800544.

NGI, 2021. *Østfoldbanen VL, Sandbukta – Moss – Såstad,Km 56,075 – 66,410, Vurdering av områdestabilitet,* Oslo: NGI.

Ni, J. C. & Cheng, W.-C., 2014. Quality control of double fluid jet grouting below groundwater table : Case history. *Soils and Foundations,* 52(6), pp. 1039-1053.

Nor, B., n.d. s.l.: s.n.

Okpoli, C., 2013. Sensitivity and resolution capacity of electrode configurations. *International Journal of Geophysics,* Volume 2013, pp. 1-12.

Parsekian, A., Claes, N., Singha, K. & Minsley, B., 2017. Comparing Measurement Response and Inverted Results of Electrical Resistivity Tomography Instruments. *Journal of Environmental and Engineering Geophysics,* 22(3), pp. 249-266.

Perrone, A., Lapenna, V. & Piscitelli, S., 2014. Electrical resistivity tomography technique for landslide investigation: A review. *Earth-Science Reviews,* 135(1), pp. 65-82.

Pierce, K., Liethty, D. & Rittgers, J., 2012. *Geopysical Investigations Electrical Resistivity Surveys,* Santee, California: U.S. Department of the Interior.

Reynolds, J. M., 2011. Electrical Resistivity Methods. In: *An Introduction to Applied and Environmental Geophysics: Second edition.* Chichester: John Wiley & Sons, Ltd, pp. 289-346.

Ribeiro, D. & Cardoso, R., 2017. A review on models for the prediction of the diameter of jet grouting columns. *European Journal of Environmental and Civil Engineering,* 21(6), pp. 641-669.

Roy, A. & Apparao, A., 1971. Depth of Investigation in direct current methods. *Geophysics,* 36(5), pp. 943-959.

Rücker, C., Günther, T. & Wagner, F., 2017. pyGIMLi: An open-source library for modelling and inversion in geophysics. *Computers and Geosciences,* pp. 1-15.

Safetec Nordic, 2022. *Nytt Dobbeltspor Sandbukta-Moss-Såstad Helhetlig geoteknisk riskovurdering, prosjektering og utførelse,* Oslo: Safetec Nordic.

Scales, J., 1988. Robust method in inverse theory. *Inverse problems,* 4(4), pp. 1071-1091.

Shen, S.-L., Wang, Z.-F., Yang, J. & Ho, C.-E., 2013. Generalized Approach for prediction of Jet Grout Column Diameter. *Journal of Geotechnical and Geoenvironmental Engineering,* 139(12), pp. 2060-2069.

Shorr, C.-P., Traegner, R. & Micciche, R., 2007. *Evaluating In-Situ Jet Grout Column Diameters Utilizing Wave Analysis.* Denver, Geo-Denver.

Skinner, A. & Covil, C. S., 1994. Grouting in the ground. In: A. L. Bell, ed. *Jet grouting - a review of some of the operating parameters that form the basis of the jet grouting process.* London: ICE Publishing, pp. 605-629.

Summer, J., 1976. *Principles of Induced Polarization for Geophysical Exploration.* 1 ed. Tucson: Elsevier Scientific Publishing Company.

The World Bank, 2020. *Urban Development,* s.l.: The World Bank.

Tsourlos, P., Kim, J.-H., Vargemezis, G. & Yi, M.-J., 2007. *Monitoring water injection with borehole ERT: preliminary results of an experiment carried out in Sindos (N. Greece),* Sindos, Greece: Aristotile University of Thessaloniki.

United Nations, 2018. *The World's Cities in 2018 - Data Booklet,* s.l.: United Nations.

Wang, Z., Shen, S., Ho, C. & Kim, Y., 2013. Jet Grouting Practice: an Overview. *Geotechnical Engineering Journal of the SEAGS & AGSSEA,* 44(4), pp. 88-90.

Yoshida, H., 1996. Development and practical applications of large diameter soil improvement method. In: *Proceedings of the Conference on Grouting and Deep Mixing.* Tokyo: Balkema, pp. 721-726.

Zhou, B. & Greenhalgh, S., 2001. Cross-hole resistivity tomography using diffrent electrode configurations. *Geophysical Prospecting,* 48(5), pp. 887-912.

APPENDICIES

pyGIMLI-code

```
from glob import glob
import numpy as np
import matplotlib.pyplot as plt
import pygimli as pg
from pygimli.physics import ert
import pygimli.meshtools as mt

datfiles = glob("DataMoss/*.dat")
print(datfiles)
data = ert.load(datfiles[2])
print(data)

ert.show(data, cMin=1, cMax=40);

if not data.haveData("r"):
    data["k"] = ert.geometricFactors(data)
    data["r"] = data["rhoa"] / data["k"]

z0 = 0.05
dz = 0.5
ze = np.arange(data.sensorCount()) * dz + z0
print(ze)

for i in range(data.sensorCount()):
    data.setSensor(i, [0, 0, -ze[i]])

print(pg.z(data))

data["k"] = ert.geometricFactors(data, dim=3)

data["rhoa"] = data["r"] * data["k"]
data["err"] = ert.estimateError(data, relativeError=0.03, absoluteUError=100e-6)
print(max(data["err"]))

ert.show(data, data['err']*100, label="error [%]");

r = [0, 0.25, 0.5, 0.8, 2]
world = mt.createCircle(radius=4, marker=0, isClosed=True)
world.createNode([0, 0])
for b in world.boundaries():
    b.setMarker(-2)
for i ,rad in enumerate(r[1:]):
    circle = mt.createCircle(radius=rad, marker=i+1, isClosed=True)
    world += circle
```

```
pg.show(world);

mesh2d = mt.createMesh(world, quality=34)
pg.show(mesh2d, markers=True, showMesh=True);

z = -np.arange(data.sensorCount()*2+6)*dz/2 - z0 + dz/2
z[0] = 0
z[-2] -= 1
z[-1] -=3
print(z)

mesh3d = mt.extrudeMesh(mesh2d, z)
print(mesh3d)

minz = pg.min(pg.z(data)) - 1
for c in mesh3d.cells():
    nlay = int(np.ceil(-(c.center().z()+z0)/(dz/2)))
    rad = np.sqrt(c.center().x()**2 + c.center().y()**2)
    if rad < r[-1]:
        c.setMarker(c.marker()*100 + nlay)

    if c.center().z() < minz:
        c.setMarker(0)

for b in mesh3d.boundaries():
    if b.outside():
        if b.center().z() == 0:
            b.setMarker(pg.core.MARKER_BOUND_HOMOGEN_NEUMANN)
        else:
            b.setMarker(pg.core.MARKER_BOUND_MIXED)
mesh3d.exportVTK("mesh3d.vtk")

mgr = ert.ERTManager(data, verbose=True)
mgr.setMesh(mesh3d)

mgr.inv.setRegularization("*", single=True)
mgr.inv.setRegularization(0, background=True)
mgr.fop.setInterRegionCoupling("*", "*", 1.0)

mgr.invert(robustData=True)

mgr.saveResult()

mgr.showFit();
plt.savefig('C:/Users/enils/transform2021-main/*/showfit.svg')
```

```
mgr.showMisfit()

zz = z[:-2]
grid = mt.createGrid(zz, r)

print(grid, len(mgr.model))
grid.swapCoordinates(0, 1)

pg.show(grid, mgr.model, cMin=1, cMax=100, xlabel="x (m)", ylabel="z (m)",
        label=r"$\rho$ ($\Omega$m)", cMap="Spectral_r", logScale=True,
orientation="vertical");
plt.savefig('C:/Users/enils/transform2021-main/*/2D1.svg')
```

Pseudosections

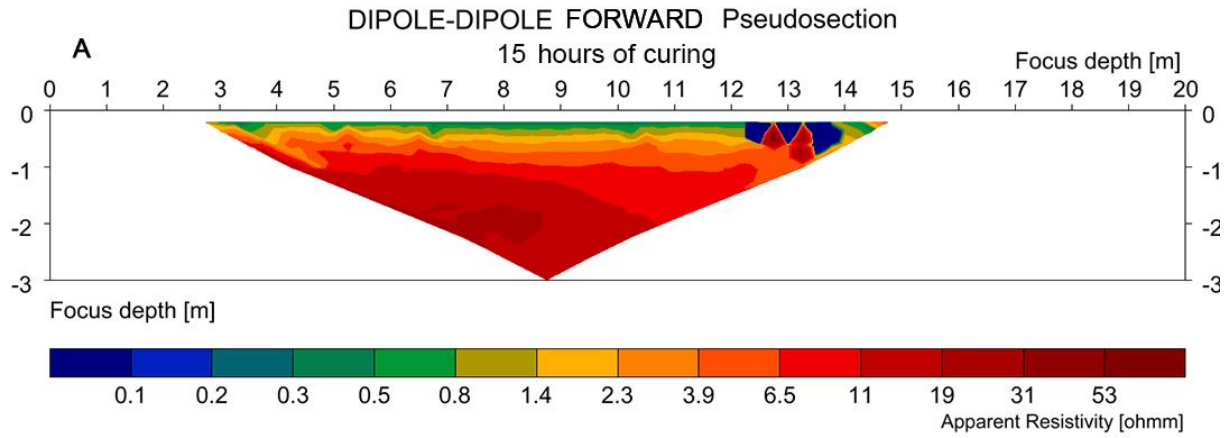

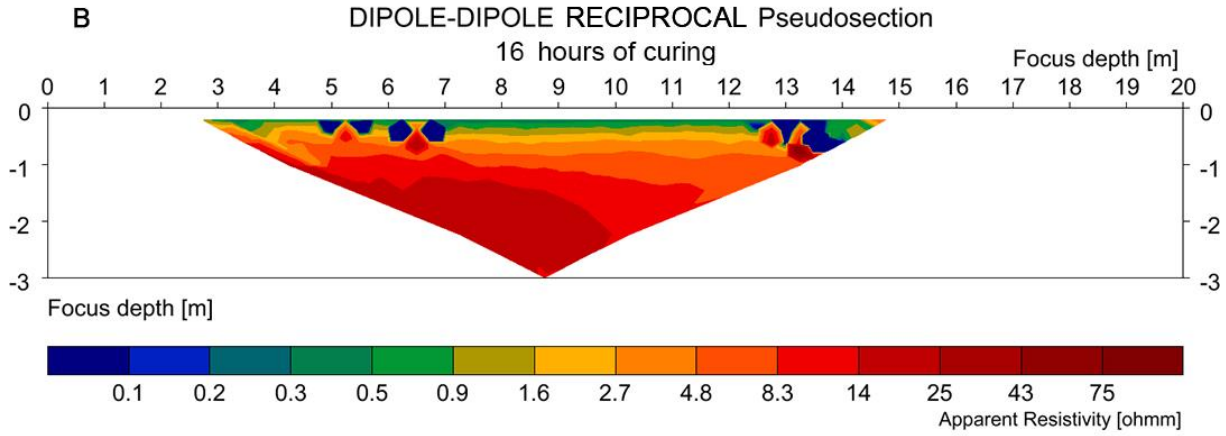

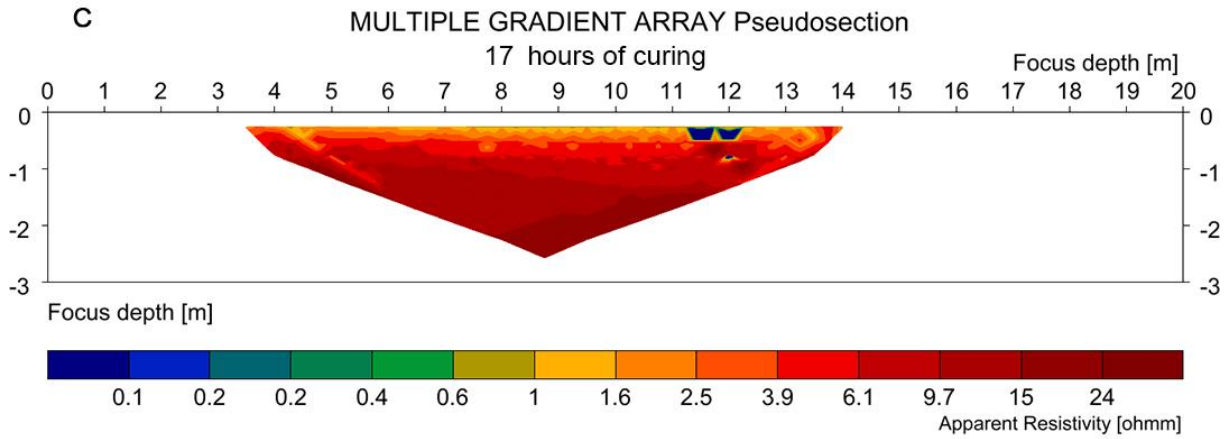

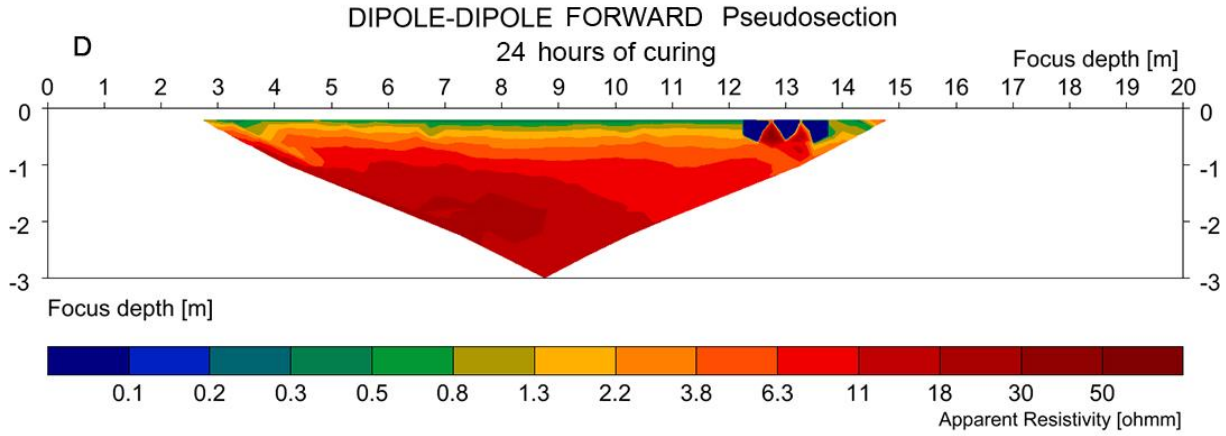
D
DIPOLE-DIPOLE FORWARD Pseudosection
24 hours of curing
Focus depth [m]
0 1 2 3 4 5 6 7 8 9 10 11 12 13 14 15 16 17 18 19 20
0
-1
-2
-3
Focus depth [m]
0.1 0.2 0.3 0.5 0.8 1.3 2.2 3.8 6.3 11 18 30 50
Apparent Resistivity [ohmm]

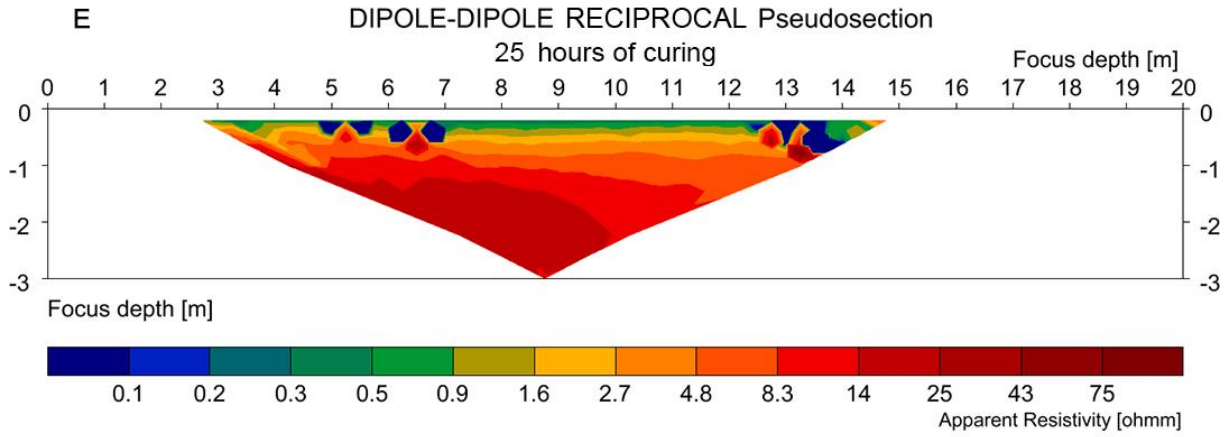
E
DIPOLE-DIPOLE RECIPROCAL Pseudosection
25 hours of curing
Focus depth [m]
0 1 2 3 4 5 6 7 8 9 10 11 12 13 14 15 16 17 18 19 20
0
-1
-2
-3
Focus depth [m]
0.1 0.2 0.3 0.5 0.9 1.6 2.7 4.8 8.3 14 25 43 75
Apparent Resistivity [ohmm]

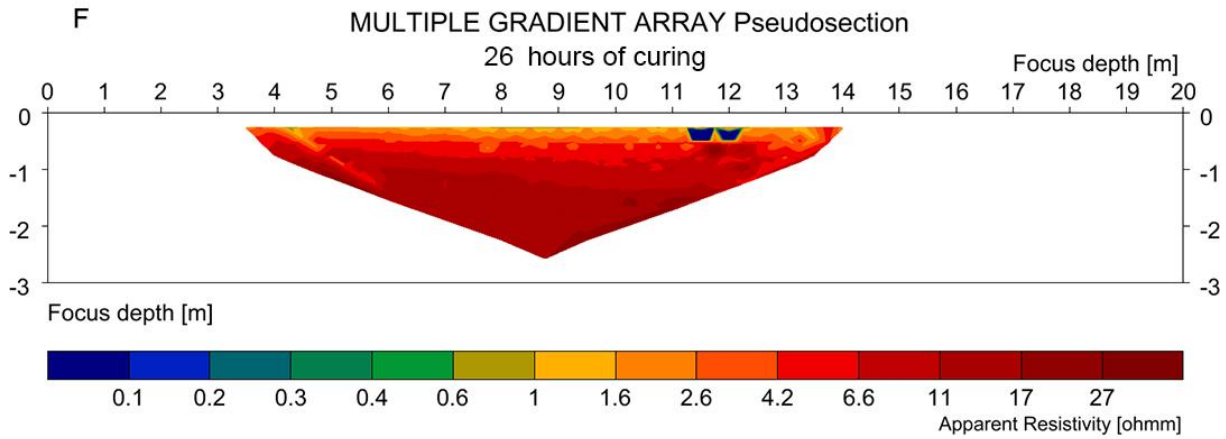
F
MULTIPLE GRADIENT ARRAY Pseudosection
26 hours of curing
Focus depth [m]
0 1 2 3 4 5 6 7 8 9 10 11 12 13 14 15 16 17 18 19 20
0
-1
-2
-3
Focus depth [m]
0.1 0.2 0.3 0.4 0.6 1 1.6 2.6 4.2 6.6 11 17 27
Apparent Resistivity [ohmm]

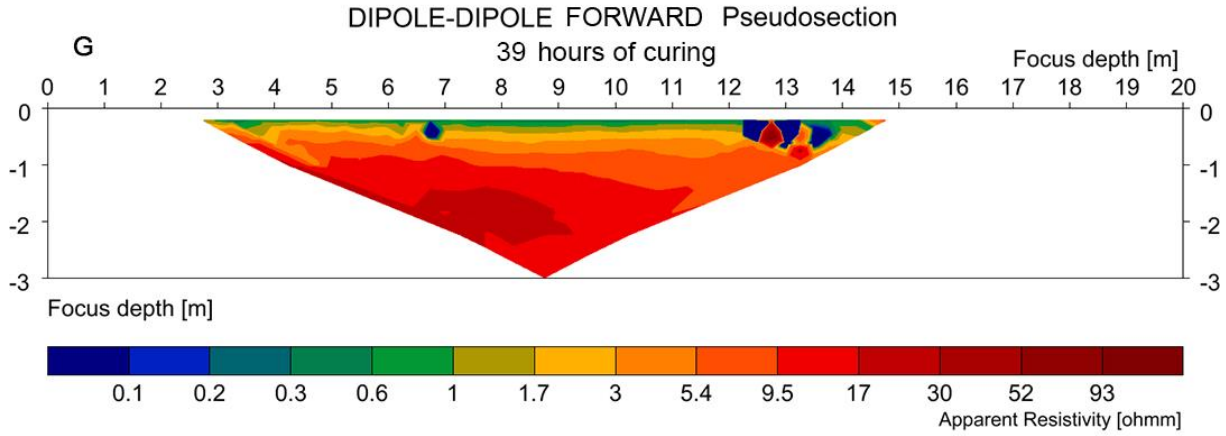
G
DIPOLE-DIPOLE FORWARD Pseudosection
39 hours of curing
Focus depth [m]
0 1 2 3 4 5 6 7 8 9 10 11 12 13 14 15 16 17 18 19 20
0
-1
-2
-3
Focus depth [m]
0.1 0.2 0.3 0.6 1 1.7 3 5.4 9.5 17 30 52 93
Apparent Resistivity [ohmm]

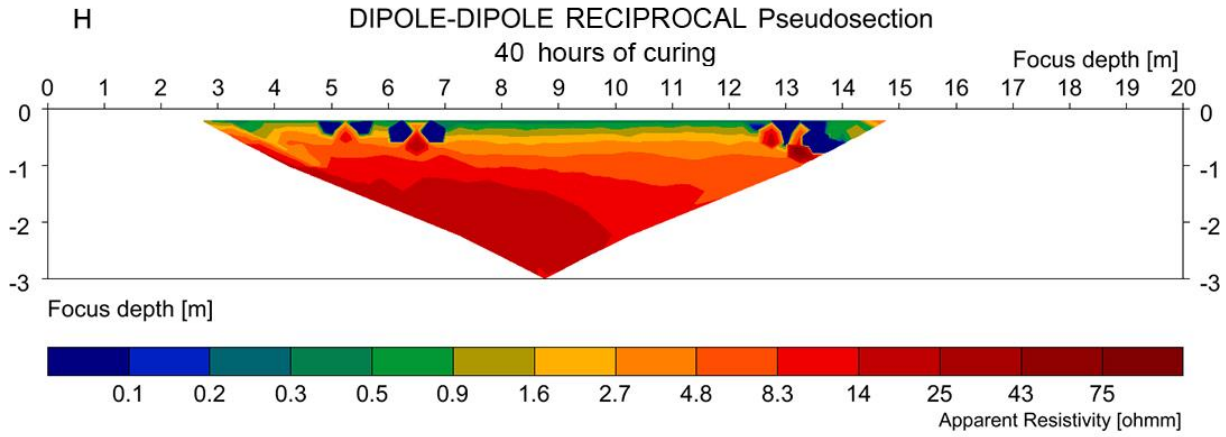
H
DIPOLE-DIPOLE RECIPROCAL Pseudosection
40 hours of curing
Focus depth [m]
0 1 2 3 4 5 6 7 8 9 10 11 12 13 14 15 16 17 18 19 20
0
-1
-2
-3
Focus depth [m]
0.1 0.2 0.3 0.5 0.9 1.6 2.7 4.8 8.3 14 25 43 75
Apparent Resistivity [ohmm]

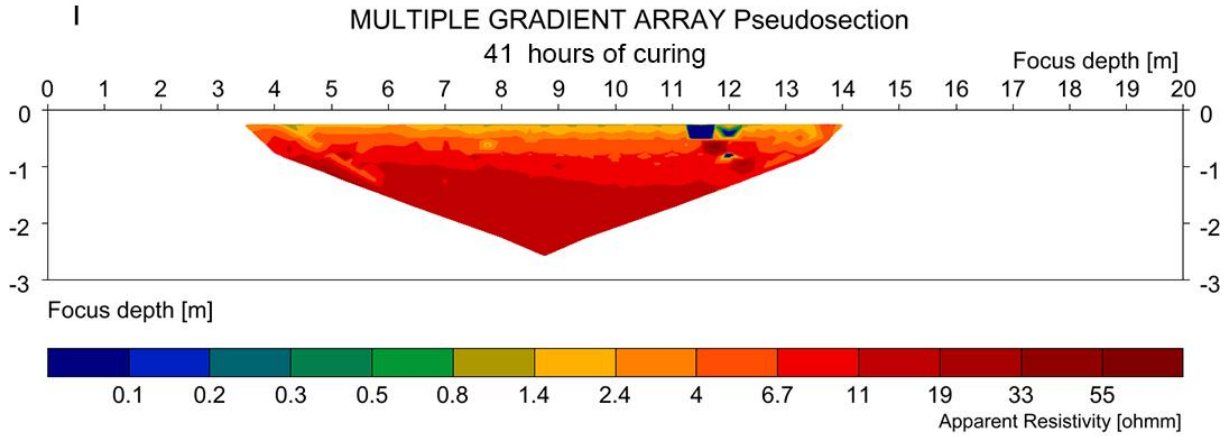
I
MULTIPLE GRADIENT ARRAY Pseudosection
41 hours of curing
Focus depth [m]
0 1 2 3 4 5 6 7 8 9 10 11 12 13 14 15 16 17 18 19 20
0
-1
-2
-3
Focus depth [m]
0.1 0.2 0.3 0.5 0.8 1.4 2.4 4 6.7 11 19 33 55
Apparent Resistivity [ohmm]

Dipole-dipole Res2DInv inversions

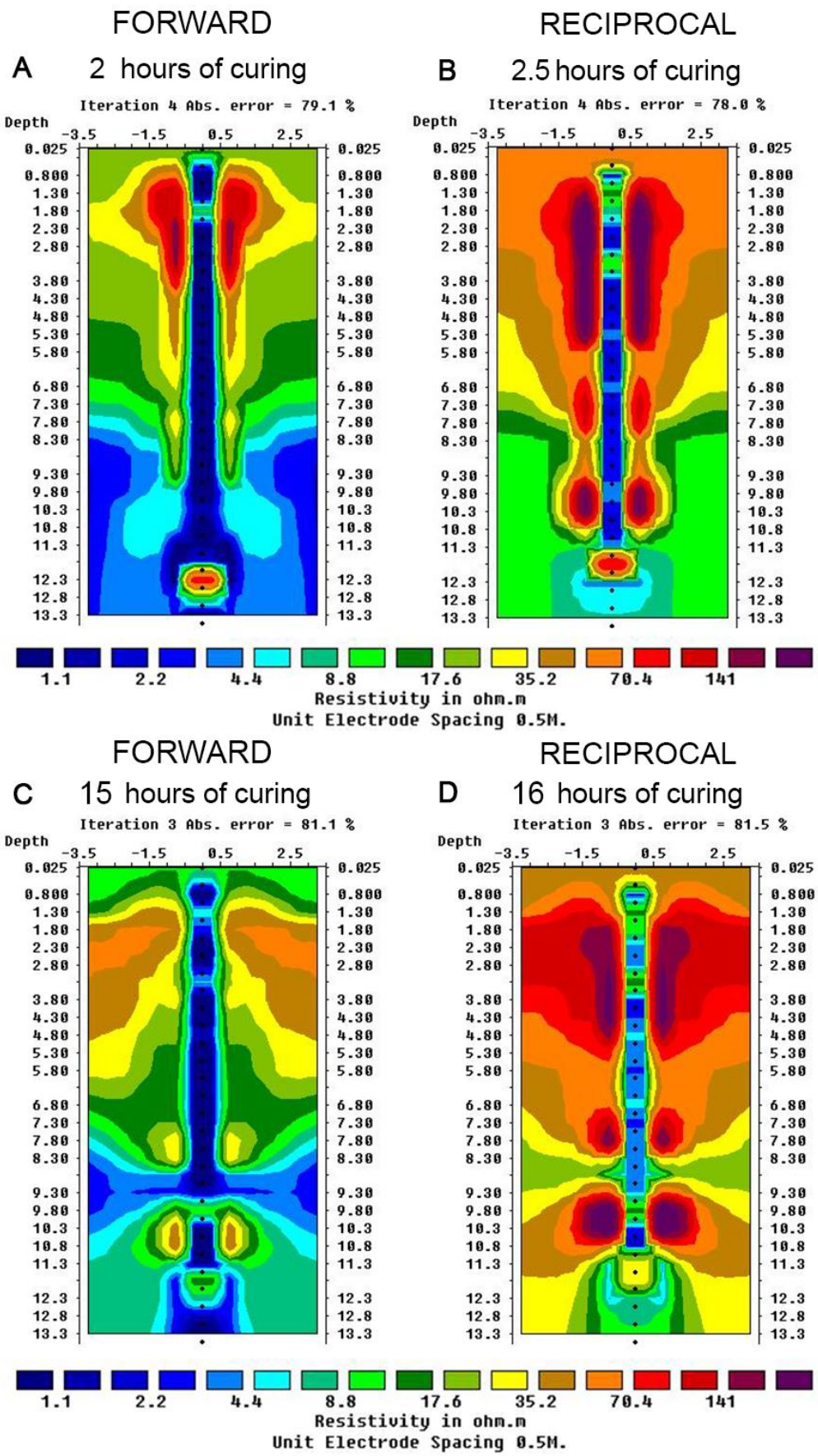

FORWARD

E 24 hours of curing

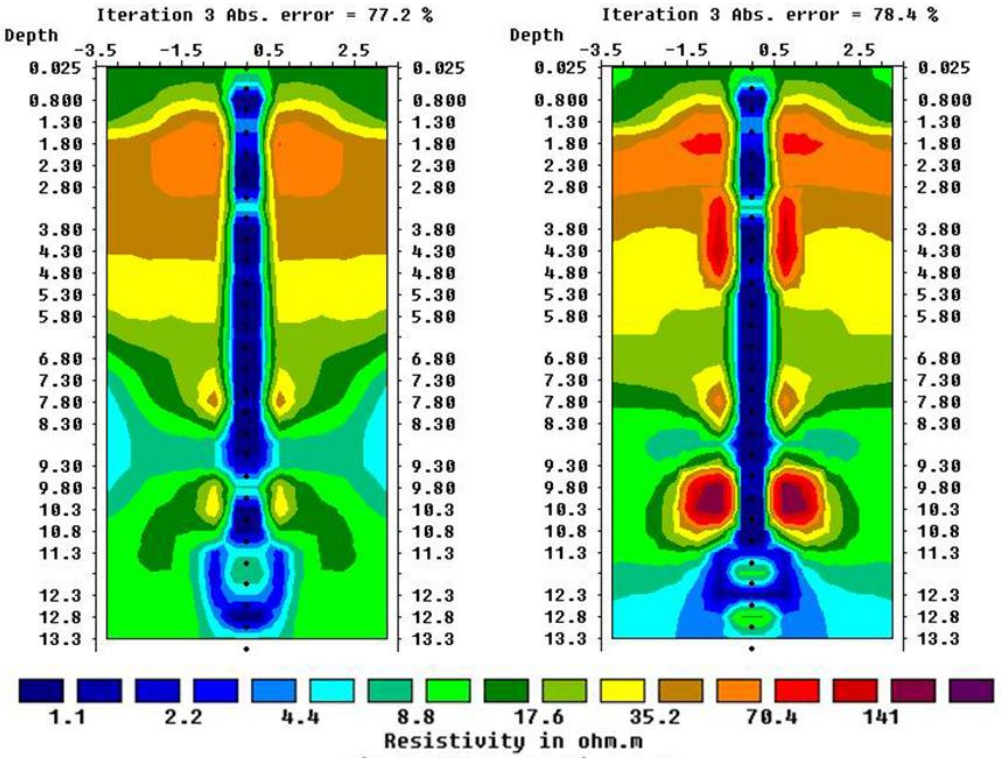

RECIPROCAL

F 25 hours of curing

FORWARD

G 39 hours of curing

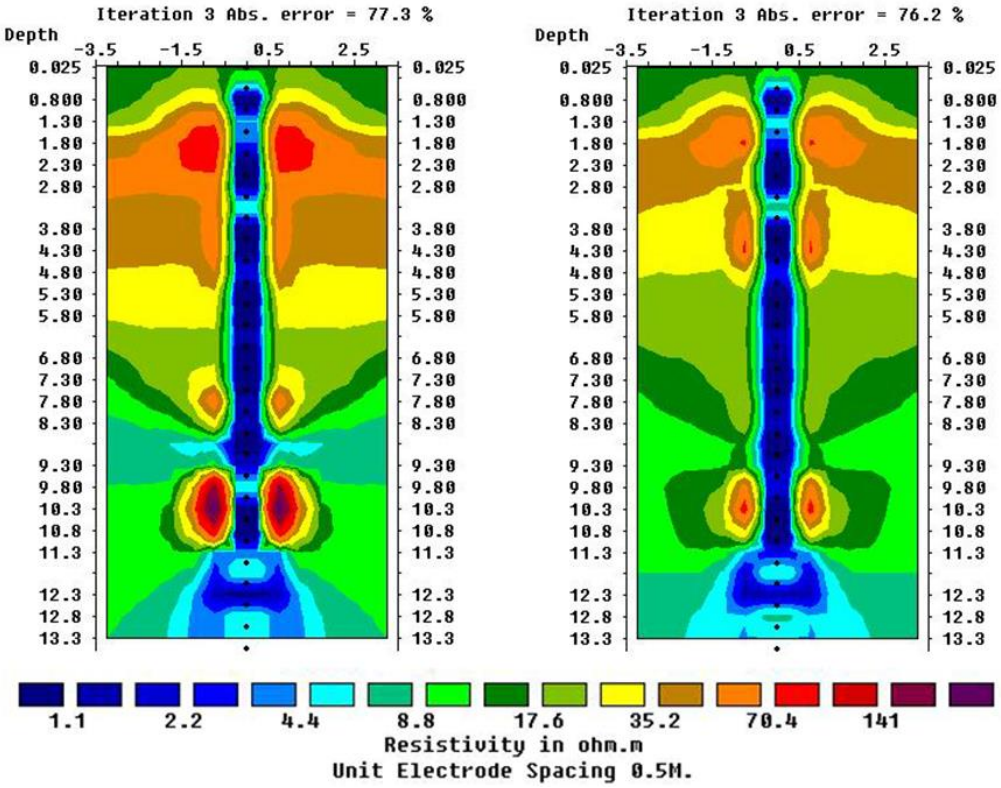

RECIPROCAL

H 40 hours of curing

FORWARD

I 790 hours of curing

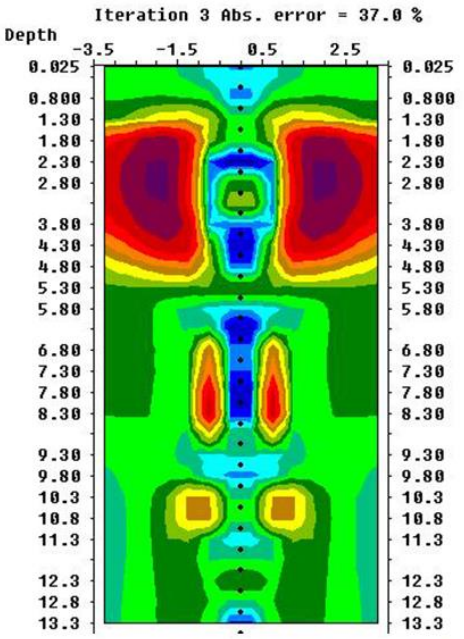

RECIPROCAL

J 790 hours of curing

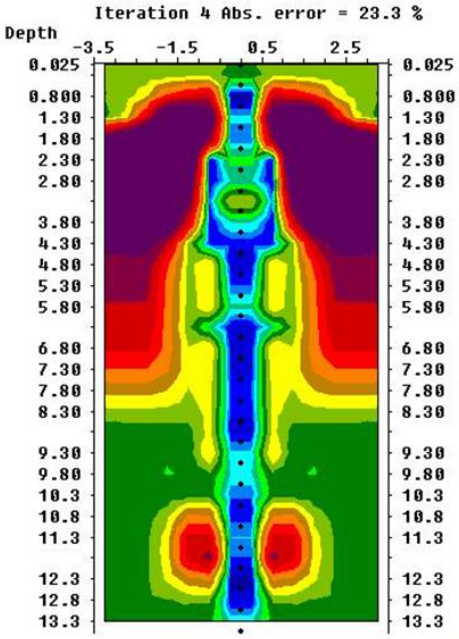

Resistivity in ohm.m

Unit Electrode Spacing 0.5M.